SYNTHESIS AND CHARACTERIZATION OF DIAMOND-LIKE CARBON AND DLC-MOS_2 COMPOSITE THIN FILMS

A Thesis Submitted to the College of

Graduate Studies and Research

In Partial Fulfillment of the Requirements

For the Degree of Doctor of Philosophy

In the Department of Mechanical Engineering

University of Saskatchewan

Saskatoon

By

HAMID NIAKAN

PERMISSION TO USE

In presenting this thesis in partial fulfilment of the requirements for a Postgraduate degree from the University of Saskatchewan, I agree that the Libraries of this University may make it freely available for inspection. I further agree that permission for copying of this thesis in any manner, in whole or in part, for scholarly purposes may be granted by the professor or professors who supervised my thesis work or, in their absence, by the Head of the Department or the Dean of the College in which my thesis work was done. It is understood that any copying or publication or use of this thesis or parts thereof for financial gain shall not be allowed without my written permission. It is also understood that due recognition shall be given to me and to the University of Saskatchewan in any scholarly use which may be made of any material in my thesis.

Requests for permission to copy or to make other use of material in this thesis in whole or part should be addressed to:

Head of the Department of Mechanical Engineering

57 Campus Drive

University of Saskatchewan

Saskatoon, Saskatchewan, S7N 5A9, Canada

ABSTRACT

In order to obtain diamond-like carbon (DLC) thin films with improved mechanical, tribological, thermal and corrosion properties for practical applications, the structure and properties of various DLC thin films including hydrogen-free DLC, hydrogenated DLC, and DLC-MoS_2 composites synthesized under different conditions were investigated in this thesis. The research methodologies and the main results are summarized in following paragraphs.

Hydrogen-free DLC thin films were synthesized by biased target ion beam deposition (BTIBD) method, while hydrogenated DLC thin films were deposited by ion beam deposition technique using a Kaufman-type ion source and an end-Hall ion source. DLC-MoS_2 composite thin films were also synthesized using BTIBD technique in which MoS_2 was produced by sputtering a MoS_2 target while DLC was simultaneously deposited by ion beam deposition. The influence of processing parameters on the bonding structure, morphology and properties of the deposited films was investigated using atomic force microscopy, Raman spectroscopy, X-ray photoelectron spectroscopy, synchrotron based near edge X-ray absorption fine structure spectroscopy, X-ray diffraction, scanning electron microscopy, nanoindentation, ball-on-disk and corrosion testing. Finally, the influence of annealing temperature on the structure and properties of pure DLC and DLC-MoS_2 composite films in ambient air and low pressure environments was studied.

In the case of BTIBD method, hydrogen-free DLC thin films with exceptionally high smoothness and low friction coefficient were prepared by biased target sputtering of graphite target without additional ion bombardment either by negative bias of substrate or assisting ion source. For ion beam deposition technique with Kaufman ion source, the DLC thin films synthesized at ion energies of 300 eV showed the highest sp^3 content and optimum properties.

Regarding end-Hall ion source, the best properties achieved in DLC films synthesized at ion energies of 100 eV.

Comparing with pure DLC and pure MoS_2 films, the DLC-MoS_2 films deposited at low biasing voltages showed better tribological properties including lower coefficient of friction and wear coefficient in ambient air environment. Also, comparing with pure DLC films, the DLC-MoS_2 thin films showed a slower rate of graphitization and higher structure stability throughout the range of annealing temperatures, indicating a relatively higher thermal stability.

ACKNOWLEDGMENTS

First of all, I would like to express my deepest gratitude to my supervisors, Profs. Qiaoqin Yang and Jerzy Szpunar, for their great guidance and support throughout this investigation. I would also like to thank my advisory committee members, Profs. Akindele Odeshi, Akira Hirose and Ike Oguocha, for their constructive criticism and useful suggestions. I specially thank Dr. Yongji Tang and Robert Peace, for all of their helping to do this research. I am grateful to Dr. D. Karpuzov in the Alberta Centre for Surface Engineering and Science for XPS measurement, which was established with the support from Canada Foundation for Innovation (CFI) and Alberta Innovation and Science, Dr. Y. Hu in the Canadian Light Source (CLS) for helping in the Synchrotron-based XANES measurement and Mr. Jason Maley in the Saskatchewan Structural Sciences Centre for helping in the atomic force microscopy study. The financial support granted by the Natural Sciences and Engineering Research Council of Canada (NSERC), the Canada Research Chair Program (CRC), and the University of Saskatchewan is acknowledged with appreciation.

Finally, I wish to express my heartfelt gratitude to my family for their support and love during the whole of my life.

DEDICATION

To my father and my mother

TABLE OF CONTENTS

LIST OF TABLES

LIST OF FIGURES

LIST OF ACRONYMS

a-C	Hydrogen-free amorphous carbon
a-C:H	Hydrogenated amorphous carbon
a-CN_x	Amorphous carbon nitride
AFM	Atomic force microscopy
Ar	Argon
B	Boron
BSE	Backscattered electrons
BTIBD	Biased target ion beam deposition
C	Carbon
CCD	Charge-coupled device
CH_4	Methane
CLS	Canadian Light Source Inc.
Co	Cobalt
COF	Coefficient of friction
Cr	Chromium
CTF	Conventional tube furnace
Cu	Copper
CVD	Chemical vapor deposition
DB	Dangling bond
DLC	Diamond-like carbon
EDS	Energy dispersive spectroscopy
EH	End-Hall
EPA	Environmental Protection Agency

EPMA	Electron probe microanalysis
ESCA	Electron spectroscopy for chemical analysis
EXAFS	Extended X-ray absorption fine structure
F	Fluorine
FCC	Face centered cubic
FLY	Fluorescence yield
H	Hydrogen
HCES	Hollow cathode electron source
IBAD	Ion beam assisted deposition
IBD	Ion beam deposition
IBS	Ion beam sputtering
IR	Infrared
MEMS	Microelectromechanical systems
Mo	Molybdenum
MoS_2	Molybdenum disulfide
MSIBD	Mass selected ion beam deposition
N	Nitrogen
Nb	Niobium
NEXAFS	Near edge X-ray absorption fine structure
Ni	Nickel
O	Oxygen
OCP	Open circuit potential
P	Pressure

PECVD	Plasma enhanced chemical vapor deposition
PLD	Pulsed laser deposition
PVD	Physical vapor deposition
RMS	Root mean square
S	Sulfur
SCE	Saturated calomel electrode
SE	Secondary electrons
SEM	Scanning electron microscopy
Si	Silicon
SPM	Scanning probe microscopy
SSSC	Saskatchewan Structural Science Centre
STM	Scanning tunneling microscopy
SXRMB	Soft X-ray Microanalysis Beamline
ta-C	Hydrogen-free tetrahedral amorphous carbon
ta-C:H	Hydrogenated tetrahedral amorphous carbon
TEY	Total electron yield
Ti	Titanium
UHV	Ultra-high vacuum
UMT	Universal Mechanical Tester
W	Tungsten
XAS	X-ray absorption spectroscopy
XPS	X-ray photoelectron spectroscopy
XRD	X-ray diffraction

CHAPTER 1 INTRODUCTION

1.1 Research Motivation

Metastable amorphous carbon which includes a high percentage of sp^3 bonding is called Diamond-like carbon (DLC) (Robertson, 2002). DLC thin film has many interesting properties such as high chemical inertness, high hardness, high corrosion and wear resistance, very low coefficient of friction and outstanding biocompatibility, which makes it an excellent wear and corrosion resistant coating for a number of scientific and industrial applications, including automotive components, bearings, biomedical implants and magnetic storage disks.

Although DLC thin films have interesting mechanical, tribological and corrosion properties, these properties change based on deposition technique and parameters, and working environment. Considering the fact that there is a possibility to synthesize DLC films using various deposition techniques with different structure and properties, determination of the processing-structure-property relationships in DLC films prepared by different methods would enable us to design and produce the films with desired mechanical, tribological and corrosion characteristics. Among deposition techniques, biased target ion beam deposition (BTIBD) technique has been employed to prepare thin films with high quality. However, there is no previous study on the deposition of pure DLC film by this method. It would be interesting to find out that hydrogen-free DLC thin film can be synthesized by biased target sputtering of graphite target without additional ion bombardment either by negative bias of substrate or assisting ion source, while additional ion bombardment is essential to obtain DLC by other sputtering methods.

Pure DLC films do not have a sufficiently low friction coefficient and wear coefficient in ambient air environment which is demanded for some industrial applications. Therefore,

improving the tribological performance of the film by means of the addition of some elements would be beneficial for their industrial applications. For most of industrial applications, the coatings may be exposed to localized heating induced by friction or working environments at elevated temperatures. Therefore, the thermal stability of DLC films not only determines the temperature range in which the DLC films can be used but also is very important for their long-term performance. Pure DLC films are unable to keep their superior properties at high working temperatures because of an irreversible conversion in their structure, which restricts the application of these films. So, improving their thermal stability would be useful and important for their high temperature applications.

1.2 Research Objectives

This thesis work aims to produce DLC coatings with improved properties (thermal stability, tribological behavior, mechanical properties and corrosion resistance). The research has the following specific objectives:

(1) To produce hydrogen-free and hydrogenated DLC coatings by different techniques

(2) To optimize the processing methods for obtaining DLC coatings with desired mechanical, tribological and corrosion characteristics

(3) To improve the tribological properties of DLC based coatings in ambient air environment

(4) To improve the thermal stability of DLC based coatings

1.3 Thesis Organization

This thesis consists of nine chapters. This chapter includes a brief introduction of the research motivation and contribution, the objectives of this research, and overview of the thesis. The rest of this thesis is arranged as follows.

In chapter 2, comprehensive literature review and background information about structure, properties, applications, deposition methods and mechanisms, doping and thermal stability of diamond-like carbon thin films will be presented.

Chapter 3 explains the experimental methodologies which have been used in this study. An ion beam system, which has been employed for deposition of diamond-like carbon and DLC-MoS_2 thin films, and furnaces, which have been used for thermal annealing of the films, will be described in details. Furthermore, different characterization methods employed in this investigation will be reported.

Chapter 4 focuses on the deposition of hydrogen-free diamond-like carbon thin films by biased target ion beam deposition method. The influence of target bias voltage, as a processing parameter, on the structure and properties of the films will be presented to determine the processing-structure-property relationships in hydrogen-free DLC films.

Chapter 5 deals with the structural characterization and properties of hydrogenated DLC thin films deposited by a Kaufman ion source with energy ranging from 300 to 700 eV. The effect of ion energy, as a processing parameter, on the structure and properties of the films prepared by the Kaufman ion source will be reported in this chapter to identify the optimum parameters to get the desired characteristics.

In chapter 6, the structure and properties of hydrogenated DLC films synthesized by an end-Hall ion source with energy ranging from 50 to 110 eV are reported . The influence of ion energy on the structure and properties of the films prepared by the end-Hall ion source will be discussed to determine the optimum parameters to reach the desired properties.

Chapter 7 focuses on the synthesis and characterization of DLC-MoS_2 composite thin films which have been employed to improve the tribological properties of pure DLC films. The

effect of MoS_2 target bias voltage, as a processing parameter, on the bonding structure and properties of the DLC-MoS_2 films will be studied in this chapter.

In chapter 8, the thermal stability of pure DLC and DLC-MoS_2 thin films in ambient air and low pressure environments is investigated. The influence of thermal annealing on the structure, mechanical and tribological properties of the deposited films will be discussed in this chapter.

Chapter 9 summarizes the conclusions of this research and provides some recommendations for future studies.

CHAPTER 2 LITERATURE REVIEW

2.1 Carbon Structures

Carbon creates a large spectrum of amorphous and crystalline structures since it is capable of being in three electronic configurations, sp^1, sp^2 and sp^3. Four electrons exist in the carbon atom's valence shell, which can be shared to create covalent bonds with other carbon atoms. The three different bonding hybridizations of carbon atoms are presented in Figure 2.1. In the case of sp^3 hybridization, like in diamond, four valence electrons of a carbon atom are each allocated to a tetrahedrally directed sp^3 orbital, which creates a strong σ bond with a neighboring atom. In the case of sp^2 hybridization, like in graphite, three of the four valence electrons go into trigonally directed sp^2 orbitals, which create σ bonds. The fourth electron of the sp^2 atom enters in a π orbital, which is located normal to the σ bonding plane. The π orbital creates a weaker π bond with a π orbital on one or more adjacent atoms. In the case of sp^1 hybridization, two of the four valence electrons go into σ orbitals, each creating an σ bond, and the other two electrons go into π orbitals (Robertson, 2002).

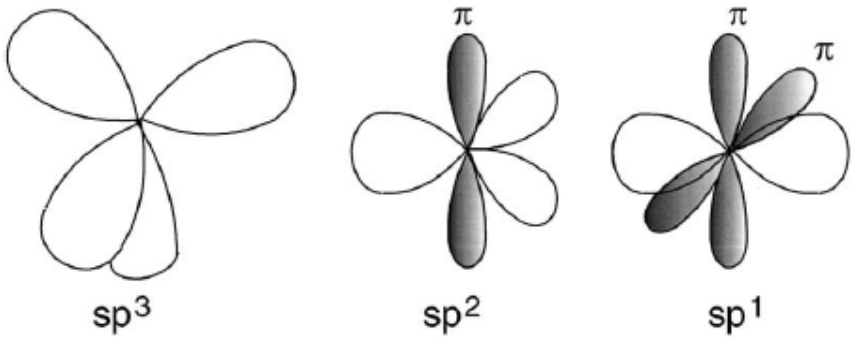

Figure 2.1. Bonding hybridizations for carbon atoms (Robertson, 2002).

According to these various bonding hybridizations, carbon creates different allotropes including diamond (sp^3), graphite (sp^2), nanostructures, and amorphous carbon (combination of

sp^3 and sp^2). The allotropes have various structures and completely different properties. The atomic configuration of some carbon allotropes is shown in Figure 2.2.

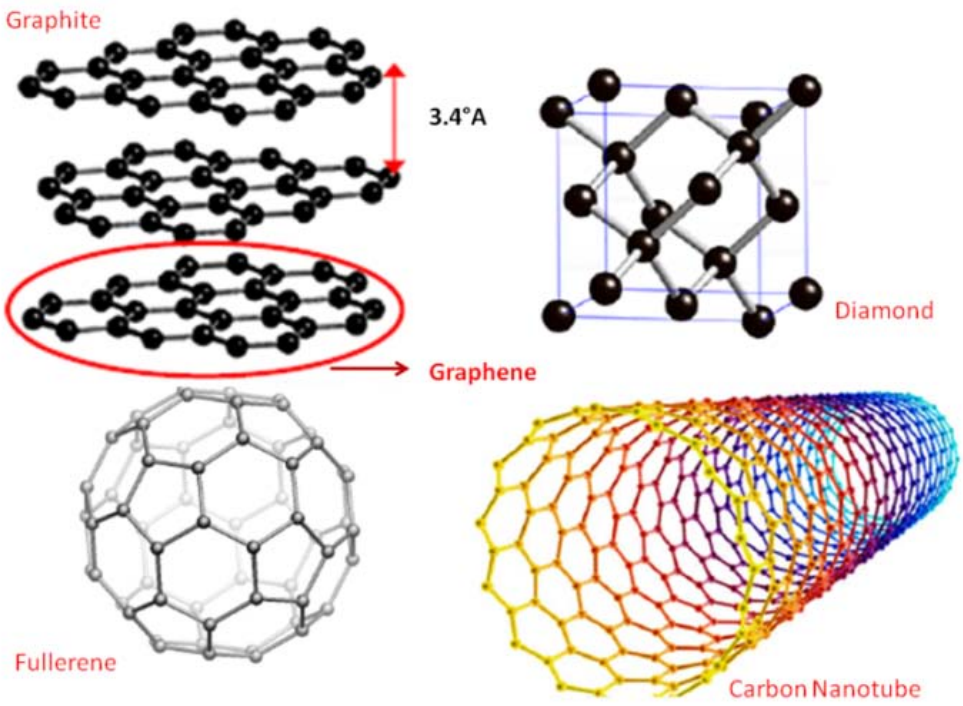

Figure 2.2. Atomic configurations of some carbon allotropes (Singh *et al.*, 2012).

Diamond has sp^3 configuration and all of its carbon bonds are strong and equivalent in a symmetrical manner. In diamond, the tetrahedral carbon bonds crystallize into a rigid FCC (face centered cubic) based lattice. Diamond has some excellent properties such as high chemical inertness, highest thermal conductivity, very high hardness, very low electrical conductivity and superior transparency because of the particular structure and strong σ bonding. In graphite the carbon atoms have sp^2 configuration, which leads to a layered planar structure. In each layer carbon atoms are bonded with each other covalently to form hexagonal lattice and these two dimensional layers are bonded together by weak Van der Waals forces. These planar layers

might slide easily over each other leading to a weak overall structure. In comparison to diamond, graphite has different characteristics because of its different configuration. It is black and not transparent, electrically conductive, and very soft. In fact, both of them (graphite and diamond) are extremely important for industrial applications (Zhang, 2012).

Carbon can be available in the form of nanostructures as well, such as carbon nanotube and Buckminsterfullerene (C_{60}), or amorphous structure. Carbon nanotube has a nanostructure which is cylindrical, with a single rolled layer (single-walled nanotube) or multiple rolled layers (multi-walled nanotube) of one-atom-thick carbon (graphite) sheet. It has sp^2 bonding configuration, exceptional thermal conductivity and very high strength. C_{60} is in a form of soccer ball and composed of sixty carbon atoms which have been bonded covalently in pentagonal and hexagonal rings. C_{60} is able to create a semiconductor solid by means of van der Waals forces. Also, it may produce films with strong non-linear optical characteristics in favor of photovoltaic applications. Amorphous carbon is composed of a random network of carbon atoms with various bonding configurations (combination of sp^3 and sp^2). They can be diamond-like or graphite-like based on their bonding states (Robertson, 1986). Diamond-like carbon (DLC) contains a large amount of sp^3 bonded carbon with properties comparable to diamond, while Graphite-like carbon includes a significant portion of sp^2 bonded carbon with properties comparable to graphite.

2.2 Diamond-Like Carbon Thin Films

2.2.1 Structure and Characteristics of DLC Films

DLC is a metastable type of amorphous carbon with a high percentage of sp^3 bonding in its structure. It can be classified into two major categories. Hydrogenated amorphous carbon (a-C:H) is one category of DLC with a moderate percentage of sp^3 bonding and a hydrogen percentage between 10 to 40%, or hydrogenated tetrahedral amorphous carbon (ta-C:H) with a

high percentage of sp^3 bonding and a relatively low percentage of hydrogen. Hydrogen-free amorphous carbon (a-C) is another category of DLC with a relatively high portion of sp^2 bonding and relatively low portion of sp^3 bonding, or hydrogen-free tetrahedral amorphous carbon (ta-C) with an extremely high percentage of sp^3 bonding up to 90% (Lifshitz, 2003). Different types of DLC films can be illustrated on a ternary phase diagram, as presented in Figure 2.3. The diagram reveals that two key factors conclude the structure and properties of DLCs; the fraction of sp^3 bonded carbon sites and the hydrogen content. Structural characterization of DLC focuses strongly on these two factors. The ordering of sp^2 sites is a third significant parameter, especially for electronic properties (Robertson, 2002).

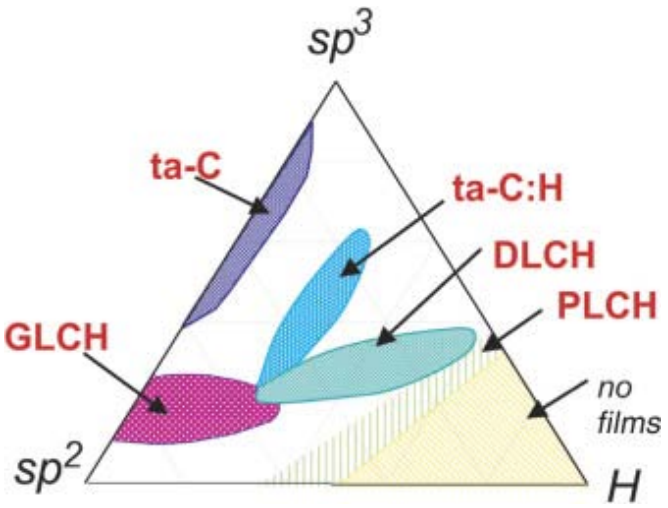

Figure 2.3. Ternary phase diagram presenting different DLC films (Casiraghi *et al.*, 2007).

Different models have been proposed to understand the DLC bonding and its electronic configuration. A cluster model has been developed by Robertson (1995) showing a relatively simple perspective from structure and bonding of DLC. In this model, the sp^2 areas in planar clusters with specific size are embedded in a matrix of sp^3 bonds. Electronic characteristics and optical gap of DLC are determined by the sp^2 cluster configuration, and mechanical properties of

DLC are induced by the sp^3 matrix. Figure 2.4 presents a view from this cluster model. The comprehensive structure of DLC in atomic scale still has not been empirically concluded, despite the fact that numerous theoretical models have been developed. A molecular dynamic simulation of an a-C:H thin film structure includes a carbon atom network with three- and four-fold atomic coordination and various types of hydrogen inside the structure (Erdemir *et al.*, 2006).

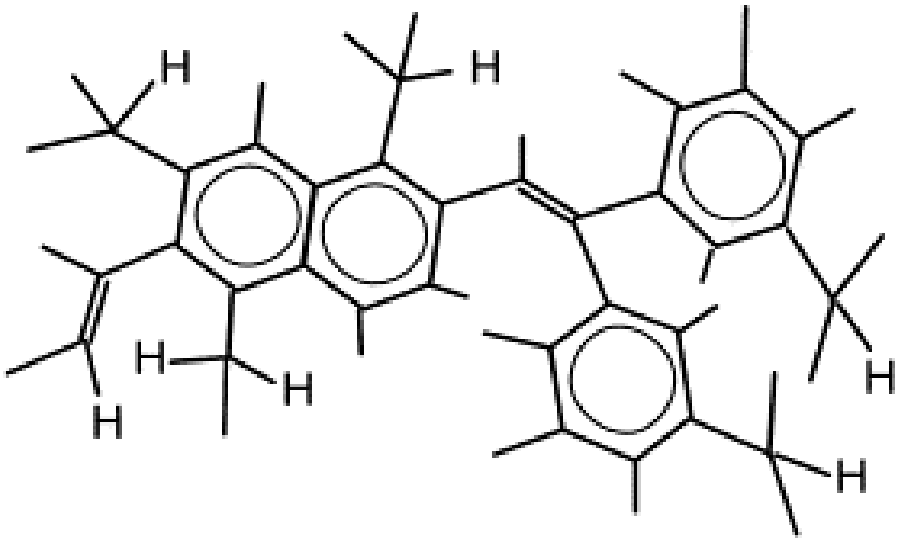

Figure 2.4. A view from cluster model in a-C:H thin film (Robertson, 1995).

Previous investigations show that deposition method, processing parameters and precursors alter the DLC bonding structure and chemical composition remarkably leading to a great variation of properties in DLC thin films. Hydrogenated DLC films might have a high percentage of hydrogen in their structure if they are synthesized from a hydrocarbon source such as methane. In fact, it is very unusual to produce DLC films without any hydrogen, so in general terms, hydrogen-free indicates low percentage of hydrogen in the thin films (less than 5%) and non-hydrogenated particles included in the synthesis procedure (Monteiro, 2001).

2.2.2 DLC Deposition Methods

The initial DLC films were processed by Aisenberg and Chabot (1971) applying ion beam deposition (IBD) technique. The DLC film deposition requires an energy source and a carbon source to produce the carbon species. Control of the deposition parameters (such as energy distribution and type of species) requires an additional filtering stage (Lifshitz, 1999). There is a possibility to synthesize DLC films with various properties by a large spectrum of chemical vapor deposition (CVD) and physical vapor deposition (PVD) techniques. These methods include sputtering, ion beam, mass selected ion beam (MSIBD), cathodic arc, pulsed laser deposition (PLD) and plasma enhanced chemical vapor deposition (PECVD) (Robertson, 2002). The techniques can be classified based on their suitability for large scale production or laboratory investigations. Each method has its own benefits and drawbacks regarding the quality and uniformity of the film, and deposition rate. The synthesized thin films have a large spectrum of structures and properties depending on the synthesis conditions which come from different deposition parameters and conditions in a particular synthesis experiment. These parameters include energy distribution of the carbon particles, their incident angle, deposition rate, substrate temperature and ambient pressure during synthesis (Lifshitz, 1999). Some DLC deposition techniques are illustrated schematically in Figure 2.5.

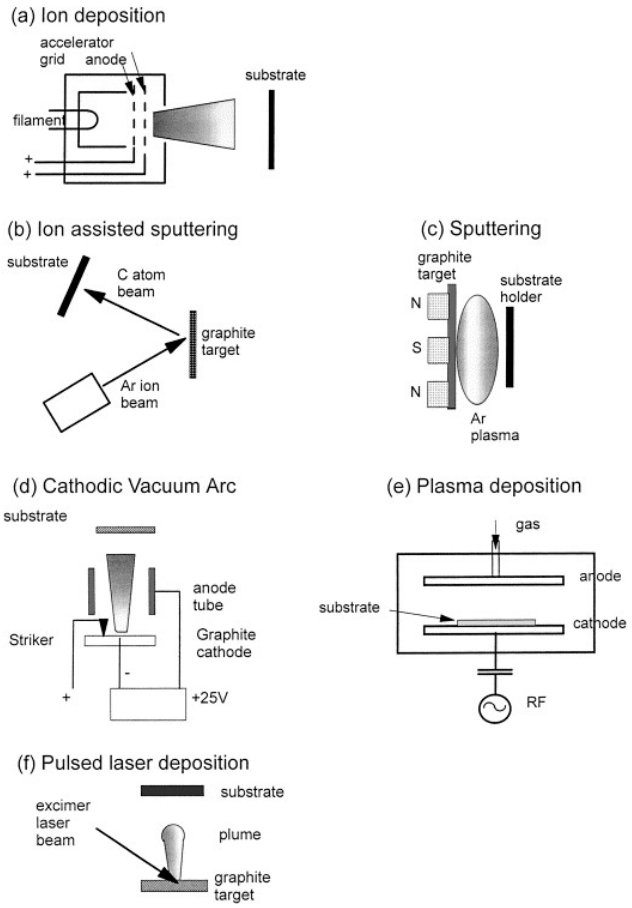

Figure 2.5. Schematic figures for different DLC deposition techniques (Robertson, 2002).

Normally, in an ion beam deposition technique, plasma sputtering of a graphite cathode in an ion source creates the carbon ions. As an alternative, a hydrocarbon gas e.g. methane is ionized in a plasma, like in the Kaufman source. Afterwards, an ion beam is extracted via a grid from the plasma source by a bias voltage. Subsequently the hydrocarbon ions or carbon ions are accelerated to create the ion beam in a high vacuum deposition system. In both situations, the ion source operates at a limited pressure, thus the beam contains a large amount of unionised (neutral) particles as well (Kaufmann, 1978). In this method, some important parameters like ion current density and ion energy can be managed independently over a large spectrum of deposition conditions, while in most of plasma methods a number of parameters such as gas flow

rate, gas pressure, plasma power, system geometry and gas composition are controlled to adjust the bombardment situations (Aisenberg *et al.*, 1991). Combination of ion bombardment with another PVD technique, such as sputtering or electron beam evaporation, leads to a method so-called ion beam assisted deposition. In this technique, it is possible to control the synthesis parameters such as ion current density, ion energy and temperature independently. By means of this method a gradual transition between synthesized film and substrate can be formed and less internal stress in the synthesized film would be created, which results in a much better adhesion of the film to the substrate. A schematic figure of this technique is shown in Figure 2.6.

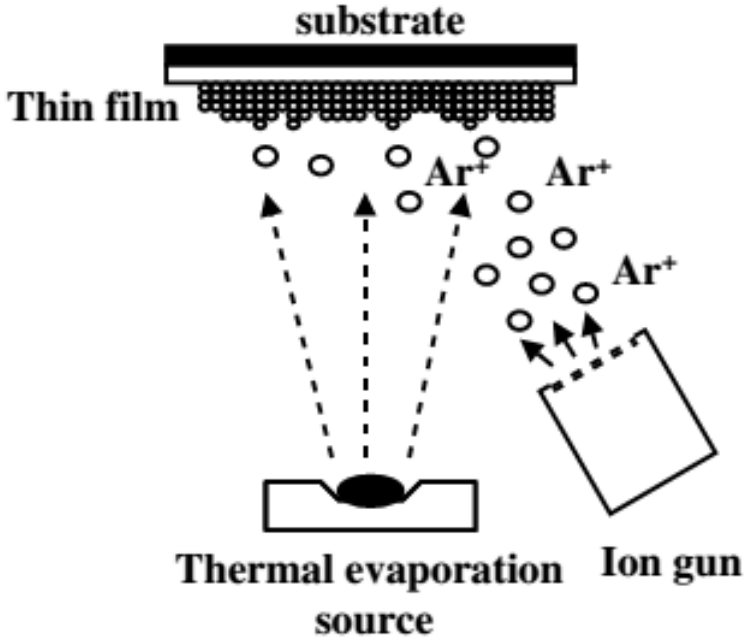

Figure 2.6. Schematic figure of ion beam assisted deposition technique (Jeong *et al.*, 2005).

MSIBD is an unusual version of direct ion beam deposition method which enables a controlled synthesis from one ion species at a specific ion energy. In this method, carbon ions are created from a graphite target in an ion source with small ion energy dispersion. Afterwards, the ions are accelerated and travelled through a magnetic filter which filters out any neutrals. The ion

beam will go off in different directions due to its Coulombic repulsion. Afterwards, the ions are slowed down to the desired ion energy by electrostatic lens, and the beam is concentrated on the substrate (Robertson, 2002). This technique is mostly employed for laboratory investigations and offers manageable ion energies, and a capability of doping by exchanging the ion species. The drawbacks of this technique are the low deposition rate, the high cost, and the small size of the deposition area which make MSIBD an unsuitable option for large scale production (Lifshitz, 1996).

The most important industrial method for synthesis of DLC films is sputtering. In this technique, the DLC film is synthesized by the sputtering of a graphite target with Ar ion plasma. In many cases due to low sputtering rate of graphite, magnetron sputtering is utilized to raise the deposition rate, particularly for the synthesis of super-dense DLC thin films (Robertson, 2002). Magnets are located in back of the target to make the electrons move spirally and expand their travelling distance leading to an increase in the degree of plasma ionization. Since the ion bombardment assists sp^3 bonding formation, the magnetic field can be arranged to pass through the substrate leading to bombardment of the substrate by the argon ions to produce an 'unbalanced magnetron'. In order to change the ion energy, a bias can be implemented to the substrate. The a-C:H can be synthesized by reactive sputtering, with a plasma of argon and methane or hydrogen, and amorphous carbon nitride (a-CN_x) can be deposited employing a plasma of Ar and nitrogen. For ion beam sputtering, a beam of argon ions can be employed to sputter the graphite target to produce the flux of carbon. In order to densify the film or promote sp^3 bonding, a second argon ion beam can be employed to bombard the growing film which is known as ion beam assisted deposition (IBAD) or ion plating. The major disadvantage is that a lot of maintenance is required to keep the ion source functional (Wolf, 1995). Among different

DLC deposition methods, sputtering is the first option for industrial applications due to its extensive application in sputtering various materials, its versatility, and its ease for large scale production. Furthermore, the synthesis parameters can be controlled by the gas pressure and plasma power, and independently from the condition or geometry of the substrate. Similar to ion beam deposition, sputtering has the drawback of a fairly low ratio of energetic ions to neutral particles leading to inability to create super hard DLC thin films (Robertson, 2002). Nevertheless, fairly high sp^3 content can be achieved in DLC thin films by developing sputtering with extremely high portion of ions, but with the drawback of decreasing the growth rate (Schwan *et al.*, 1996).

Cathodic arc is an uncommon technique for industrial and laboratory application. In a high vacuum system, an arc is started when a tiny carbon striker electrode touches the graphite cathode removing the striker which creates a high ion density energetic plasma. The benefits of the cathodic arc method include creation of a highly ionized plasma involving energetic particles, a relatively narrow ion energy distribution, and high deposition rate for a low capital cost. In contrast to ion beam deposition, the depositing beam in this method is a neutral plasma beam; therefore it is able to deposit on the insulating substrates. The drawbacks of this method include the inadequate filtering and instability of the cathode spot (Robertson, 2002).

In the PLD technique, pulsed excimer lasers like ArF produce extremely short and strong energy pulses that can be employed to vaporize materials as a strong plasma. Afterwards, the plasma spreads out towards the substrate. The kinetic energy of this expansion creates an ion energy comparable to the cathodic arc or MSIB ion energy. Pulsed laser deposition has been applied to synthesize ta-C films. The main advantage of this method is its multi-purpose

laboratory scale, which can be employed to synthesize a large spectrum of materials, from hard coatings to high temperature superconductors (Voevodin, 1996a).

RF PECVD is the most widely used laboratory synthesis technique for deposition of DLC coatings. The reactor is composed of two electrodes with unsimilar area. Normally, the RF power is attached to the electrode with smaller size which the substrate is mounted on that, and another electrode is attached to the earth. The RF power creates a plasma between these electrodes. Electrons have higher mobility than ions in the plasma producing a sheath beside the electrodes with extra ions which have a positive space charge. Therefore, the plasma creates a positive voltage regarding to the electrodes, which makes the average electron and ion current equal. In the PECVD method, a glow discharge is used to activate gas particles required for synthesis. Different hydrocarbon gases including methane, acetylene, ethylene, benzene, propane and ethane have been employed as carbon source for synthesis of DLC by this method (Lieberman *et al.*, 1994).

2.2.3 Deposition Mechanism of DLC Films

The high amount of sp^3 bonding is the most important characteristic of DLC thin films. It is known that the main factor to achieve metastable sp^3 C-C bonding comes from the ion-assisted character of the synthesis process, more specifically, the energetic particle bombardment throughout the synthesis. In the synthesis process, the impinging particles go into subsurface interstitial atomic locations to create sp^3 bonding and cause a quenched-in density growth (Robertson, 2002). This indicates that the deposited DLC film is dependent mainly on this ion energy (the mean impact energy of the incident particles). More specifically, the energy per incident C ion determines the sp^3 bonding content of the film. In the case of hydrogenated amorphous carbon, it relies to some extent on the precursor hydrocarbon molecule as well. In

addition, the hydrogen percentage of the hydrogenated amorphous carbon is less than the hydrogen percentage of the precursor hydrocarbon particles. Hydrogen is lost because of ion bombardment which relies mainly on the ion energy (Donnet *et al.*, 2008). Typically, the mean ion energy for synthesis of DLC varies between 10 and 1000 eV. McKenzie *et al.* (1991) mentioned that graphite with sp^2 bonding possesses 50% further volume than diamond with sp^3 bonding concluding the pressure-temperature phase diagram of graphite and diamond, as presented in Figure 2.7, in which diamond is stable at elevated pressures on the top of the Berman-Simon line. McKenzie *et al.* assumed that the ion beam function is to make a compressive stress into the thin film, which will shift the thin film on the top of the Berman-Simon line leading to stabilization of the diamond-like phase (a quasi-thermodynamic transformation on this phase diagram). According to this model, right after the formation of the phase it will be quenched to the state of the growing thin film.

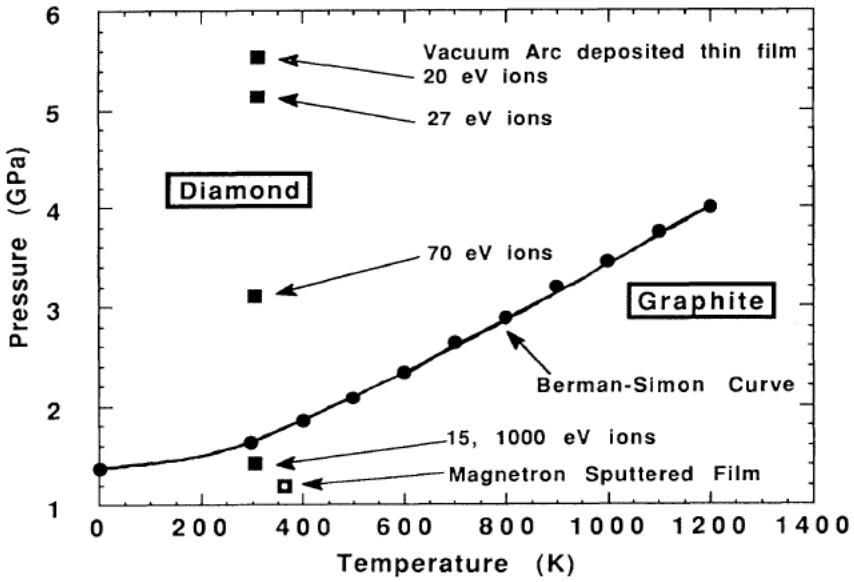

Figure 2.7. The carbon pressure-temperature phase diagram presenting the Berman-Simon curve (McKenzie *et al.*, 1991).

It is well-established that the DLC synthesis process from energetic particles is a shallow implantation, the so-called subplantation process, and not a regular surface condensation process. This subplantation process usually includes four steps: carbon particles penetration to the layers located below the surface, local stress inducement by carbon atoms incorporation, target atoms sputtering and dilution till the creation of a pure DLC layer and, finally, the pure DLC layer growth on successive bombardment (Lifshitz, 1999). Different analytical and numerical simulations have tested the subplantation fundamental theory. In these models, the structure of the film is determined by the impinging species energy and the interaction between two procedures of densification by incoming energetic ions, and relaxation of density. Figure 2.8 illustrates the subplantation process forming sp^3 structure in amorphous carbon films. According to Robertson (1994), the optimum ion energy for synthesis of DLC with high percentage of sp^3 bonds is approximately 100 eV at which the C atoms have enough energy to penetrate into the surface of substrate, while any extra energy can anneal out the density growth. Additionally, according to Erdemir *et al.* (2006), regardless of the synthesis method used, for ion-dominated procedures the maximum of sp^3 bonding content is achieved with a mean ion energy of about 100 eV. A lower ion energy than 100 eV leads to a larger portion of adhering to the surface in form of sp^2 configuration. A higher ion energy than 100 eV causes a drop in sp^3 content as well. This happens since the extra bombarding ion energy enables atomic relaxation nearby the implanted atom and a transformation of some sp^3 domains to the sp^2 domains. The exact mechanism of this process is still under debate. Probably, it includes a thermal spike, which causes the extra carbon atoms diffusion into the surface.

Regarding the synthesis of a-C films, a minimum ion energy is needed to penetrate to layers located below the surface and promote the creation of sp^3 bonding. The carbon ions at this

minimum energy get into undersurface interstitial locations and stop because of energy loss originating from atomic collisions, ionization and phonon excitations. Afterwards, the carbon ions diffuse and chemically react with the target atoms to raise the local density and rearrange the local bonding leading to a raise in sp^3 configuration. Local relaxation and detrapping of the carbon ions may eliminate part of the densification and enable local modification in a very compact domain in which the carbon ions are implanted (Lifshitz, 1996). Whereas a maximum density is obtained, plastic deformation may happen which sets the sp^3 content and density to a fixed amount with additional ion inclusion. By decreasing the ion energy, the carbon ions will be trapped on the surface, which can lead to surface processes i.e. graphitization (raise of sp^2).

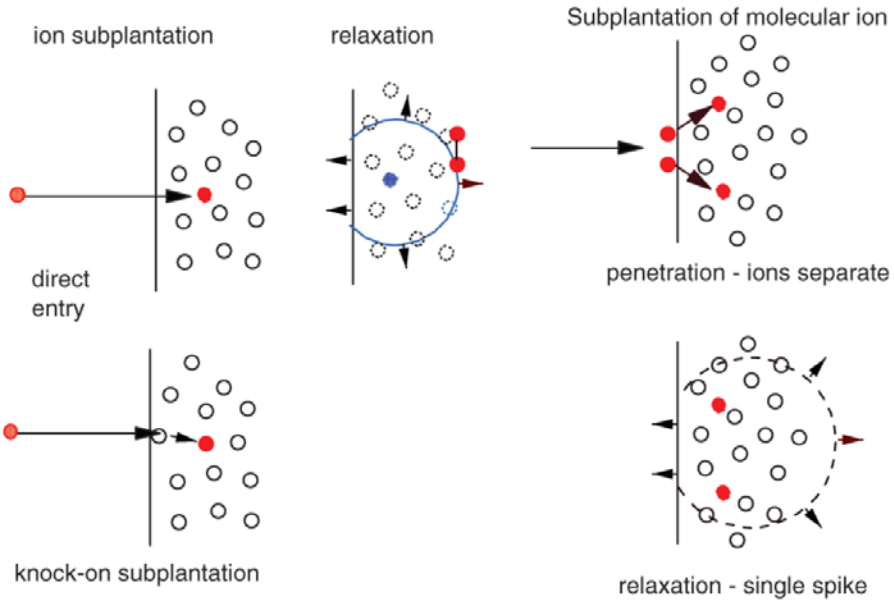

Figure 2.8. The subplantation process forming sp^3 structure in a-C films (Donnet *et al.*, 2008).

In the case of synthesis mechanism of hydrogenated amorphous carbon films, a similar subplantation process happens. But the process is more complicated, containing a stage of film growth, dehydrogenation induced by ion and compression of C-C structure. Various hydrocarbon gases including ethane, propane, acetylene, methane, benzene, and ethylene can be employed to

synthesize hydrogenated amorphous carbon films (Robertson, 1994). The energetic ions are ionized from the source gases and create an ion beam to bombard the surface of substrate. They decompose into atomic ions with equally allocated energy and afterwards the created atomic ions will subplant. Usually, besides the atomic ions, neutrals (e.g. mono-radicals and undissociated precursor gases) and atomic hydrogen impinge on the surface of substrate. The neutral particles participate in film growth by directly adding into C-C or C-H bonds of the surface or reacting with the film on dangling bonds (the so-called DBs) upon the surface to create C-C bonds. Eliminating hydrogen from a C-H bond of the surface by ion replacing or hydrogen removal can form a dangling bond. Unlike the neutral hydrocarbon particles acting solely at the surface, both atomic hydrogen and ions can pass into the film. Hydrogen atoms pass a few nanometers into the film and remove hydrogen from C-H bonds, thereby forming subsurface dangling bonds and hydrogen molecules. Carbon and hydrocarbon ions pass into the film by displacing hydrogen from C-H bonds. Hydrogen ions pass deepest into the film since they interact with carbon atoms weakly because of their small mass. Therefore, in the perfect model of hydrogenated amorphous carbon film growth, the chemical procedures of neutral particles and dehydrogenation, and the physical procedure of subplantation would be all included. The component processes in the growth of hydrogenated amorphous carbon thin film is presented in Figure 2.9 (Robertson, 2002).

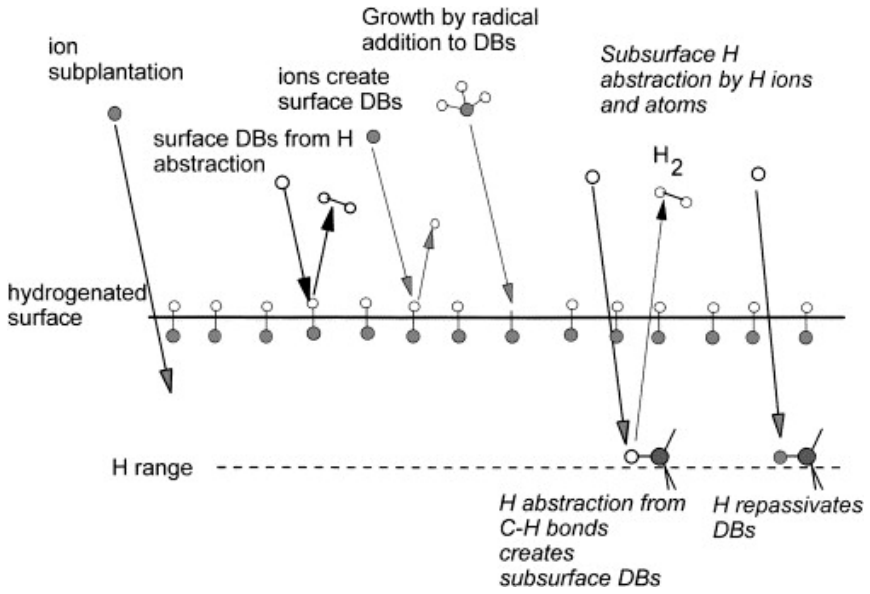

Figure 2.9. Component processes in the growth of hydrogenated carbon film (Robertson, 2002).

In hydrogenated amorphous carbon films, ion energy is the most important factor to determine the sp^3 content. For low ion energies, usually polymer-like carbon films are formed since the precursor gases might not be decomposed adequately. For intermediate ion energies, diamond-like carbon films are formed because of a decrease in the hydrogen content and an increase in the sp^3 content. In the case of high ion energies, graphite-like carbon films can be formed since the high energy causes a raise in disordered sp^2 bonding. In addition, the substrate temperature is an important factor for synthesis of the film. Whereas this temperature is higher than a transition temperature, it is detected that there is an obvious reduction in the sp^3 content. Also, by the raise of ion energy during the film synthesis the transition temperature reduces (Erdemir *et al.*, 2006).

2.2.4 DLC Properties

Due to the high content of sp^3 bonding, DLC has some exceptional properties comparable to diamond, e.g. the high hardness, high elastic modulus, low friction coefficient, high wear

resistance, high chemical inertness and corrosion resistance, excellent biocompatibility, superior optical transparency in the IR region and to some extent also in the visible region, relatively wide band gap, high electrical resistivity and dielectric strength, and good thermal conductivity (Nakazawa *et al.*, 2010), while these properties are obtained in an isotropically disordered film without any grain boundaries. Also, DLC is significantly cheaper to be produced compared to diamond leading to huge benefits for many industrial applications (Robertson, 2002). Another important benefit of DLC in comparison with CVD polycrystalline diamond is its high surface smoothness due to its amorphous structure. Furthermore, DLC can be synthesized at room temperature, which is a benefit for substrates which are sensitive to elevated temperatures like plastic.

The mechanical properties of DLC thin films are of great significance for their application as protective films. The great mechanical properties of DLC films result from their high content of sp^3 bonding. Normally, by increasing the sp^3 bonding content the hardness and Young's modulus of the DLC films rise. DLC is the only thin film or substance which is able to present simultaneously low friction and high hardness performances during dry sliding circumstances (Erdemir *et al.*, 2006). Figure 2.10 shows this matter in a superior way by classifying different categories of tribological coatings regarding their characteristic friction and hardness values.

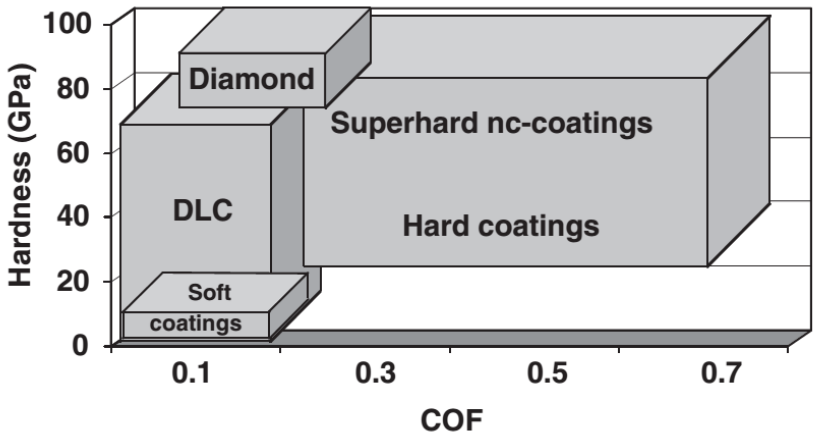

Figure 2.10. A schematic illustration of friction coefficient (COF) and hardness of DLC and other tribological coatings (Donnet *et al.*, 2008).

DLCs are also remarkable because of their low coefficients of friction (COF). The unlubricated COF of DLC on steel is comparable to the lubricated COF of steel on steel. According to Erdemir *et al*. (2000), hydrogenated amorphous carbon can have a COF as small as 0.01 in a vacuum environment. For hydrogenated amorphous carbon film, COF is strongly dependent on the percentage of humidity. COF Values less than 0.05 are achieved at low percentage of humidity and in a vacuum environment, and COF rises significantly at high percentage of humidity.

Wear coefficients for different sorts of DLC have been compared with other thin films by Gangopadhyay (1998) and Voevodin *et al.* (1996b). They observed that tetrahedral amorphous carbon (ta-C) has a very low wear coefficient in order of 10^{-9} mm^3 N^{-1} m^{-1}, which is around 1000 times less than that of a-C:H (hydrogenated amorphous carbon) in the order of 10^{-6} mm^3 N^{-1} m^{-1}. In the case of a-C:H, other wear coefficient measurements confirm these results (Grill, 1997). Due to the low wear coefficient of ta-C, it is a good candidate for application in Microelectromechanical systems (MEMS). According to Martinez *et al.* (2001), ta-C has the smallest wear coefficient at the greatest hardness value. The wear mechanism for a-C:H and ta-C

films are similar to their friction mechanisms which is adhesive wear by means of transfer layers. The ta-C converts by stress-induced conversion to a graphitic over-layer, which afterwards works as a lubricant, while a-C:H creates a carbon-hydrogen transfer layer on the surface. In ambient air atmosphere, a-C with high sp^2 bonding is worn accompanied by oxidation, forming CO_2 (Robertson, 2002).

Humidity, gas atmosphere, temperature and working environment significantly affect the wear and friction behavior of DLC films. In the case of inert or dry environments, the DLC films with high hydrogen content usually show low friction behavior, while the hydrogen-free DLC films present high friction behavior and intensified wear. In the case of humid atmosphere, the COF of both kinds of DLC films is quite similar changing from 0.05 to 0.2 and the lowest wear coefficient can be obtained with ta-C films. At elevated temperatures, the good tribological characteristics of a-C:H films may be interrupted because of hydrogen effusion and graphitization in the structure of the film. On the other side, the ta-C films are able to withstand at elevated temperatures, although the COF increases (Donnet *et al.*, 2008). From another point of view, a large difference in tribological properties of DLC films seems to come from a combined influence of extrinsic (tribotest condition) factors and intrinsic (film characteristic) factors. Extrinsically, tribotest conditions involving substance parameters, e.g. the counterface substances, motion nature, contact pressure, speed, load, surrounding temperature throughout the testing and the nature and chemistry of testing environment can have important effects (Erdemir *et al.*, 2006). Intrinsically, tribological behaviors of DLC films are significantly influenced by their structural and chemical nature (a great diversity of compositions and structures controlled by synthesis method and deposition parameters) (Grill, 1993). The combined effects of excellent mechanical properties and weak surface interactions explain the low COF and wear coefficient

of DLC films in a large spectrum of tribological applications. Depending on the environmental and tribological conditions; graphitization, triboreaction with supplements and tribo-oxidation, gaseous adsorption or desorption can happen at the film's sliding contact interfaces, which will determine the tribological performance of the film (Donnet *et al.*, 2008). However, DLC films do not have a sufficiently low coefficient of friction and high wear resistance on some working environments. Therefore, investigations on expanding the working environment and improving the performance of the film by means of the addition of metal or non-metal elements have been extensively conducted. Investigators have developed novel DLC films which are alloyed, composite or nano-structured by applying modern synthesis methods to improve their mechanical, physical and tribological properties. For example, it has been found that adding Ti, W and Si into DLC films enhance their tribological properties during lubricated sliding tests (Erdemir *et al.*, 2006).

Besides the mechanical and tribological applications, DLC films are appropriate for lots of diffusion-barrier and corrosion barrier applications as well due to their quite high density and very good coverage. Currently, DLC films are under research as passivation layers for interior part of beverage plastic bottles. The anticorrosion behavior of ta-C films for chemical-mechanical planarization pads has been studied as well. Protective coatings for hard drives and razor blades are two successful examples of ta-C film applications (Silva, 2003). The most common application of DLC films is in magnetic storage media (for magnetic disks and magnetic heads) due to their anti-wear and anti-corrosion nature. DLC films are particularly applicable in the place which the protective film should be extremely thin (below 50 nm), e.g. in magnetic hard drives. DLC is employed since it provides very smooth, uniform coverage, continuous, and chemically inert films leading to operation as a diffusion and corrosion barrier

with a surface roughness less than 1 nm (the major function of DLC films for this application is to create protection against corrosion) (Robertson, 2002). Also, DLC films seem to be biocompatible, and they have been employed in biological environments. DLC coatings can protect the implants against corrosion and work as diffusion barriers due to their chemical inertness and their quality of being impermeable to the liquids (Kim *et al.*, 2005).

According to Sharma *et al.* (2008), DLC films are chemically inert to almost any solvent at room temperature and are not attacked by alkalis, acid or organic solvent. DLC films are found chemically inert even to strong acid solutions. Also they found that the corrosion resistance of DLC films was improved by raising the film thickness. In spite of the fact that DLC films are normally nobler than substrates, the nanopores formation in the films can cause the electrochemical deterioration of the substrates because of water permeation and surrounding oxygen (Khun *et al.*, 2009). Doping of DLC films with Si can cause a great improvement in the corrosion resistance of the films, which could be associated with the creation of a film with higher density and consequently preventing the penetration of water ions or molecules (Masami *et al.*, 2009). But; the corrosion resistance of the nitrogen doped tetrahedral amorphous carbon films reduced with increased nitrogen flow rate (Khun *et al.*, 2009) and the corrosion resistance of the nickel doped DLC films dropped with increased Ni content (Khun *et al.*, 2010) due to the formation of more sp^2 bonds. According to Liu *et al.* (2006), the adhesion strength of DLC films affects their corrosion resistance, which means that the higher the film adhesion strength, the better the film corrosion resistance. Additionally, synthesis methods and parameters can have influence on the DLC film corrosion resistance. They can influence the corrosion resistance of the films by affecting bonding structure (e.g. sp^3 content), surface roughness, porosity density and electrical conductivity of DLC films (Bai *et al.*, 2011).

Erosive wear interacting with corrosion is called erosion–corrosion and is famous to deteriorate materials at elevated rates than anticipated, due to a synergistic influence between corrosion and wear. Erosion–corrosion degradation of stainless steel employed in the food manufacturing has been found and some simple surface modification techniques can be technologically the best solution to face this challenge, such as surface hardening at low temperatures and DLC protective films. According to Jellesen *et al.* (2009), the combined use of low temperature nitriding and DLC film significantly decreases the erosion–corrosion rate of stainless steel AISI 316 under particles impingement in a corrosive environment.

2.2.5 Applications of DLC based thin films

DLC coatings have appeared as one of the most important engineering coatings for different industrial applications, such as optics, transportation, microelectronics, manufacturing, and biomedical areas. The low COF of DLC makes DLC coating applicable on various mechanical parts in aerospace, automobile industry, textile industry, food transformation, and biomedical fields. Primarily, it enables us to diminish the consumption of energy and consequently helps to decrease the gas emissions which lead to global warming. Secondly, low COF causes the decrease of wear since the energy wasted in the mechanical contact is reduced.

DLC coatings have established their applications in many devices including magnetic storage media and razor blades. For instance, the carbon overcoats have been applied on magnetic hard disks to decrease friction and adhesion of the disc to the head since mid-80s. With the development of the coating techniques, the film thickness has reduced linearly with time to a few nanometers currently and their efficiency and durability have also considerably improved. DLC coatings have been applied on razor blades by many suppliers and the lifetime and comfortability of the blades have been significantly improved. In addition, DLC as antireflective

and wear resistant coating for IR windows has been industrialized (Lifshitz, 1999) and some companies have applied DLC coatings on laser barcode scanners and eyeglasses to enhance their scratching and abrasion resistance.

DLC coatings have had an important influence on the transportation industries. A large number of fuel injectors in diesel engines with excellent performance and a number of other engine components used in race cars are now covered with a layer of DLC film. It is absolutely clear that in future DLC films will be applied on some other critical engine components because next engine systems are anticipated to be a lot more compact, stronger and more efficient than the ones which came before. In the case of transportation industry despite the fact that some of the applications are routine and well-developed, other applications are still under progress. A huge application which is currently under investigation for automobiles contains valve lifters, tappets, and wrist pins. Also, the locking systems and door hinges of certain cars are being covered with DLC films instead of a thick grease layer.

DLC films are also employed in large scales in different manufacturing industries to hinder material transfer and wear throughout stamping, molding, drawing, and rolling processes. Due to the exceptional tribological performance and chemical inertness, DLC film can be applied on cutting tools in both dry and lubricated situations, which makes it a good candidate for applications demanding processing without lubricant such as food industry and biomedical areas. In biomedical areas, novel application of DLC coatings is for implantable and invasive medical instruments. Currently, these coatings are being tested for their performance and durability in specific biomedical implants such as load-bearing joints like hip and knee joints, and those which have direct contact with blood such as blood pumps, heart valves and coronary stents

(Donnet *et al.*, 2008). A fast spreading industrial application for DLC is in the textile field, where different parts and needles are covered with a layer of DLC to improve abrasion resistance.

Aerospace industry is one of the new fields for DLC application. Electroplated hard chromium coating has been employed to protect different parts against friction and wear in aerospace industry. But, hard chromium electroplating technique employs hexavalent chromium which is a famous human carcinogen. In fact, hexavalent chromium has been connected to cancer in humans subsequent of extended inhalation, and mortality investigations performed on chromium electroplaters revealed a raise in cancer-induced deaths. Environmental Protection Agency (EPA) has specified strict protocol for chromium electroplating solutions handling and disposal. So, there is a significant necessity to substitute hard chromium coating with an environmentally friendly and also excellent protective coating for high strength steel parts. Synthesis of DLC coating is an environmentally friendly procedure and consequently it is a better substitute to the hard chromium coating for protecting the steel surfaces (Sundaram, 2006). Also solid films are employed over a wide area for the lubrication of components working in space environment since they satisfy the severe requirements of that atmosphere, such as a large spectrum of working temperature, oxygen absence, the state of being in an ultra-high vacuum, the gravity absence, and the ionizing radiation existence. But, space systems are needed to work in ambient air as well because the assembly, test and storage stages are carried out on earth. Consequently, the excellent wear and friction behavior in ambient atmosphere is significantly demanded (Vanhulsel *et al.*, 2007). Currently, sputtered molybdenum disulfide (MoS_2) film is a well-established solid lubricant in aerospace industry which meets these requirements to some extent. MoS_2 thin film displays an extremely low COF in an ultra-high vacuum situation (Donnet *et al.*, 1996). The extremely low COF of MoS_2 comes from its laminar structure (Martin *et al.*,

1993). The films deposited by sputtering methods are non-stoichiometric (Weise *et al.*, 1997) and oxygen atoms replace the sulfur ones in crystal lattice of MoS_2 (Lince *et al.*, 1990), and thus passivation to environment containing oxygen similar to ambient air throughout a long storage time leads to deterioration in the tribological performance of the MoS_2 film. Fabricating a composite coating containing MoS_2 might be one solution to hinder the oxidation throughout the storage stage. As discussed earlier in this chapter, DLC is a thin film which has demonstrated excellent tribological properties, including low wear coefficient and low COF, and thus promising to be used as a solid lubricant for aerospace applications (Vanhulsel *et al.*, 2007). However, previous studies show that the friction and wear of DLC coatings are largely dependent upon the atmospheric situations and the coating characteristics induced by the synthesis method and parameters (Donnet *et al.*, 1997a). The employment of pure DLC films might not be the best option where elevated temperature and different atmospheres are anticipated. In this matter, design of novel thin films like a composite film of MoS_2 and DLC might be favorable and synergy effect of both components may enhance the tribological performance of the coating especially for ambient air environments and elevated temperatures.

2.3 Doped DLC Thin Films

DLC has two disadvantages; thermal instability and large compressive stress. However, due to the amorphous nature of DLC it has the ability to be doped with metals and non-metal elements which moves it in the right direction to overcome these challenges (Robertson, 2002). Regardless of the film deposition method, there is a huge amount of intrinsic compressive stress (macroscopic stress) created in DLC films during the deposition, as explained in section 2.2.3. The total residual stress of deposited DLC films is composed of a thermal stress and the intrinsic compressive stress. The thermal stress arises from the difference in the thermal expansion

coefficients of the substrate materials and the DLC coatings (Wang *et al.*, 2007). The intrinsic stress is attributed to the deposition mechanism of DLC coatings known as subplantation, which creates the sp^3 bonding into the film during deposition (the energetic particle bombardment during the synthesis makes a compressive stress into the thin film, which will shift the thin film on the top of the Berman-Simon line leading to stabilization of the diamond-like phase). This huge compressive stress may lead to the film's peel off from the substrate which consequently restricts the applications to thin DLC films. So, reduction or removal of compressive stresses in DLC films proposes a big challenge for industrial applications of DLC films. The most common techniques for measuring the residual stresses in coated surfaces are those based on direct measurement of the elastic strains in the film by X-ray diffraction method, and those based on measuring the curvature radii of the initial substrate and the curvature radii of the substrate coated with the DLC film using Stoney's equation (Holmberg *et al.*, 2009). Substrate material and deposition parameters are two important factors which affect and determine the residual stress induced by DLC coatings. Usual methods to achieve DLC films with small amount of internal stress required raising the synthesis temperature or reducing the carbon particles impinging energy, which leads to a large decrease in sp^3content of the film. So, the reduction or removal of compressive stresses in DLC films by doping with metals and the employment of metallic interlayers between the substrate and the film has been developed. A small decrease in the sp^3 content and reduction in average coordination number of the network are two main reasons for the reduction of internal stress in metal-doped DLC coatings. On the other hand, in some industrial applications other necessities and enhanced properties are demanded which are achieved by doping light elements such as F, N, O or Si in the DLC structure.

Doped DLC thin films are an important class of DLC which are described by the inclusion of various elements in DLC structure to obtain enhanced properties in comparison with pure DLC thin films. By managing the dopant's nature, amount and distribution, altered deposition of doped-DLC with suitable characteristics for particular applications can be achieved. Usual dopants are metals, light elements and combinations from this to improve properties like adhesion, thermal stability, internal stress, hardness, tribological properties, biocompatibility or electrical conductivity. Various possibilities for doping DLC with different elements are shown schematically in Figure 2.11. The doped DLC films are synthesized by the same methods similar to the pure films by introducing species including the doping elements to the deposition chamber. In spite of the fact that there are some discovered correlations between the deposition parameters and the ultimate performance of the film, but there is not much discovered correlation between the properties and microstructure and the actual performance of the film for specific applications. Also, it is usually hard to foreseen the effect of a doped element on the final performance, particularly the tribological performance, which is influenced by various parameters (Donnet *et al.*, 2008).

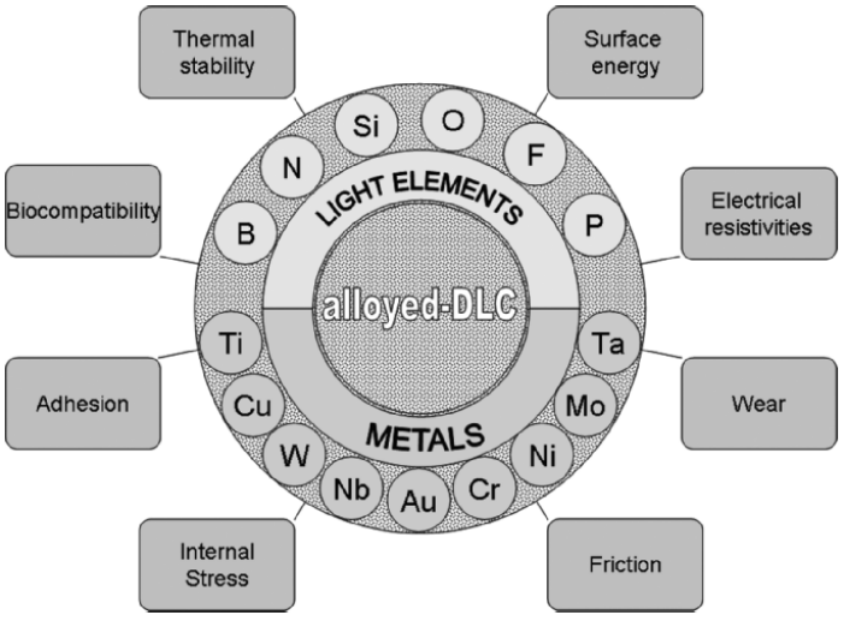

Figure 2.11. A schematic representation of various possibilities for doping DLC with different elements (Donnet *et al.*, 2008).

2.3.1 Light Element Doped DLC Films

Silicon doped DLC thin film can be used as a wear-resistant film similar to the pure a-C:H film (Grill *et al.*, 1996). Doping Si into DLC can reduce its COF during sliding versus steel and make the steel counterpart's wear less sensitive to humidity (Gangopadhyay *et al.*, 1997). It has been also reported by Oguri *et al.* (1990) and Meneve *et al.* (1993) that doping Si into DLC causes decreasing the COF in ambient air to less than 0.1, with a small raise in the wear coefficient. Fluorine doped DLC thin film can also be applied as a wear-resistant film, because doping F into DLC can decrease the microwear and COF of DLC (Trojan *et al.*, 1994; Donnet *et al.*, 1997b). Miyake *et al.* (1991) have doped the combined mixture of F and Si into DLC film structure. The microtribological performance of the Si-doped film was enhanced additionally by addition of F whereas the adhesion of the film and the DLC strength is significantly increased by doping low percentage of Si. In another study, doping a combined mixture of fluorine and B into

DLC film structure to create hard films with hydrophobic characteristics has been reported by He *et al.* (2005).

PVD techniques have been successfully employed to dope nitrogen into DLC films (a-C:N) (Chan *et al.*, 1998). For example, Cutiongco *et al.* (1996) used magnetron sputtering to synthesize thin nitrogen doped DLC films. Khurshudov *et al.* (1996) used ion beam assisted deposition technique to synthesize a-C:N films for magnetic storage disc application. According to Franceschini *et al.* (1992), doping N into DLC films decreases the compressive stress and based on the Hauert *et al.* (1995), it enhances the thermal stability of DLC coatings as well.

2.3.2 Metal Doped DLC Films

The reduction of compressive stress leading to the adhesion improvement is the most important advantage of doping metals into DLC film. The high adhesion of the metal doped DLC films to the substrates is very important for their industrial applications (Michler *et al.*, 1999). Some improvements have been obtained by designing functionally graded DLC films while chemical composition and mechanical properties are gradually changing from the metal substrate to the DLC film top layer. Voevodin *et al.* (1995) employed titanium and titanium carbide graded underlayers to improve the wear resistance of DLC coatings. Dahan *et al.* (2001) used this gradient design for tungsten carbide and steels substrates to enhance the adhesion properties of the DLC films.

DLC thin films has been doped with various metals, such as Nb, Ti, Cr, Cu, Co, Mo, W, and Au, mostly by magnetron sputtering of metallic targets where methane or another hydrocarbon gas has been used as carbon source simultaneously. Till now, the structure of these coatings has not been studied comprehensively. However, they are mostly in the form of tiny

pure metal or metal carbide nanocrystallites embedded into the amorphous DLC matrix (Donnet *et al.*, 2008).

The tribological behaviors of the metal doped DLC films can be different from each other severely. According to Wei *et al.* (1998), small amount of titanium or copper reduces the wear coefficient of the composite film in comparison with the pure DLC film. According to Dimigen *et al.* (1991), in the case of tungsten and tantalum doped DLC films, COF lower than 0.1 and very low wear coefficient have been obtained. Also according to Hauert *et al.* (1997), the optical characteristics of hydrogenated DLC films can be improved by doping chromium or tungsten into the DLC film.

2.4 Thermal Stability of DLC Thin Films

As stated earlier in this chapter, DLC is a metastable type of amorphous carbon including a very high percentage of sp^3 bonding, which has a natural tendency to turn to stable graphitic structure, sp^2-bonded carbon, after an energy barrier is provided (the energy barrier for transformation of metastable sp^3 bonding to stable sp^2 bonding). For some industrial applications, the DLC coatings may be exposed to high temperature environments or to localized elevated temperature induced by friction which can supply the needed energy barrier for the transformation of sp^3 bonding to sp^2 bonding. Liu and Meletis (1997) showed that the sliding friction procedure supplies the demanded energy for the transformation of DLC (sp^3 cubic structure) to graphite (sp^2 hexagonal structure). The low COF and very low wear coefficient of DLC films has been attributed to a graphite-like layer with low shear strength created at the sliding interface due to strain and thermal influences produced throughout sliding. It has been assumed that this transfer layer is created by the friction-induced transformation of the DLC film. Generally, the high temperature performance of the DLC coatings is extremely affected by

the coatings structure and nature. The water vapor and hydrogen have strong effect on the high temperature performance of the DLC coatings as well. For hydrogenated DLC coatings (a-C:H), the removal of hydrogen from the DLC structure will alter the film structure and consequently the film performance. In the case of hydrogen-free DLC coatings, the water vapor thermal desorption is harmful for their high temperature tribological performance (Donnet *et al.*, 2008).

2.4.1 Thermal Stability of a-C:H Coatings

In a-C:H coatings, the hydrogen has a crucial influence on the bonding structure by making the sp^3 bonding stable and consequently controlling the characteristics of the film. The hydrogen presence in DLC coating raises the percentage of sp^3 bonding. Annealing the a-C:H coating at elevated temperatures leads to hydrogen desorption in the coating. Because hydrogen atoms are anticipated to enhance the sp^3 bonding of the a-C:H structure, the hydrogen release will make the tetrahedral bonding unstable and intensify the transformation of tetrahedral sp^3 bonding structure to sp^2 bonding structure. Therefore, the hydrogen removal can activate the conversion of the sp^3 structure into a sp^2 structure, and the conversion of a-C:H structure to graphite is proposed to gradually continue resulting in microcrystalline type of graphite (raise of graphite microcrystallites in number and size) (Louro *et al.*, 2011). On the other side, thermal annealing of hydrogenated DLC decreases the film stress, similar to ta-C. But, due to the less bonding stability in hydrogenated DLC during annealing, this stress relaxation is less applicable comparing to ta-C (Robertson, 2002).

Hydrogen effusion will happen in hydrogenated DLC coatings at elevated temperatures ranging from 150 °C to 700 °C based on the coating synthesis parameters (Wild *et al.*, 1987). In the case of softer hydrogenated DLC coatings, hydrogen effusion and the film structure transformation to nanocrystalline graphite happens at lower temperatures ranged from 150 to 350

°C relative to the harder films which happens around 550 °C. The dense ta-C:H films have an hydrogen effusion temperature in the range of 700 °C during heating in air (Tallant *et al.*, 1995). According to Gao *et al.* (2005), the thermal annealing of a-C:H structure until 150 °C leads to high percentage of surface hydrogen desorption, as measured by mass spectroscopy. This influence came up with a raise in COF. According to Miyoshi *et al.* (1989), a raise in COF of hydrogenated DLC coating happened when the heating temperature increased from 500 °C to 600 °C. In dry nitrogen and ultra-high vacuum (UHV) environments, the removal of hydrogen from DLC film detected when it heated at temperature higher than 550 °C accompanied with severe raise in COF (Memming *et al.*, 1986). But, in humid environment the severe shift has been reported at lower temperature ranges (Grill, 1997).

In general, higher temperature induces higher wear (Liu *et al.*, 1999). As mentioned before, the hydrogen evolution is accompanied with the conversion of the sp^3 structure into a sp^2 structure. This graphitization and also oxidation of the a-C:H coating will wear out the DLC structure quickly at elevated temperatures. A raise in wear coefficient of DLC has been reported at elevated temperatures starting from 100 °C (Erdemir *et al.*, 1996). In comparison with the room temperature tests, the wear coefficient intensified largely for the hydrogenated DLC coating in 250 °C. Another study showed a quite unchanged wear performance for hydrogenated DLC coatings sliding versus Al_2O_3 in humid air environment at elevated temperatures until 200 °C, while in 300 °C and higher temperatures, the wear coefficient intensified largely causing the coating delaminating because of graphitization (Liu *et al.*, 1999). During the testing of the annealed a-C:H coatings in room temperature, stable wear resistance was observed until an annealing temperature ranging from 200 °C to 400 °C (Venkatraman *et al.*, 1999). Another study showed that the hydrogenated DLC coatings synthesized in higher temperature are tribologically

more stable at elevated temperatures (Grill *et al.*, 1991). According to Liu *et al.* (1993), the structure of hydrogenated DLC displayed no substantial shift after heating until 400 °C, while at higher temperatures the removal of hydrogen from the structure happened accompanied with small graphite crystals precipitation. But, hardness stayed almost unchanged after heating at temperatures ranged from 200 to 700 °C.

The thermal stability of hydrogenated DLC coatings can be improved by doping, for example with silicon. It has been observed that the doped Si stabilizes the structure and this silicon doped DLC coating graphitizes at a higher temperature in comparison with pure hydrogenated DLC coating (Wu *et al.*, 1999). However, there are some doping elements which reduce the thermal stability of hydrogenated DLC films, such as fluorine (Müller *et al.*, 1995).

2.4.2 Thermal Stability of Hydrogen-Free DLC Coatings

In the case of hydrogen-free DLC coatings, phase transformation or oxidation happens at much higher temperatures relative to a-C:H coatings. The tetrahedral amorphous carbon (ta-C) has hydrogen only in the form of impurity and the structure contains a high percentage of sp^3 bonding. Because of their structure, the ta-C coatings synthesized by vacuum arc discharge are thermally stable until 727 °C during annealing in vacuum environment (McKenzie *et al.*, 1994). However, during annealing in ambient air, coating oxidation is detected at temperatures ranging from 450 °C to 500 °C (Robertson, 2002). It has been also found that heating at 400 °C reduces the wear resistance of ta-C during sliding versus stainless steel after annealing (Leng *et al.*, 2003). For tetrahedral amorphous carbon coatings synthesized by pulsed laser (PLD) method, the thermal stability has been found to be dependent on the structure (sp^3 bonding content) and chemical properties of the film. It has been reported that alteration in sp^3 bonding content happens by heating in air at 300 °C (Jung *et al.*, 1999). But, high thermal stability has been

detected until 627 °C in ultra high vacuum environments (Rey *et al.*, 2000). A raise in COF of tetrahedral amorphous carbon coating was observed at slightly elevated temperatures in comparison to those measured at room temperature (Ostrovskaya *et al.*, 2001).

Annealing the tetrahedral amorphous carbon up to 500-600 °C enables a relaxation of the compressive stress to around zero. The initiation of relaxation occurs at low temperatures starting from 100 °C (local relaxation) and almost full relaxation has been detected at 600 °C (permanent relaxation via diffusion). This has a significant effect since stress restricts the synthesis of thick and adherent coatings. Thermal annealing to 600 °C enables the deposition of tetrahedral amorphous carbon coatings with thickness of about 1 μm. The annealed coatings keep their high Young's modulus and hardness since the sp^3 bonding content is unchanged (Robertson, 2002).

It has been reported that the softer hydrogen-free amorphous carbon (a-C) coatings, synthesized by magnetron sputtering method, are thermally stable till 300 °C, and for higher temperatures the hardness reduces significantly as a result of graphitization in the film structure. Tribological tests with hydrogen-free amorphous carbon films disclosed intensified wear coefficient at 120 °C as a result of stability loss and considerable oxidation of the film in ambient air. COF of hydrogen-free amorphous carbon films is intensified significantly when tested at elevated temperatures as well. The intensified COF is associated with the lack of adsorbed water which is essential for the friction performance of the hydrogen-free DLC films (Konca *et al.*, 2006). But, the thermal stability can be improved by designing nanocomposite structures (Zhang *et al.*, 2006).

CHAPTER 3 EXPERIMENTAL METHODS

In this investigation, an ion beam deposition system was employed for deposition of diamond-like carbon and DLC-MoS_2 thin films. The detail configuration of this coating machine will be explained in this chapter. Thermal stability of pure DLC and DLC-MoS_2 thin films were studied by thermal annealing in furnaces with various environments of ambient air and low pressure. Annealing in these furnaces will be discussed here. Structure and properties of the deposited and processed films were characterized by different methods, including atomic force microscopy (AFM), Raman spectroscopy, X-ray photoelectron spectroscopy (XPS), synchrotron based near edge X-ray absorption fine structure spectroscopy (NEXAFS), X-ray diffraction (XRD), scanning electron microscopy (SEM), nanoindentation, ball-on-disc testing, and corrosion testing. The principles of those methods will be described in this chapter as well.

3.1 Experimental Equipment

3.1.1 Ion Beam Deposition System

The ion beam deposition system was made by 4Wave Inc. This system is composed of a power supply and a computer control system, a pumping system, and a vacuum chamber. The pictures of this ion beam deposition (IBD) system are displayed in Figure 3.1. Figure 3.2 presents a schematic diagram of the system configuration. Inside the vacuum chamber, there are an ion source for deposition, precleaning and assisting (ion source I), another ion source for sputtering (end Hall ion source II), targets, substrate holder and shutters for targets and substrates. The substrate holder is at the distance of 300 mm from the ion source I and is tilted 45° with respect to this ion source. The system is multi-purpose and can do ion beam etching, ion beam deposition, as well as ion beam sputtering.

(a)

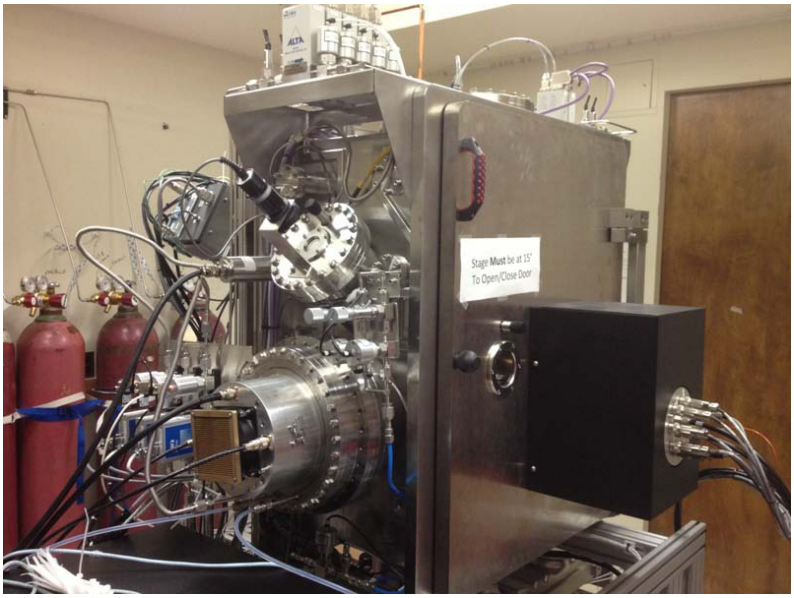

(b)

Figure 3.1. Pictures of the IBD system, (a) power supply and control system, (b) vacuum deposition chamber.

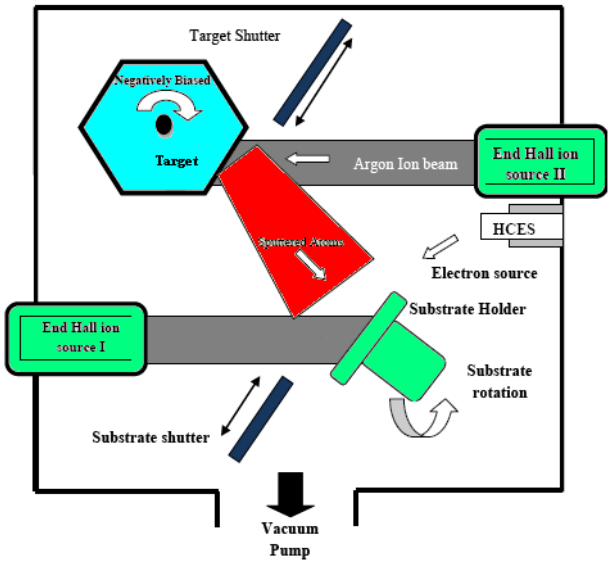

Figure 3.2. A schematic diagram of the ion beam deposition system configuration.

When an end-Hall ion source (ion source I) is installed in the position of precleaning and assisting ion source, the source can be employed to etch the substrates (Ion Beam Etching) or deposit the hydrogenated DLC film on the substrates (Ion Beam Deposition) as will be explained in Chapter 6. If a Kaufman ion source is installed in the position of precleaning and assisting ion source (instead of end Hall ion source I), again the ion beam can be used to etch the substrates (Ion Beam Etching) or deposit the hydrogenated DLC film on the substrates (Ion Beam Deposition) as will be reported in Chapter 5. In both cases, precursor gas (in this investigation CH_4/Ar) is inserted into the ion source and ionized to free radicals of carbon. The radicals of carbon are able to react and deposit a thin film on the substrate.

When sputter ion source is working, target materials will be sputtered and deposited on the surface of substrate, known as biased target ion beam sputtering technique. The hydrogen-free DLC film to be discussed in Chapter 4 was synthesized by this method using a graphite target as carbon source. Composite DLC thin films can also be synthesized using this system by

applying biased target ion beam sputtering and ion beam deposition simultaneously. Metal or non-metal clusters, ions or atoms are produced by the biased target ion beam sputtering and doped into the DLC structure which is produced simultaneously by the ion beam deposition source (end Hall ion source I). This technique was used to synthesize DLC-MoS_2 composite thin films which will be described in Chapter 7.

3.1.2 Annealing Furnaces

After the synthesis of pure DLC and DLC-MoS_2 thin films, thermal stability of the films were studied by thermal annealing in the furnaces with various environments of ambient air and low pressure for 2 h. The annealing temperatures ranged from 100 to 600 ºC at an interval of 100 ºC. The heating rate was set at a constant value of 20 ºC/min, and the samples were heated from room temperature to the desired annealing temperature. After heating for 2 h at the set temperature, the samples were cooled down to the room temperature in the furnace. Thermal annealing was performed with a Thermo Scientific Lindberg/Blue M Moldatherm Box Furnace in ambient air atmosphere. This furnace includes unique insulation and heating element composites to minimize outer surface temperatures while maintaining uniform heat distribution within the chamber. Heat treatment in a low pressure atmosphere was performed with a conventional tube furnace (CTF). In the tube furnace the samples are placed in a quartz tube, which can be vacuumed. The tube furnace has three heating zones to obtain homogeneous temperature distribution. Before the annealing, the quartz chamber was pumped down to low pressure (at a pressure of about 10^{-2} Torr). Figure 3.3 shows pictures of the annealing furnaces, (a) Thermo Scientific Lindberg/Blue M Moldatherm Box Furnace and (b) conventional tube furnace.

(a)

(b)

Figure 3.3. Pictures of annealing furnaces, (a) Thermo Scientific Lindberg/Blue M Moldatherm Box Furnace, (b) conventional tube furnace.

3.2 Characterization Methods

3.2.1 Atomic Force Microscopy

Scanning tunneling microscopy (STM) and atomic force microscopy (AFM) are the two types of scanning probe microscopy (SPM) in which a tiny probe scans from side to side of the samples to achieve the surface information. AFM was designed to overcome some disadvantages of STM, which requires ultra-high vacuum and conductive surfaces. AFM can operate under ambient environment or even a liquid environment and can image nearly any kind of surfaces, such as ceramics and polymers. Typically, height resolution below 0.1 nm and lateral resolution less than 1 nm can be achieved with AFM. AFM is a powerful method to monitor and precisely evaluate the surface morphology of thin films with ultra smooth surfaces (Lifshitz, 1999).

AFM includes a cantilever with a sharp tip located at the end of it which is employed to probe the surface of a material. The cantilever and tip are made from Si_3N_4 or Si. Typically, radius of tip is between a few to tens of nm. When the tip comes near to the surface of the sample, the cantilever deflects because of the forces between the sample and the tip. Contingent upon the conditions, the forces might be van der Waals forces, capillary forces, mechanical contact force, electrostatic forces, magnetic forces, or chemical bonding. The cantilever deflection induced by the forces can be measured with Hook's Law. The tip does not operate at a fixed height because of the risk of damage induced by crashes between the surface of the specimen and the tip. In most AFMs, a vertical piezoelectric probe is used to arrange the distance between the surface of the specimen and the tip on the basis of a feedback mechanism to keep the force fixed. The cantilever deflection induced by the vertical piezoelectric probe is measured using a laser spot reflected from the cantilever top surface into an array of photodiodes. When the tip moves across the surface of the specimen, the cantilever deflection induced by the force,

and the cantilever deflection induced by the vertical piezoelectric probe are monitored to illustrate the topography of the specimen.

Various AFM modes of operation have been designed for different applications. The main operation modes are dynamic mode and static mode. The dynamic mode includes tapping mode (or intermittent contact mode) and non-contact mode. The non-contact mode operates well to evaluate soft specimens and rigid specimens containing a few monolayers of adsorbed fluid on the surface. The tapping mode (intermittent contact mode) creates higher lateral resolution and it is widely employed for biological specimens and thin films. The static mode is known as contact mode where the AFM probe scans at a fixed force from a distance extremely close to the surface of the sample. Contact mode is usually employed for rigid surfaces.

In this study, the AFM images were taken from an Agilent 4500AFM (Agilent Technologies, Chandler, AZ, USA) operating in the tapping mode (intermittent contact mode), located in the Saskatchewan Structural Science Centre (SSSC), University of Saskatchewan. The surface roughness was calculated using WSxM software based on five measurements at different locations of the thin films. A silicon cantilever (Nanoscience Instruments Inc., Tempe, AZ) with a curvature radius of approximately 10 nm, a resonant frequency of approximately 60 kHz, and a force constant of 3 N/m were employed for AFM measurements. All the AFM measurements were done at a set-point ratio of about 0.8 - 0.9 from the free-amplitude of the cantilever and they were all conducted in a vibration isolation system with the scan rate of 0.5 - 1.0 Hz (512 pixels per line). A picture of this AFM instrument is shown in Figure 3.4.

Figure 3.4. Picture of Agilent 4500AFM.

3.2.2 Raman Spectroscopy

When a molecule scatters light, majority of photons will be scattered elastically and have the energy equal to the energy of incident photons. But, a tiny part of light (around 1 in 10^7 photons) will be scattered inelastically and have an energy value which is not equal to the energy of incident photons. The process causing this inelastic scattering is known as Raman effect. The energy difference between the Raman scattered photon and the incident photon is equal to the scattering molecule vibration energy. Raman spectrum is a plot of scattered light intensity versus the energy difference. Raman spectroscopy is widely employed to investigate rotational, vibrational and other low frequency modes in condensed materials and to identify the materials bonding type. It contains illuminating the surface of the sample with a monochromatic light and studying the light scattered by the sample with a spectrometer. The spectra of two molecules are not the same if these molecules have different isotopic distributions, constitutions, or conformations. The spectra present specific bands of distinctive vibrations. Raman spectra, like fingerprints, can be used to identify matters.

Raman spectroscopy is a powerful technique for distinguishing and analyzing different C-C bonds in diamond, graphite, carbon nanotubes, fullerenes, amorphous carbon and DLC. Due to the fact that Raman spectroscopy is extremely sensitive to recognize sp^3 and sp^2 bonds of carbon, it has been employed as a routine method, to detect different carbon materials. For different carbon materials, Raman spectra present various typical peaks. Figure 3.5 provides typical Raman spectra of different carbon materials which are captured by applying a 514.5 nm laser radiation. Natural diamond shows two typical peaks at 1332 cm^{-1} and 2750 cm^{-1} in its Raman spectrum. Large single crystal graphite shows one sharp peak at 1580 cm^{-1} in its Raman spectrum which is tagged with G in favor of graphite. Regarding disordered graphite or graphite with small crystallite size, the sharp graphite G peak turns into a broad G band and a second peak comes into view at 1350 cm^{-1} in its Raman spectrum which is tagged with D in favor of disorder. Amorphous carbon illustrates a broad non-symmetrical hump from 1000 to 1600 cm^{-1} in its Raman spectrum. DLC thin films exhibit very broad G and D peaks in their Raman spectra, in contrast with the extremely sharp Raman peaks of single crystal graphite and diamond (Robertson, 2002).

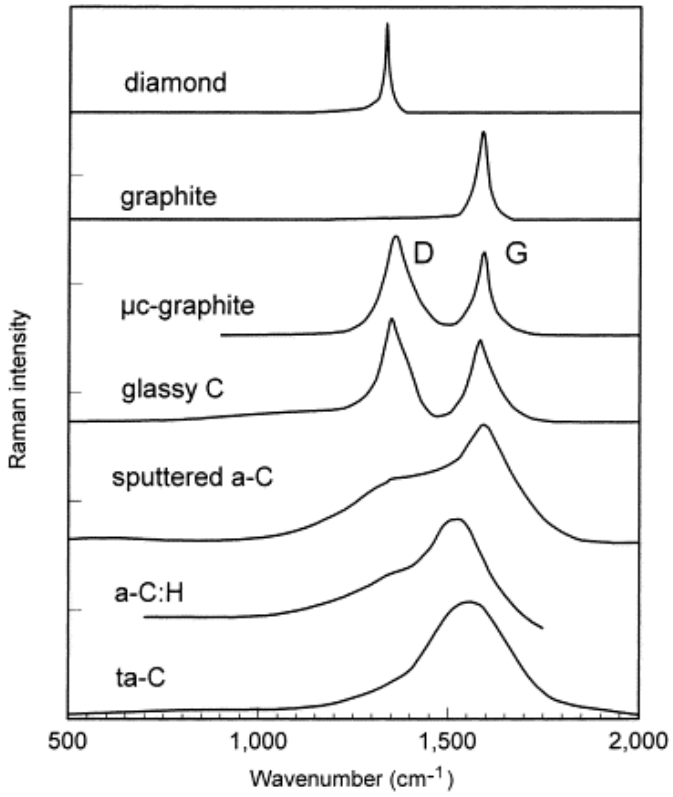

Figure 3.5. Typical Raman spectra of carbons (Robertson, 2002).

In this work, Raman spectra of thin films were achieved using a Renishaw 2000 micro-Raman system operated at an argon laser wavelength of 514.5 nm and an 1800 line/mm grating (located at the SSSC, University of Saskatchewan). The spot size was approximately 2 μm. A picture of this Raman spectroscope instrument is presented in Figure 3.6.

Figure 3.6. A picture of Renishaw 2000 micro-Raman system.

3.2.3 X-ray Photoelectron Spectroscopy

X-ray Photoelectron Spectroscopy (XPS), also known as electron spectroscopy for chemical analysis (ESCA), is a quantitative electron spectroscopic method to get information about elemental composition, electronic state and chemical state of the elements. This method is on the basis of photoelectric effect. When the surface of a substance is exposed to the radiation of soft X-ray photons, the inner shell electrons of the target atoms are emitted and escape out of the surface after the absorption of the photons. An electron energy analyzer detects the emitted photoelectrons, and simultaneously measures their kinetic energies and numbers. Based on Einstein's law, the absorbed photon energy is more than the kinetic energy of the emitted free photoelectron and their energy difference is considered as the electron binding energy which is distinctive for each element. Therefore, the kinetic energy values of the emitted photoelectron can reveal the elements in the substance. Each element’s fraction is proportional to peak areas, which can be employed to obtain quantitative composition information.

XPS can be employed to detect all elements except helium and hydrogen since normal X-ray photon energies are too far from resonance of their ionization potentials, which leads to very low ionization probability and causes outgoing signals go below sensitivity thresholds of regular XPS systems. Limit of detection of XPS for majority of the elements is in the order of parts per thousand and it might reach to the order of parts per million (ppm) depend on particular circumstances of concentration at top surface. XPS measurements need extremely high vacuum and may degrade samples, specifically organic chemicals, which can be degraded by the heat generated from the incident X-rays. Also, XPS can be done with synchrotron radiation sources, which provides bright and wavelength tunable X-ray beams.

Furthermore, XPS reveals each element's chemical bonding state by the shifting of core level binding energy. For example, C 1s has a core level shift of approximately 0.9 eV between graphite and diamond because of the different bond length of sp^3 and sp^2 carbon (Robertson, 2002). XPS is a surface sensitive method since only the photoelectrons from the top 2-20 atomic layers can escape and be detected (Tang, 2010).

Typically there are four stages to analyze and interpret a XPS spectrum. The first stage is to identify spectral lines and connect them with special energy levels of analogous elements. The second stage is to calculate photoemission intensities by removing the inelastic scattering background. It is essential to remove this background as the photoelectrons released at different subsurface depths endure severe inelastic scattering before leaking out from the surface of a substance. The third stage is XPS peak intensities correction by considering sensitivity factors which are related to the instrument and can be obtained from standard calibration. Finally, the atomic concentration can be calculated by assuming that the XPS peak intensities are proportional to the number of atoms in the tested volume.

In this investigation, the element bonding states and composition of amorphous carbon films were examined by XPS. XPS measurements were done on a Kratos Axis 165 spectrometer (located in the Alberta Centre for Surface Engineering and Science, University of Alberta) with a monochromatic Al Kα X-ray source and a base pressure of 10^{-6}-10^{-7} Pa in the analytical chamber. The instrument resolution was 0.4-0.5 eV.

3.2.4 Synchrotron Based Near Edge X-ray Absorption Fine Structure Spectroscopy

When charged particles are accelerated, they generate electromagnetic radiation. Within synchrotron radiation, the charged particles move at a velocity close to the light speed in a storage ring, emitting radiation over the whole electromagnetic spectrum. Synchrotron radiations

have high brightness (several orders of magnitude higher than regular X-ray sources). Also, synchrotron radiation has high flux/intensity, high collimation, polarization, and high stability. Furthermore, synchrotron can generate a smooth energy spectrum accompanied by high energy resolution.

When a monochromatic X-ray beam created by synchrotron is projected on a substance, intensity of the beam is reduced because of the interaction with atoms in the substance. An X-ray beam with suitable energy range may excite core electrons to emit Auger electrons, fluorescence photons and photoelectrons. By tuning the X-ray beam photon energy to an appropriate absorption edge with a monochromator and gathering the data of fluorescence/electron emission, X-ray absorption spectroscopy (XAS) can be obtained. XAS is applied to investigate the local unoccupied electronic density of states in atoms. The ‘name’ of the absorption edge in XAS measurements is related to the core electron which is excited, for instance, the principal quantum numbers (n) of 1, 2 and 3 correspond to K-, L- and M-edges, respectively.

The X-ray absorption spectra exhibit an extreme increase at the absorption edge and afterwards gradually decrease in intensity with the X-ray energy. The area before the absorption edge to the beginning of the extended X-ray absorption fine structure (EXAFS) region (about 50eV above the absorption edge) is known as near edge X-ray absorption fine structure (NEXAFS or XANES). NEXAFS is specific for each element because different elements have different X-ray absorption threshold energies. Also, NEXAFS is very sensitive to the chemical state, including the oxidation state and the absorbing atom local geometry. So, NEXAFS, like fingerprints, can be employed to identify the availability of a specific chemical species. Synchrotron-based NEXAFS has been used extensively to investigate the bonding state and electronic structure of different elements in thin films.

In this study, the NEXAFS spectra of the DLC-MoS_2 thin films were conducted at the Soft X-ray Microanalysis Beamline (SXRMB) of the Canadian Light Source (CLS; Saskatoon, SK, Canada) to characterize the electronic state and the oxidation state of the films. Considering the fact that fluorescence yield (FLY) is a bulk sensitive mode and the structure of the surface and thin films was studied in this research, the spectra were recorded in total electron yield (TEY), a surface sensitive mode, by monitoring the sample current. The photon resolution of the NEXAFS measurements was less than 0.1 eV.

3.2.5 X-ray Diffraction

X-ray diffraction (XRD) is an important non-destructive method which discloses detailed information about the crystallographic structure of bulk materials and thin films. Elastic scattering from long range order structure is the basis of XRD. The spacing between crystalline planes of crystalline materials is in the similar order of the X-ray wavelength, so diffractions could happen when a monochromatic X-ray beam is incident on a crystalline substance. Bragg's Law describes the interference of X-rays scattered by crystals. Incident waves of an X-ray beam with the wavelength of λ is scattered by a crystal. The path difference between the waves reflected by two adjacent lattice planes can be formulated as $2d\sin\theta$, in which θ is the angle between the planes and the incident beam, and d is the spacing between the lattice planes. Constructive interferences happen when the path difference is an integer multiple of the incident wavelength, $2d\sin\theta=n\lambda$, and result in diffraction peaks. Each crystalline substance has a specific crystal lattice; therefore it diffracts X-rays in a characteristic pattern. X-ray scattering occurs from both crystalline and non-crystalline substances. Crystalline substances have long range order and the diffraction pattern from a crystalline substance has numerous sharp peaks matched with different crystal planes. Amorphous substances do not have long range order and the

diffraction pattern from an amorphous substance includes one or two peak with a very wide distribution in the 2θ range. The diffraction pattern from a substance including both crystalline and amorphous solids has a broad background due to the amorphous phase and sharp peaks due to the crystalline phase (He, 2009).

In this investigation, the XRD patterns of the DLC-MoS_2 thin films were recorded with a Bruker AXS D8 DISCOVER diffractometer using Cu Kα radiation (λ=1.54056 Å) at a voltage of 40 kV and a current of 30 mA over the 2θ range from 10 to 80°. Scanning steps were 0.02° (2θ) and the specimens were in as-deposited solid form. The detector and the sample were mounted on two separate rotating bases, when the sample rotated an angle θ; the detector rotated an angle 2θ. Afterwards, the data were analyzed using X'pert Highscore software and peaks were identified by comparing with standard database (JCPDS Card). Figure 3.7 illustrates a picture of this X-ray diffractometer instrument.

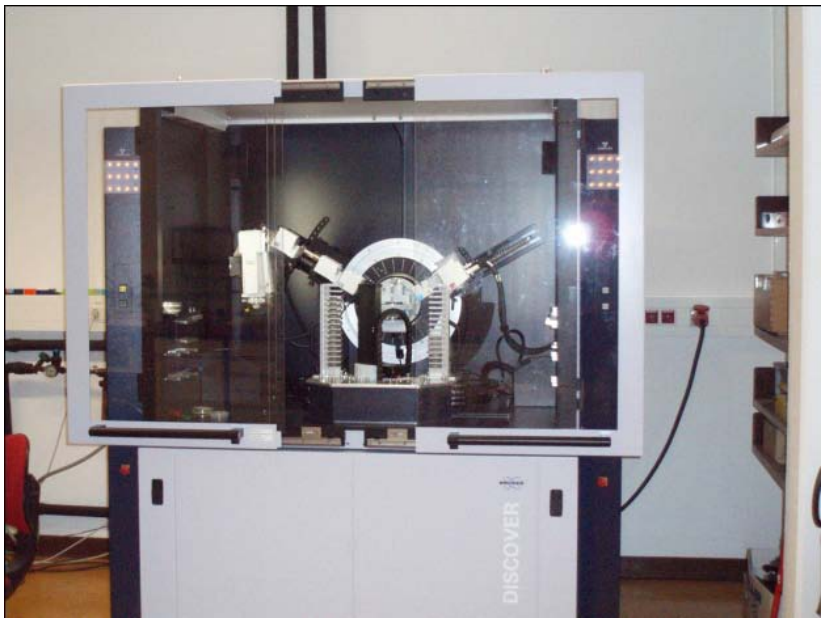

Figure 3.7. A picture of Bruker AXS D8 DISCOVER diffractometer.

3.2.6 Scanning Electron Microscopy

One of the most multi-purpose methods to analyze the surface morphology, texture and chemical composition of substances is scanning electron microscopy (SEM). SEM uses electron beams as a source of radiation and magnetic coils to concentrate the beam of electrons on the surface of specimens. The large depth of focus comparing to other kinds of microscopy is one of the main characteristics of SEM, which allows to image extremely rough surfaces. SEM is a non-destructive analysis method since the interactions between electron and material do not cause volume loss of the sample. A large spectrum of magnifications can be obtained in SEM, from around 10 times to higher than 500,000 times. SEM is able to create high resolution images, revealing details about a few nanometers in size. The backscattered electrons (BSE) mode of SEM displays the atomic number contrast of the sample and reveals information about the elemental mapping of the samples; While, secondary electrons (SE) detector is usually employed to study the surface topography of the samples.

In this investigation, a Hitachi SU6600 field emission SEM equipped with an Oxford Instrument EDS attachment (located in Room#3C95, Engineering Building, University of Saskatchewan) was used to characterize the surface morphology and to analyze the chemical composition of the specimens. The SEM operating voltage was 10 kV in both SEM and EDS works and as-produced specimens were examined. The specimens were mounted onto an aluminum stub using double sided carbon conducting tapes. Figure 3.8 presents a picture of this SEM instrument.

Figure 3.8. Picture of Hitachi SU6600 SEM.

3.2.7 Nanoindentation

Nanoindentation is the main practical technique to measure the mechanical properties of coatings and thin films. In this technique, usually a diamond nanoindenter is pressed into and afterwards unloaded from the film with small loads down to milli-Newtons or even micro-Newtons, and finally the loads and penetration depths or displacements are monitored precisely. The monitored data can be employed to measure hardness, elastic modulus, fracture toughness and yield strength of a thin film or surface layer according to various calculation methods. The main constituent of nanoindentation is nanoindenter. Different types of nanoindenters with various tip geometries have been used for nanoindentation testing including Berkovich nanoindenters. The thin film hardness measurements by nanoindentation method can be influenced by various factors such as surface roughness of the film and substrate. The absolute value of the hardness for a thin film might change based on the calculation technique; therefore it is essential to mention the calculation technique when illustrating the value of hardness.

Currently, software is employed as the best technique to assemble the measurement data and analyze curves of load versus displacement in order to calculate the elastic modulus and hardness.

In this study, a nanohead made by Center for Tribology Inc. (CETR), as presented in Figure 3.9, was employed to perform nanoindentation testing to measure the elastic modulus and hardness of the synthesized films. The 100 nm Berkovich-type diamond indenter tip employed for the nanoindentation testing was normal to the surface of the films and moved into the surfaces by applying an increasing load up to a preset value equal to 2 mN. After 10 second of holding, the load was gradually reduced until the films were relaxed. The speed of loading and unloading was 0.5 mN/min. The load and displacement were monitored continuously during the whole of process (Figure 3.10) and employed to calculate the Young's modulus and hardness of the film by an built-in software using the Oliver and Pharr technique (Oliver *et al.*, 2004). Multiple indents (9 indents) on a particular area of the film were achieved automatically with a longitudinal and lateral resolution equal to 50 μm, and the average values are reported. Also, in order to evaluate the adherence between the film and the substrate, a constant load in the value of 20 mN was applied on the surface. After unloading if no delamination or pilling off occurs on a film, the adherence is considered good.

Figure 3.9. Picture of Universal Material Tester designed and made by CETR.

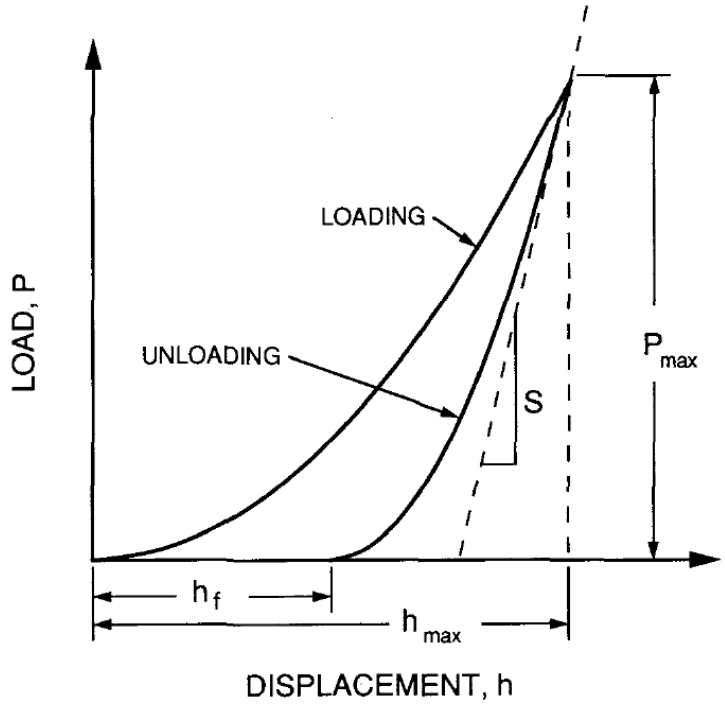

Figure 3.10. Schematic of load-displacement curve for an instrumented nanoindentation test (Oliver *et al.*, 2004).

3.2.8 Friction and Wear Test

Tribometers or friction testers with various configurations and special simulated contact conditions, like ball-on-disc, ball-on-flat, pin-on-disc and flat-on-flat, have been employed to evaluate thin films frictional behavior. For the application of tribometers, mathematical models have been established to calculate the coefficient of friction on the basis of Coulomb approximation, supposing that the surfaces are in atomically close contact over the contact area and the friction force is proportional to the normal force. However, the actual contact occurs only at the tips of surface asperities, and usually the actual contact area is only an extremely tiny portion of the apparent area. The Coulomb approximation is only a useful principle to simplify and evaluate the result of a complex physical interaction. Figure 3.11 presents a schematic figure of ball-on-disc sliding test. The non-moving sample of the substance pair is mounted on a specimen stage, and the flexible one is mounted on a mobile head. At the time of applying a specific load, the sliding is started; and a strain-gage transducer is employed to evaluate the frictional force. Under some conditions, piezoelectric force transducers are employed for evaluation of dynamic frictional forces.

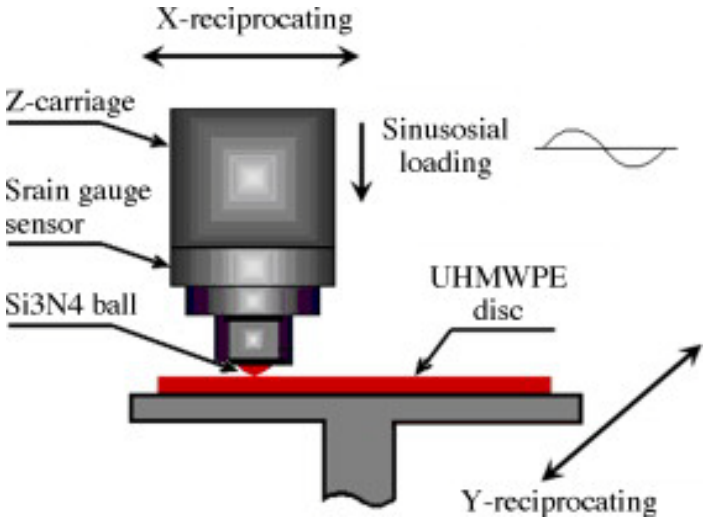

Figure 3.11. A schematic figure of ball-on-disc sliding test (Ge *et al.*, 2008).

In this investigation, The Universal Mechanical Tester (UMT) manufactured by Center for Tribology Inc. was employed to do ball-on-disk testing to examine the tribological characteristics of the synthesized thin films (Figure 3.12). The tests were performed with a AISI 440C steel ball (4 mm diameter) as the counterpart material in reciprocating mode. They were done with a normal load of 5.0 N and a linear sliding speed of 0.5 mm/s for 1000 cycles under dry lubrication in ambient atmosphere (22 °C and a relative humidity of 40%). The sliding distance was 10 mm and the coefficient of friction (COF) of the films was measured. The coefficient of friction of the films reported in this investigation is the average value during the steady state. The wear coefficient (specific wear rate coefficient) of the films was evaluated as worn volume per sliding distance per load.

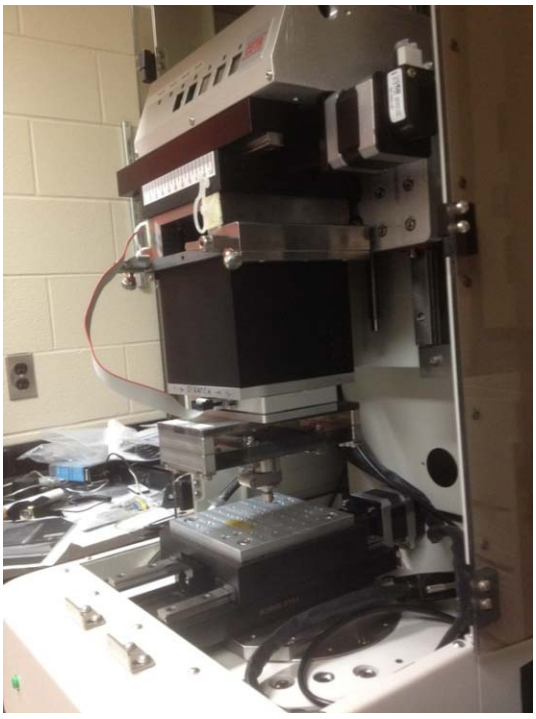

Figure 3.12. UMT during the ball-on-disk testing.

3.2.9 Corrosion Test

Potentiodynamic polarization measurements were conducted to evaluate the corrosion resistance of pure DLC and DLC-MoS_2 coatings, synthesized with different processing parameters, using a Gamry Series G^{TM}750 potentiostat. Potentiodynamic polarization test was done in a solution of 3.5wt% NaCl in distilled water at room temperature. For this experiment, an electrochemical cell of the three-electrode type was used. The specimen was the working electrode, the counter electrode was a pure graphite sheet and the reference was the saturated calomel electrode (SCE). A picture of the electrochemical cell and the potentiostat is presented in Figure 3.13. Working and counter electrodes are designed to be clamped in the end plates (Figure 3.14). A reference electrode in the included bridge tube should go through the top port on the same end plate as the working electrode. The working electrode was in the shape of a plate and the coatings were still attached to the substrate at the time of testing. Subsequent to connecting the electrodes, the platinum wire and the specimen were exposed to the solution for 6 h to stabilize the specimen potential. Afterwards, the Tafel test script was chosen from the potentiostat software menu. The corrosion test started with the electrode stabilization in the electrolyte (3.5% NaCl solution), during which the open circuit potential (OCP) was monitored and recorded. Finally, a potentiodynamic polarization test was carried out starting from 250 mV below the OCP in the cathodic zone, to a potential of 250 mV above the OCP to determine corrosion potential (E_{corr}) and current (I_{corr}). The sampling period for each scan was 1 second.The potential scan rate was 1mV/s (Pauleau *et al.*, 1997). The working electrode exposed area was 0.25 cm^2. In order to calculate the corrosion potential and current by means of Tafel extrapolation method, Gamry Echem Analyst software was employed. Five specimens of each coating were tested to ensure reproducibility of the results.

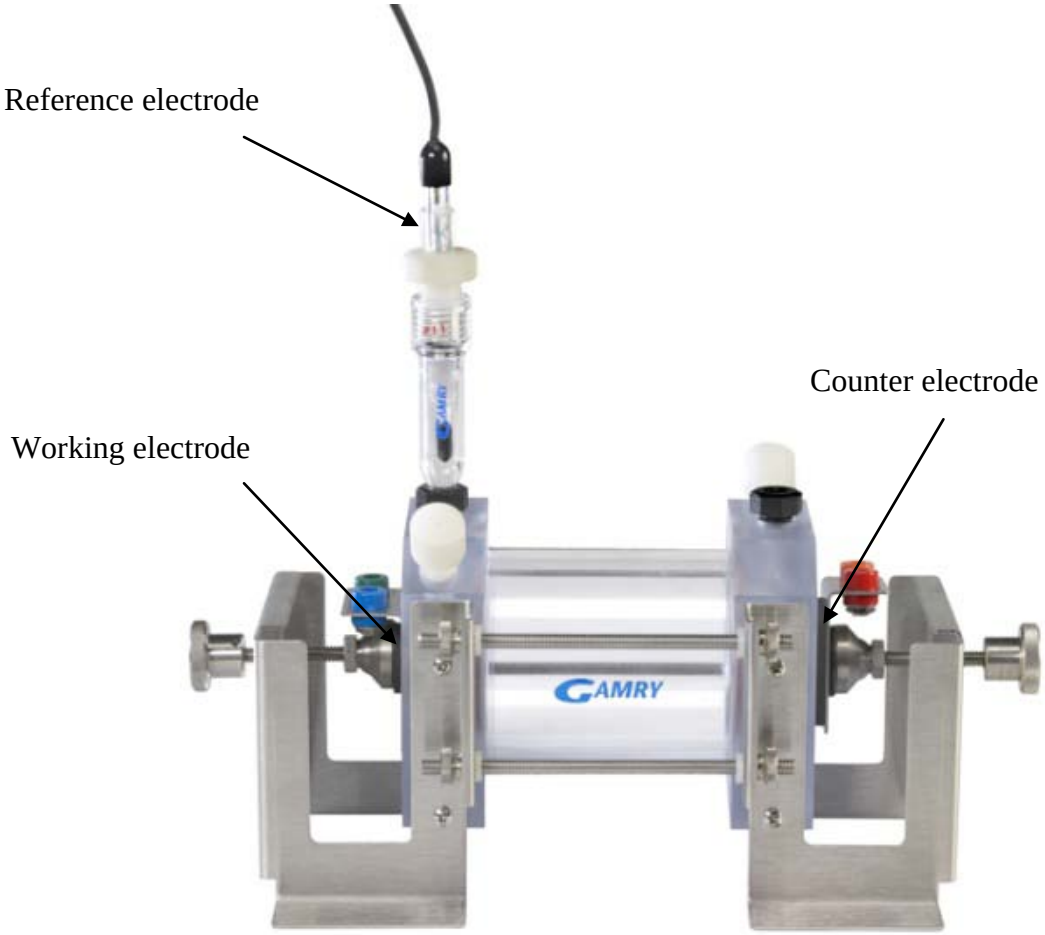

(a)

(b)

Figure 3.13. Picture of (a) electrochemical cell and (b) Gamry Series G^{TM}750 potentiostat.

Figure 3.14. Position of working electrode in electrochemical cell.

CHAPTER 4 STRUCTURE AND PROPERTIES OF HYDROGEN-FREE DIAMOND-LIKE CARBON THIN FILMS SYNTHESIZED BY BIASED TARGET ION BEAM DEPOSITION

Transition

In this chapter, production of hydrogen-free DLC thin films by BTIBD technique is studied. The effect of target bias voltage, as a processing parameter, on the structure and properties of the films will also be investigated to get optimum mechanical, tribological and corrosion properties by this technique. This chapter has been published in "*Surface and Coatings Technology*" as follows: "Niakan H., Q. Yang, J.A. Szpunar. 2013. Structure and properties of diamond-like carbon thin films synthesized by biased target ion beam deposition. Surface and Coatings Technology 223: 11-16".The PhD candidate designed and conducted the experiments, analyzed the results of the experiments and prepared the manuscript for publication under the supervision of Profs. Qiaoqin Yang and Jerzy Szpunar. The manuscript has been reformatted from the original version for inclusion in the thesis and the text has been slightly modified to ensure clarity and avoid repetition.

4.1 Introduction

Sputtering is the most common industrial technique for the synthesis of DLC because of its high deposition rate, good uniformity of the deposits, reproducibility of properties, good film adhesion and possibility of the deposition onto large surface areas (Cuomo *et al.*, 1991). Sputtering techniques mainly include ion beam sputtering (IBS) and magnetron sputtering. Ion beam sputtering technique has some disadvantages. The minimum energy that can be achieved in commercially available grid ion beam gun is approximately 50 eV, while is significantly greater than the ideal energy wanted for many applications. Also, the initial sputtering ions must impact the target at an oblique incident angle that may cause high energy and flux of reflected neutrals.

Furthermore, despite the fact that IBS systems are designed to direct all the ions onto the target, a fraction of the ion beam may miss the target. These high-energy ions may sputter off unwanted materials from the vacuum system hardware, causing the growth film overspill contamination. Finally, in ion beam sputtering it is difficult to implement low adatom energy that is needed for the interface deposition. This is due to the fact that at low beam voltages, it is more difficult to focus the sputtering ion beam, causing larger overspill contamination. In addition, deposition rates in IBS systems are lower relative to other sputtering methods (normally 0.1 to 2 Å/sec) (Hylton *et al.*, 2000). Magnetron sputtering has drawbacks of large system size, operation at much higher pressures, and significant adatom flux scattering by the background gas before reaching the substrate (Chen *et al.*, 2009).

In order to overcome the disadvantages of those conventional sputtering methods, another technique called biased target ion beam deposition (BTIBD) was developed (Zhurin *et al.*, 2000), which combines the advantages and avoids the disadvantages of both conventional sputtering methods. The BTIBD technique employs an end-Hall ion source combined with a hollow cathode electron source instead of a gridded ion source. The end-Hall ion source can produce ions with both high density and low energy (down to several eV). By applying a negative bias to the sputtering target, the ions accelerated by the negative bias can achieve high energy and hit the target at a near-normal incidence which decreases both the energy and flux of reflected neutrals. In this case, only the biased target materials are sputtered off for synthesis. Depending on the bias voltage applied, the impact energy of the ions on the target can be simply controlled in the range of 100 eV to 1500 eV, which is appropriate for sputtering. In the BTIBD system, the maximum energy of the ions from the end-hall ion source is approximately 25 eV, below the sputter threshold of the vacuum system materials, thus no undesired sputtering occurs.

Consequently, the ion beam can be much broader than the target for enhancing illumination uniformity. In particular, the illumination profile and the ion current reaching the target are independent of the target voltage since the plasma sheath formed at the surface of the target for acceleration of ions is narrow (~ 2 mm). Furthermore, the ion sources can operate over a wide range of pressures (10^{-4} to 5×10^{-3} Torr), enabling the control of adatom scattering from the background gas (Hylton *et al.*, 2000). Because of a large scope of process pressures, control of adatom energies, and exceptional uniformity of deposits, BTIBD is well suited for the applications demanding atomically high precision engineered interfaces and thin films. The films deposited by this technique are very smooth with very small amount of contaminations (Tang *et al.*, 2011a). High performance multilayer devices such as optical interference filters, giant magnetoresistive multilayers, and gate dielectric stacks have been made using BTIBD (Quan *et al.*, 2007). BTIBD has been used to prepare some thin films with high purity, low roughness, and high uniformity by Tang *et al* (2011a) and Bharathy *et al* (2010a). However, up to now, there is no literature reporting on the synthesis of hydrogen-free DLC films by BTIBD.

In the present investigation, the synthesis of hydrogen-free DLC thin films using BTIBD method is reported. It is very interesting to find that hydrogen-free DLC thin films with exceptionally high smoothness and low friction coefficient can be synthesized by biased target sputtering of graphite target without additional ion bombardment either by negative bias of substrate or assisting ion source, while additional ion bombardment is essential to obtain DLC by other sputtering methods. The effect of target bias voltage as a key processing parameter, ranging from -200 to -1000 V, on the structure and properties of the films was further investigated. This would help to determine the processing-structure-property relationships in the hydrogen-free DLC thin films.

4.2 Experimental

4.2.1 Synthesis of Hydrogen-Free DLC Thin Films by BTIBD Technique

Ti–6Al–4V alloy and mirror polished p-type Si (100) wafers were used as substrates for this investigation. Specimens of size 10×10×1 mm were prepared from Ti–6Al–4V plates in mill annealed condition. All Ti alloy specimens were prepared by polishing (10×10 mm face) with four grades of silicon carbide emery papers (grit 240, 320, 400 and 600) followed by diamond pastes (6, 3 and 1 μm) and then washed with deionized water. The substrates (Ti alloy and Si wafer) were cleaned in an ultrasonic bath for 10 min, first with acetone and then with methanol, and fully dried before being put into the vacuum chamber for the film deposition. The deposition experiments were carried out using a 4Wave Inc BTIBD system (see section 3.1.1). A schematic diagram of the DLC synthesis using BTIBD technique is shown in Figure 4.1. The system was pumped down to a base pressure of 5×10^{-7} Torr. Prior to the deposition, the surface of substrates was cleaned and etched to remove surface residual contaminants and surface oxides by introducing Ar gas into the assisting end-Hall ion source using the parameters listed in Table 4.1. These pre-treatments also helped to improve the adhesion of the coatings to the substrates. Then carbon thin film deposition on the substrate was carried out by sputtering a graphite target of 99.99% purity for 3 hours using the parameters listed in Table 4.2. The target bias voltage was varied between -200 and -1000 V to study the effects of processing conditions on the structure and properties of the films.

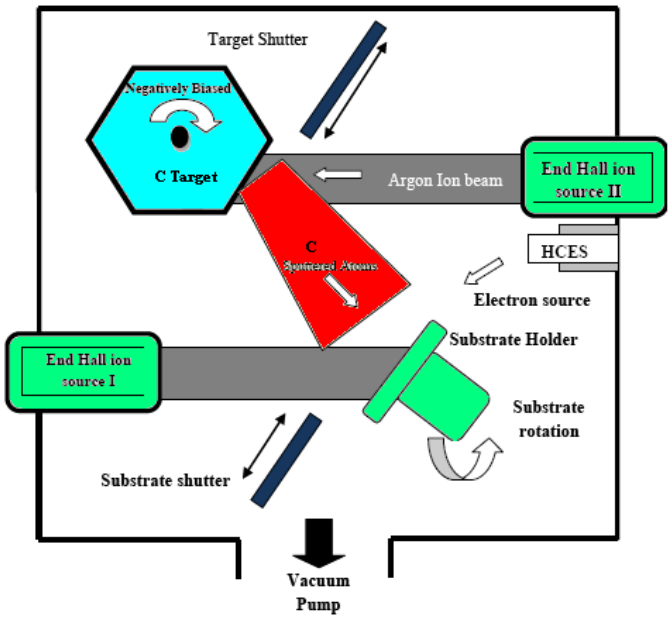

Figure 4.1. A schematic diagram of the DLC synthesis using BTIBD technique.

Table 4.1. Substrate cleaning conditions before film deposition.

Ar flow rate (sccm)	5
Mean ion energy (eV)	50
Ion current (A)	2
Time (min)	10

Table 4.2. Deposition conditions for hydrogen-free DLC thin films.

Target Bias Voltage (-V)	200-1000
Discharge current (A)	4
Time (hr)	3
Substrate temperature (°C)	<50
Working pressure (Torr)	1×10^{-4}

4.2.2 Characterization of Hydrogen-Free DLC Thin Films

After the film deposition, the samples were analyzed using a scanning electron microscope (SEM), an atomic force microscopy (AFM), a Raman spectroscopy, and an X-ray photoelectron spectroscopy (XPS). The surface morphology was analyzed using a Hitachi SU-6600 field emission SEM (see section 3.2.6). The AFM data were taken on an area of 500 nm×500 nm and the surface roughness was calculated as described in section 3.2.1. Raman spectra were obtained using a micro-Raman system which explained in section 3.2.2. XPS measurements were done on a Kratos Axis 165 spectrometer as mentioned in section 3.2.3. XPSPEAK software was employed to normalize raw data, subtract background and deconvolute the extracted spectra with a combination of Gaussian-Lorentzian (G-L) line profile. Mechanical properties (hardness and Young's modulus) of the films were measured by nanoindentation technique which discussed in section 3.2.7. The tribological characteristics of the films were obtained using a ball-on-disc tribometer as explained in section 3.2.8. Potentiodynamic polarization measurements were conducted to evaluate the corrosion resistance of the films as described in section 3.2.9.

4.3 Results and Discussion

4.3.1 Surface Morphology and Roughness

All the deposited films were continuous and uniform with a thickness of approximately 300 nm as measured by profilometry. Figure 4.2 shows the cross-sectional SEM micrograph of DLC film on Ti-6Al-4V alloy deposited at -800 V target bias voltage. It can be seen that the DLC thin film is well adhered to the substrate. AFM was further used to observe the topography and to evaluate the surface roughness of the samples. A typical AFM image of the film synthesized at target bias voltage of -800 V is shown in Figure 4.3. The root-mean squared

(RMS) roughness of the samples versus the absolute value of target bias voltage is described in Figure 4.4. It can be seen that the RMS roughness decreases gradually with increasing the absolute value of target bias voltage up to 800 V, and then raises when the absolute value of target bias voltage increases. When the negative target bias increases, the average incident energy of inert gas ions used for sputtering increases, consequently the average kinetic energy of carbon atoms sputtered from the target increases, which affects the films properties (Quan *et al.*, 2007). According to Gilmer *et al.* (1998), higher energetic particle bombardment could increase the carbon atoms mobility on the surface of growing film, and as a result decreases the magnitude of voids in the film, increases the film density and makes the film smooth. However, when the bombardment energy is too high, the surface of the film can be damaged, resulting in the increase of roughness. Peng *et al.* (2001) believe that gradual transition from a rough surface with many sp^2-rich clusters at low ion beam energies to an atomically smooth surface at higher energies happens. They indicated that there is a competition between this influence and a trend for such high energies resulting in substantial heating of the substrate and hence to promote roughening by diffusional cluster formation at the surface, causing the increase of roughness at too high energies. The RMS roughness of the coated samples was homogenous, i.e. there was not substantial difference between different micro-regions; and location on the substrate did not affect the roughness level of the coated samples. The RMS roughness of the starting Si wafer substrate is 0.15 nm which shows that DLC coated samples by BTIBD technique can produce films smother than Si substrate using optimized deposition parameters e.g. at -800 V target bias voltage. By comparing the results with carbon films prepared by other sputtering methods (Pandey *et al.*, 2004; Bai *et al.*, 2011), this BTIBD technique produces smoother a-C thin films. This is probably due to the high degree of mobility of the sputtered atoms provide the mobility to

promote the formation of smoother films. Since the pressure of the gas is 10^{-4} torr, all the sputtered atoms arrive at the substrate with virtually all their kinetic energy, before they have a chance to thermalize with the background gas. Comparing the results of BTIBD deposited films with that of the films deposited by ion beam sputtering (IBS) methods (Bai *et al.*, 2011), BTIBD deposited films have a higher deposition rate and smoother surface. The higher deposition rate is due to the higher ion current density of the end-hall ion source and the smoother surface is probably due to the fact that BTIBD technique deposition occurs at a near-normal adatom incident angle, while in IBS deposition happens at an oblique adatom incident angle and, therefore, higher values of surface roughness is observed in IBS deposited films (Zhurin *et al.*, 2000).

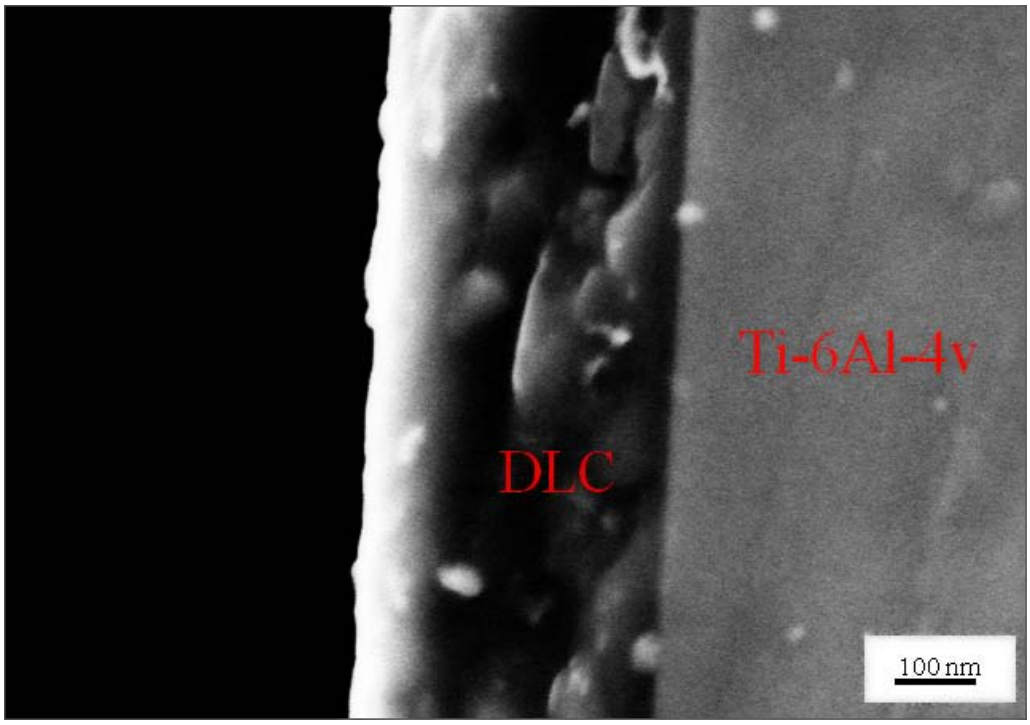

Figure 4.2. Cross-sectional SEM micrograph of DLC film on Ti-6Al-4V alloy synthesized at -800 V target bias voltage.

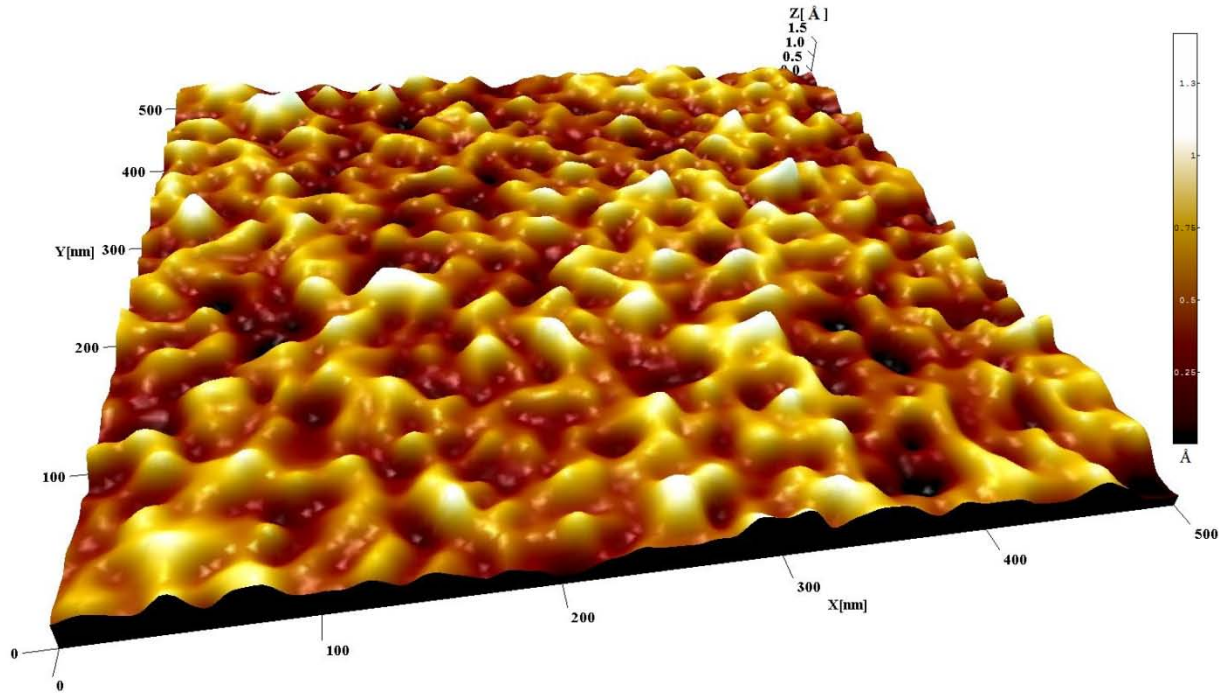

Figure 4.3. Typical topographic image (500 nm×500 nm) of the DLC film prepared at target bias voltage of -800 V (color scale of the sample height is in angstrom).

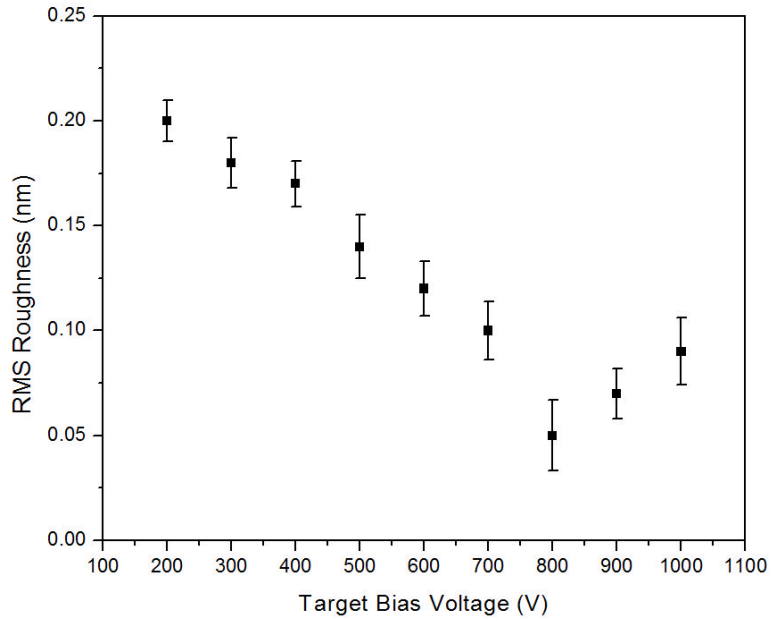

Figure 4.4. RMS roughness values of carbon films synthesized by BTIBD technique at various target bias voltages.

4.3.2 Bonding Structure

Raman spectroscopy is an effective method for distinguishing various C-C bonds in carbon materials (Abrasonis *et al.*, 2006). Raman spectrum with a broad single peak centered around 1500-1600 cm^{-1} (G-band which is tagged with G in favor of graphite) with a shoulder at around 1300-1400 cm^{-1} (D-band which is tagged with D in favor of disorder) is the signature of DLC films (Zhang *et al.*, 2000). The G peak is attributed to the bond stretching mode of all pairs of sp^2 sites, either in carbon rings or carbon chains. The D peak is attributed to the breathing modes of sp^2 sites in carbon rings (Ferrari *et al.*, 2004). Figure 4.5 illustrates Raman spectra of the carbon films deposited using different target bias voltages. For target bias voltages in the range of 400-1000 V, the signature of a typical DLC film can be observed in the spectra (D and G peaks); while for target bias voltages of -300 and -200 V, the spectra are more similar to those of graphite than DLC. After deconvolution and fitting of the Raman spectra (mixed Gaussian/Lorentzian) into the D and G peaks, the G peak position and the intensity ratio of the G and D peaks (I(D)/I(G)) were derived and the results are shown in Figure 4.6. It can be seen that G peak position shifts down and the I(D)/I(G) peak intensity ratio reduces with increasing the absolute value of sputtering target bias voltage from 200 V to 800 V. However, with a further raise in the absolute value of target bias voltage (from 800 to 1000 V), both G peak position and I(D)/I(G) show the same trend of increase. The reduction in I(D)/I(G) implies a decrease in the total number and/or size of disordered graphitic-like micro domains resulting in an enlargement in the sp^3 content of the carbon films. Also, the downward shift of G peak position implies an increase in the sp^3 content of the carbon films (Zhang *et al.*, 2000). Based on the correlation between sp^3 content of the carbon thin films and the G position or I(D)/I(G), proposed by Ferrari *et al.* (2004), the sp^3 content (% sp^3/ sp^3+ sp^2) of the carbon films was estimated. The estimated

sp^3 content of the films versus their target bias voltage based on I(D)/I(G) is plotted in Figure 4.7.

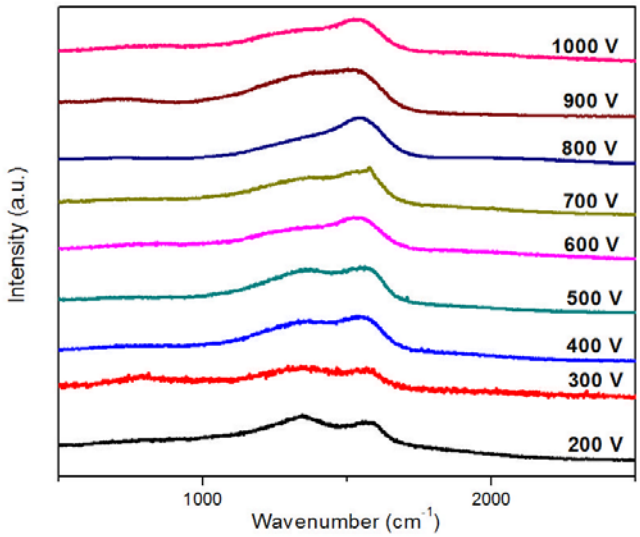

Figure 4.5. Raman spectra of carbon thin films with different target bias voltages.

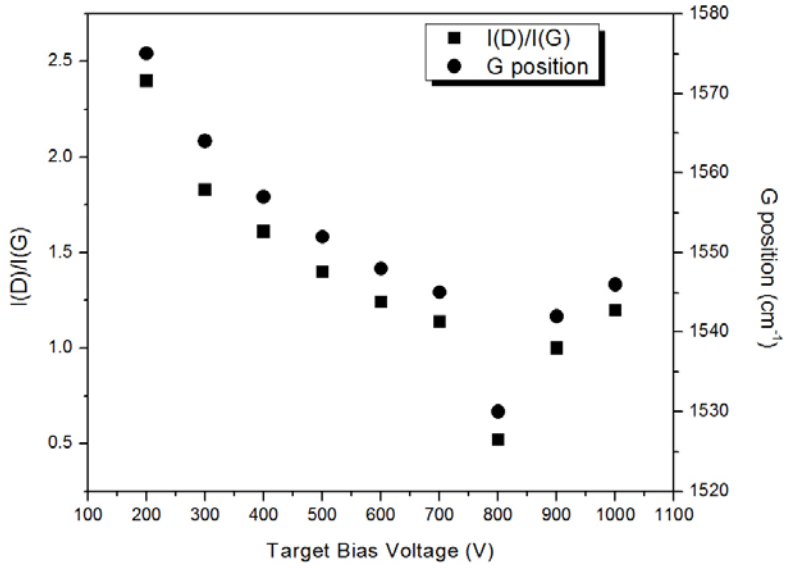

Figure 4.6. Raman G peak position and intensity ratio of the G and D peaks versus target bias voltage.

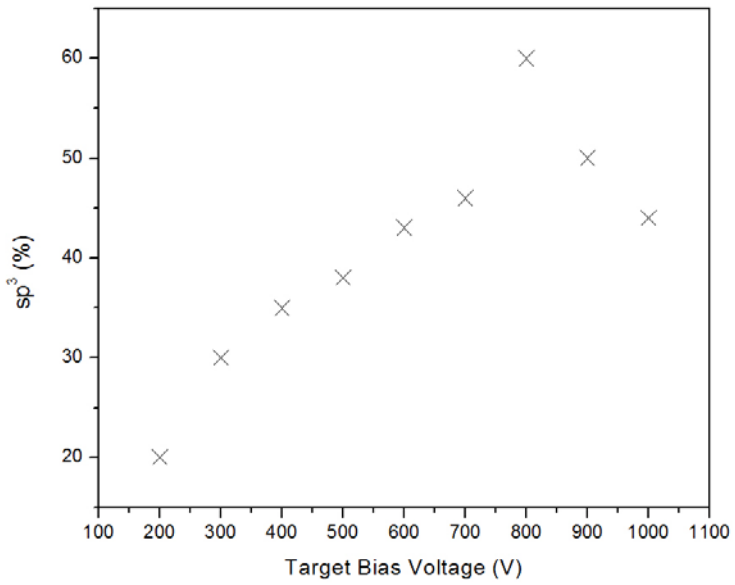

Figure 4.7. sp^3 percentage for as-deposited carbon films versus target bias voltage.

Typical XPS survey spectra of as deposited samples before and after Ar sputtering cleaning are illustrated in Figure 4.8. It shows that only carbon and oxygen are present in the surface of the samples. The strong C 1s peak reveals the carbon nature of the films. The presence of small amount of oxygen at the surface is probably a result of the physical absorption in the time of the air exposure because it can be significantly decreased by Ar plasma cleaning. C 1s core-level spectrum can be broken down into two constituents: sp^2 hybridization (graphite-type bonding), and sp^3 hybridization (diamond-type bonding). Since oxygen is present in the thin films, as illustrated by the survey spectrum, the contribution of C–O is included in the deconvolution analysis as well. At first based on a method used by Merel *et al.* (1998) and Tang *et al.* (2011b), a Shirley-type function was employed to eliminate the background which arises mainly due to inelastic electron scattering. Afterwards, the extracted spectra were fitted with a combination of Gaussian-Lorentzian (G-L) line profile. Figure 4.9 presents a typical

deconvoluted spectrum which is for the sample deposited at target bias voltage of -200 V. Similar deconvolution analysis was conducted on the spectra of the other samples. The relative fraction of sp^3 bonding was then estimated from the area ratio of sp^3 peak over the area of total C 1s peak. The binding energy and relative fraction of the sp^3, sp^2 and C–O components are stated in Table 4.3. In Figure 4.10, the sp^3 content in the samples estimated by XPS technique are compared to those estimated by Raman spectroscopy. It can be seen that the estimations by these two techniques correlate well with each other. These results demonstrate that the sp^3 bonding content in the carbon films increases when the absolute value of target bias voltage increases from 200 to 800 V and decreases when the absolute value of target bias voltage is higher than 800 V (from 800 to 1000 V). Such trend can be attributed to the deposition mechanism of DLC films (subplantation model). According to this model, the sp^3 bonding results from carbon particles penetration to the layers located below the surface and creating a quenched-in density raise. Since the carbon ions should have enough energy to penetrate into the surface, the process possesses an optimum ion energy; while any extra energy can anneal out the density growth. This optimum ion energy may change based on the synthesis method and parameters. Ions with lower energies do not penetrate into the surface but only adhere to the surface in form of sp^2 configuration. Also in the case of high ion beam energies, thermal spikes induced by the bombardment of carbon ions into the films exceed normal bounds, which result in the a-C film graphitization , indicating the sp^3 content reduces and graphite-like bond (sp^2 content) increases (Robertson, 1994). In BTIBD method by increasing the negative target bias voltage, the average incident energy of inert gas ions used for sputtering increases, consequently the average kinetic energy of carbon atoms sputtered from the target increases (the average impact energy of the deposition/impinging species). Therefore at target bias voltage of -800 V, the optimum energy

per C atom/ion and consequently the maximum sp^3content has been achieved. For lower or higher bias voltages, which produce lower or higher ion beam energies, the sp^3 content is less, the sp^2 content is larger and the films are more graphitic.

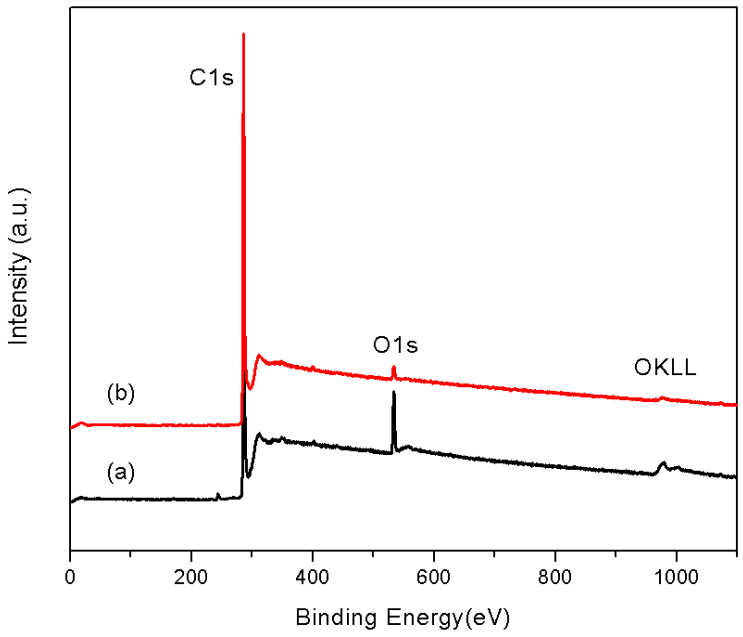

Figure 4.8. XPS survey spectrum of carbon film (a) as-deposited, (b) after Ar cleaning.

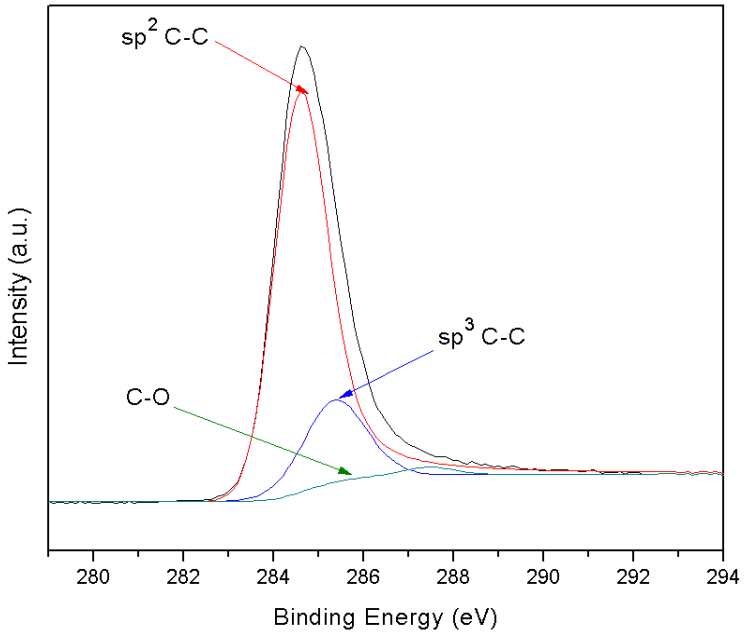

Figure 4.9. Typical C1s spectrum and its fitting of carbon film deposited at -200 V.

Table 4.3. Binding energy and relative fraction of the components which contribute to the XPS spectrum of C 1s for carbon film deposited at -200 V.

a-C	Bonding types	Position (eV)	Area (%)
C ls	sp^2 C–C	284.4	80.53
	sp^3 C–C	285.2	18.00
	C–O	286.5	1.47

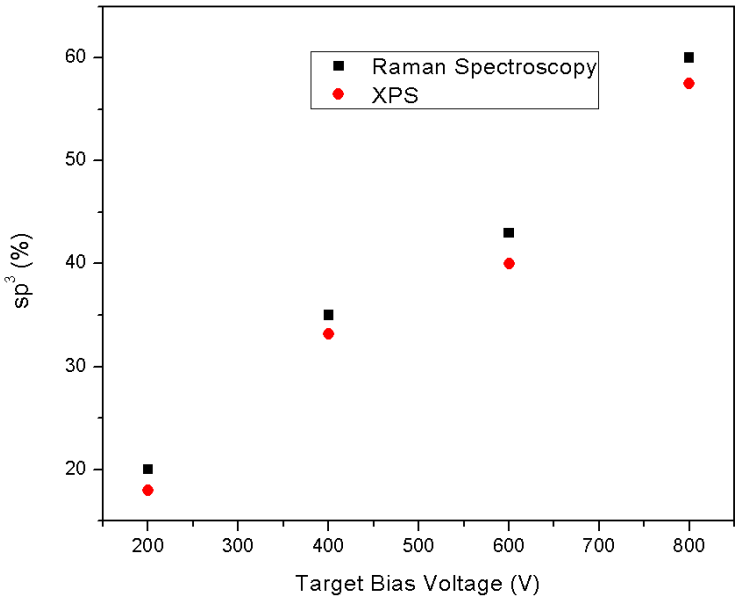

Figure 4.10. Estimation of sp^3 fraction by Raman spectroscopy and XPS for carbon films.

4.3.3 Mechanical Properties

Hardness and Young's modulus values of the deposited carbon films as a function of the absolute value of target bias voltage are presented in Figure 4.11. The indent depth reached approximately 20 nm, which was less than 10% of the film thickness. Therefore, the measurements were not influenced by the substrate (Gitis *et al.*, 2008). From Figure 4.11, it can be observed that the hardness increases from 4.5 GPa to 15 GPa, and the Young's modulus raises from 65 GPa to 170 GPa with increasing the absolute value of target bias voltage from 200 V to 800 V, while the hardness decreases to 12.9 GPa and the Young's modulus reduces to 150 GPa for bias voltage of -1000 V which correlate with the sp^3 content of the films. It is known that sp^3 is a key factor for amorphous carbon films, and the high hardness and the Young's modulus values of the carbon films are due to the strong and directional sp^3 bonding of carbon, which creates a three-dimensional (tetrahedral) network of σ bonds. However, in the case of sp^2

bonding (graphitic bonds), the existence of weak Van der Waals bonding between the layers results in a very soft film. Therefore, as sp^3 content rises, the hardness and Young's modulus increase (Lifshitz, 1999; Chowdhury *et al.*, 2004). So the variation trend of the hardness and the Young's modulus of the hydrogen-free DLC films can be attributed to the variation trend of the sp^3 content of the films due to the target bias voltage changes, and the hardness and the Young's modulus values reveal almost same agreement with the Raman spectroscopy analysis.

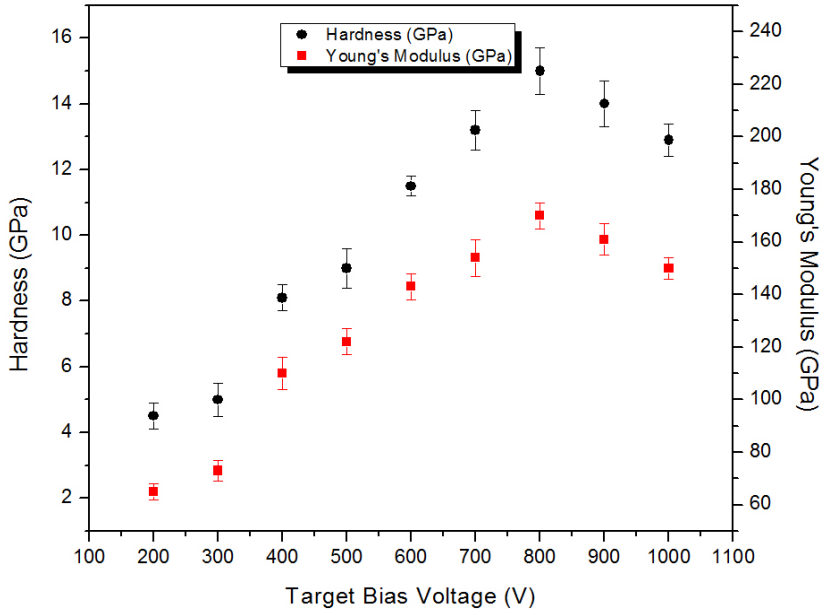

Figure 4.11. Hardness and Young's modulus of carbon films deposited at different target bias voltage values.

4.3.4 Tribological Properties

Figure 4.12 illustrates the coefficient of friction (COF) and wear coefficient, k, of the carbon films after 1000 cycle of sliding versus the absolute value of target bias voltage which they synthesized. The carbon films deposited at target bias voltages of -200 and -300 V exhibit

relatively high COF of 0.3 and 0.25 respectively, and relatively high k of 15.1×10^{-6} $mm^3N^{-1}m^{-1}$ and 11×10^{-6} $mm^3N^{-1}m^{-1}$ respectively. It can be seen that by increasing the absolute value of target bias voltage from 400 to 800 V, COF and k decrease monotonously (COF from 0.2 to 0.06 and k from 8×10^{-6} $mm^3N^{-1}m^{-1}$ to 1.6×10^{-6} $mm^3N^{-1}m^{-1}$). But at 1000 V, COF again increases to 0.11 and k raises to 3.7×10^{-6} $mm^3N^{-1}m^{-1}$. Chen *et al.* (2011) showed that the carbon film converts by a stress-induced conversion to a graphitic over-layer during the sliding and creates an adherent transfer film of this material on the counterface, which then acts as a lubricant and leads to a low friction coefficient. Regarding the decrease of friction coefficient (COF) with the increase of deposition bias voltage from 200 V to 800 V, according to Yang *et al.* (2003), the reduced COF must be induced by the reduced frictional force, which is the product of the contact area and the shear strength at the ball-film interface. In fact, the increased film hardness and Young's modulus with the raise of bias voltage from 200 V to 800 V leads to ease in supporting the load, which can decrease the contact area at the ball-film interface. So, with a raise of film hardness and Young's modulus, the COF could tend to reduce. On the other hand, based on the Li *et al.* (2006), the friction mainly results from the chemical interactions induced by the strong dangling σ-bonds at the sliding interfaces, and the weak π–π interactions of sp^2 bonds will also cause an extra friction force leading to the decrease of COF with the increasing target bias voltage induced by decrease in sp^2 bonds. By increasing the target bias voltage from 800 V to 1000 V, a reverse mechanism happens leading to a raise in COF value. In addition, Shaha *et al.* (2011) have studied the effect of surface roughness on the formation of transfer film and frictional characteristics of DLC coatings. This study showed that higher surface roughness causes a higher steady-state COF for DLC films. As the bias voltage increases from 200 to 800 V, the surface roughness on the as-deposited film would be reduced, and the decreased surface roughness of

film leads to the gradually decrease of COF. With increasing the target bias voltage from 800 V to 1000 V, a reverse mechanism happens and the surface roughness and consequently COF increase. According to Erdemir *et al.* (2006), high smoothness is essential to remove mechanical interlocking and/or asperity-asperity interactions throughout sliding to get low COF. Also, these surfaces should have the highest degree of chemical passivity or inertness in order to not get involved in any sort of adhesive bonding or chemical interactions with counterface substances which achieves at the highest sp^3 content. Moreover, the film with the higher amount of sp^3 bonding tends to produce stress-induced graphitic transfer layers much faster and with a higher degree of coverage and strong bonding than the one with lower sp^3 leading to lower friction coefficient. Based on Robertson (2002) and Archard equation, the wear coefficient of the coating is inversely proportional to the hardness of the surface. Hence harder surfaces wear less, and the increased film hardness with the raise of bias voltage from 200 to 800 V leads to the decrease of wear coefficient of the carbon films. However, with a further raise in the bias voltage (from 800 to 1000 V), the reduced film hardness induces an increase in the wear coefficient of the DLC film.

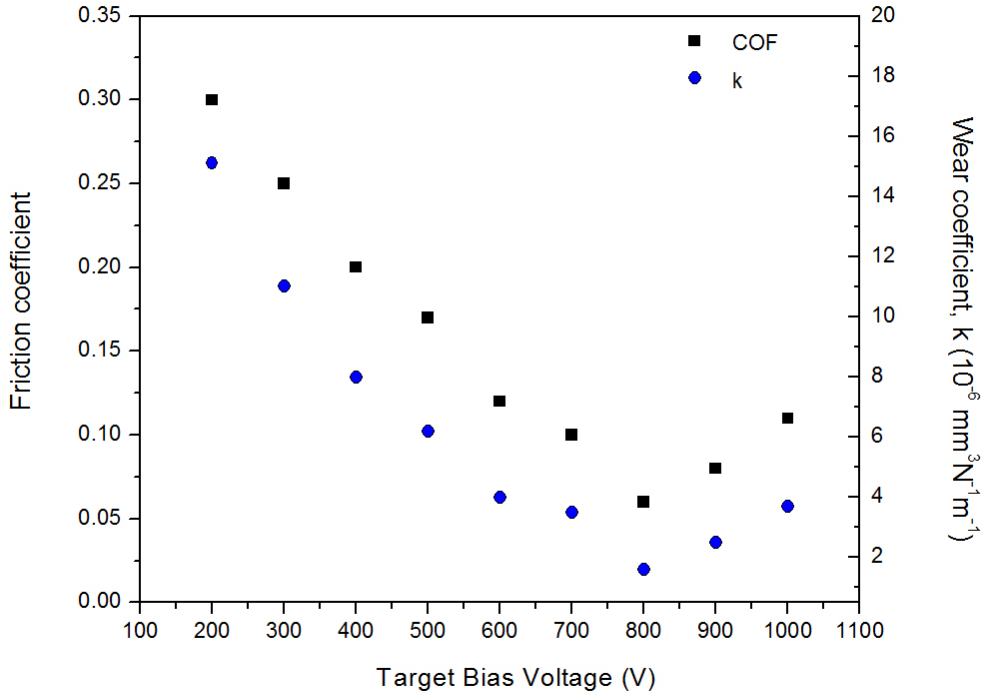

Figure 4.12. Coefficient of friction (COF) and wear coefficient (k) of hydrogen-free DLC films versus target bias voltage of deposition.

4.3.5 Corrosion Resistance

Potentiodynamic polarization tests were done in 3.5% NaCl solution at room temperature. The corrosion potential and corrosion current can be achieved from the Tafel analysis. Table 4.4 presents the corrosion potential and corrosion current of the carbon films synthesized with various target bias voltages. By increasing the bias voltage from 200 to 800 V, corrosion potential increases. It shows that the anti-corrosion behavior (nobility) of the carbon films increases with bias voltage increasing from 200 to 800 V. However, with a further increase in the target bias voltage (from 800 to 1000 V), corrosion potential reduces indicating a decrease in the anti-corrosion behavior (nobility) of the DLC film. Basically, the corrosion current is directly related to the corrosion rate, which means that the lower the corrosion current, the better

the resistance against corrosion (Choi *et al.*, 2007a). As stated in Table 4.4, when the bias voltage raises from 200 to 800 V, the corrosion current reduces, i.e. lower corrosion rate. However, with a further increase in the bias voltage (from 800 to 1000 V), the corrosion current increases accordingly, i.e. higher corrosion rate. It is known that certain factors can affect the corrosion resistance of a film including bonding structure, electrical resistivity and the film density (Khun *et al.*, 2009). Combining this with Raman spectroscopy results, one can conclude that the corrosion resistance of the carbon films is correlated with the films structure. As stated previously, the sp^3 content of the carbon films raises with increasing bias voltage from 200 to 800 V. Consequently, the film density increases with the raise of deposition target bias voltage from 200 to 800 V. Greater film density can efficiently prevent corroding ions from entering into the film subsurface. Also, it is known that the sp^3 content of the DLC films is directly related to the electrical conductivity of the films, i.e. the higher sp^3 content is regularly accompanied by lower film electrical conductivity (higher electrical resistivity) (Bai *et al.*, 2011). In a general sense, the increased corrosion resistance for films with the increased bias voltage from 200 to 800 V can be ascribed to the reduced electrical conductivity, increased electrical resistivity and raised films density. With increasing the target bias voltage from 800 V to 1000 V, a reverse mechanism happens leading to a decrease in sp^3 content and consequently corrosion resistance of the hydrogen-free DLC film.

Table 4.4. Corrosion potential and corrosion current of carbon thin films.

Target bias voltage (V)	Corrosion potential, E_{corr}, (mV)	Corrosion current, I_{corr}, (nA)
200	20	60
300	80	20
400	162	4.5
500	193	3.2
600	230	1.6
700	235	1.5
800	260	1.3
900	242	1.4
1000	233	1.55

4.4 Conclusions

Hydrogen-free DLC thin films have been successfully synthesized by biased target sputtering of graphite target without additional ion bombardment either by negative bias of substrate or assisting ion source, while additional ion bombardment is essential to obtain DLC by other sputtering techniques. The films obtained by this method are continuous and uniform with different structure and properties depending on the target bias voltage. The sp^3 contents estimated by Raman spectroscopy and XPS are similar. The films prepared at target bias voltage of -800 V show the lowest roughness, friction coefficient (COF) and wear coefficient (k) and the highest sp^3 content, hardness, Young's modulus and corrosion resistance. For higher or lower biasing voltages, the sp^3 fraction content, corrosion resistance, mechanical properties and tribological properties begin to reduce and the surface roughness rises.

CHAPTER 5 STRUCTURAL CHARACTERIZATION AND PROPERTIES OF HYDROGENATED DLC THIN FILMS PREPARED BY ION BEAM DEPOSITION USING KAUFMAN ION SOURCE

Transition

In this chapter, deposition of hydrogenated DLC thin films by ion beam deposition method using a Kaufman-type gridded ion source is investigated. The influence of ion energy, as a processing parameter, on the structure and properties of the films will also be studied to optimize the processing parameters of hydrogenated DLC thin films synthesized by Kaufman ion source for desired mechanical, tribological and corrosion characteristics. The energy range which can be provided by a Kaufman ion source is from 300 to 700 eV. This chapter has not yet been submitted as a journal paper.The PhD candidate designed and conducted the experiments, analyzed the results of the experiments and prepared the paper under the supervision of Profs. Qiaoqin Yang and Jerzy Szpunar.

5.1 Introduction

Since Aisenberg and Chabot (1971) reported that DLC thin films had been synthesized by ion-beam deposition in the early 1970s, this deposition technique has been continuously improved with the gradual development of ion sources. Gridded ion beam source was built in the late 1970s, which included a magnetic field to enhance ionization rate and grid optics to deal with the ion energy and beam size (Kaufman, 1978). Among different sorts of ion beam sources, Kaufman-type gridded ion source gives the most independent control on some important parameters like ion current density and ion energy over a large spectrum of deposition conditions. In this chapter, the synthesis of hydrogenated DLC thin films using a Kaufman-type gridded ion source with different ion energies ranging from 300 to 700 eV is reported in order to

understand the effect of ion energy on the structure and consequently the properties of the films. This would help to determine the processing-structure-property relationships in the hydrogenated DLC thin films.

5.2 Experimental

5.2.1 Synthesis of Hydrogenated DLC Thin Films Using Kaufman Ion Source

Mirror polished p-type Si (100) wafers were employed as substrate for this study. The substrates were cleaned before being inserted in the vacuum deposition chamber as explained in section 4.2.1. The deposition experiments were performed by the deposition system mentioned in section 3.1.1. A Kaufman-type gridded ion source, manufactured by Kaufman & Robinson, Inc. USA, was employed to deposit hydrogenated DLC thin films. Firstly, the surface of substrates was cleaned and etched by introducing Ar gas at a flow rate of 5 sccm into the ion source with an average ion energy of 700 eV for 10 min. Afterwards hydrogenated DLC thin film deposition was performed by introducing Methane (CH_4) gas into the ion source to produce hydrocarbon ions using the parameters listed in Table 5.1. The ion energy was varied between 300 and 700 eV to study the effects of processing conditions on the structure and properties of the films.

Table 5.1. Deposition conditions for hydrogenated DLC thin films.

Mean ion energy (eV)	300-700
CH_4 flow rate (sccm)	15
Ar flow rate (sccm)	5
Ion current (mA)	75
Time (hr)	6
Substrate temperature (°C)	<50
Working pressure (Torr)	1×10^{-4}

5.2.2 Characterization of Hydrogenated DLC Thin Films

Following the film synthesis, the samples were analyzed by an atomic force microscopy (AFM) and a Raman spectroscopy. The AFM data were collected from an area of 1.5 μm × 1.5 μm and the surface roughness was calculated as explained in section 3.2.1. Raman spectra were recorded using a micro-Raman system which described in section 3.2.2. Mechanical properties (hardness and Young's modulus) of the films were measured by nanoindentation method which mentioned in section 3.2.7. The tribological properties of the films were evaluated using a ball-on-disc tribometer as described in section 3.2.8. Potentiodynamic polarization measurements were carried out to measure the corrosion resistance of the films as discussed in section 3.2.9.

5.3 Results and Discussion

5.3.1 Surface Morphology and Roughness

All the synthesized films were uniform and continuous with a thickness of approximately 600 nm as measured by profilometry. AFM was employed to observe the topography and to

evaluate the surface roughness of the samples. A typical AFM image of the film deposited with the ion energy of 400 eV is presented in Figure 5.1. The root-mean squared (RMS) roughness of the samples versus the ion energy is shown in Figure 5.2. It can be observed that the RMS roughness rises gradually with increasing the ion energy from 300 eV to 700 eV. The results can be explained by the mechanism of continuous film formation. Two requirements must be satisfied in order to form smooth films. Firstly, the synthesized phase must have a high nucleation density on the whole surface and secondly, the synthesized species should not have surface mobility to migrate across the surface to shape islands. In the case of very low ion energies, the ions have more trouble to overcome nucleation barriers and therefore have quite low nucleation density, causing higher surface roughness. Whereas the ion energy is greater than the optimum value (around 100 eV), which is the case for the present work, the atoms have elevated energy to move across the surface and accumulate with other clusters, causing greater values of RMS roughness (Robertson, 2003). In addition, according to Gilmer *et al*. (1998), when the bombardment energy is very high, the surface of the film can be damaged, causing the raise of roughness.

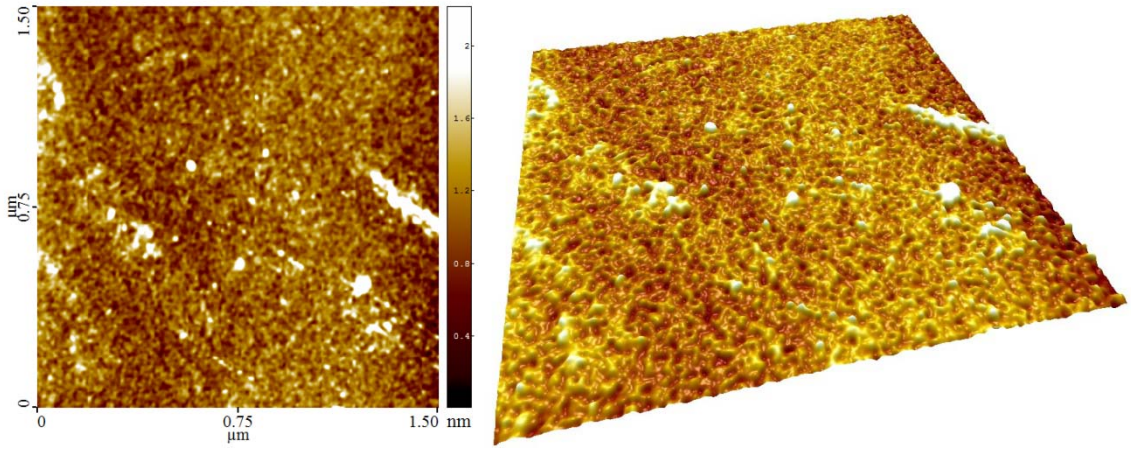

(a) (b)

Figure 5.1. Typical topographic image (1.5 µm × 1.5 µm) of the DLC film deposited with ion energy of 400 eV (a) 2-D image, (b) 3-D image.

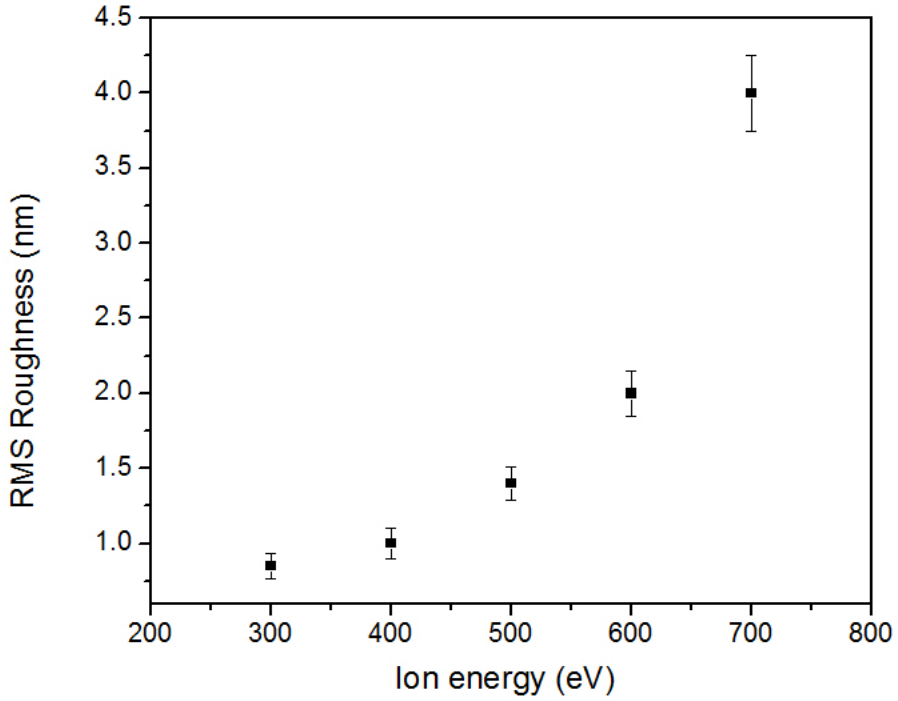

Figure 5.2. RMS roughness values of hydrogenated DLC films synthesized by Kaufman ion source at various ion energies.

5.3.2 Bonding Structure

Figure 5.3 presents typical Raman spectra of the DLC thin films synthesized by Kaufman ion source with different ion energies. For ion energies between 300 and 600 eV, the signature of a typical DLC film was observed in the spectra (D and G peaks); while for ion energy of 700 eV, the spectrum is more similar to that of graphite than DLC. After deconvolution and fitting of the Raman spectra (mixed Gaussian/Lorentzian) into the D and G peaks, the G peak position and the intensity ratio of the G and D peaks (I(D)/I(G)) were extracted, as presented in Figure 5.4. It can be observed that G peak position shifts up and the I(D)/I(G) peak intensity ratio increases by raise of the ion energy from 300 eV to 700 eV. The rise in I(D)/I(G) and the G-band upward shift indicate a reduction in the sp^3 content of the carbon films (see section 4.3.2 for exact mechanism). On the basis of the correlation between sp^3 content of the carbon thin films and the I(D)/I(G), which explained in section 4.3.2, the sp^3 content of the DLC films was estimated and the results is presented in Figure 5.5. It shows that sp^3 bonding content in the DLC films reduces when the ion energy increases from 300 to 700 eV. Such trend can be ascribed to the synthesis mechanism of DLC films (subplantation model) which discussed in section 4.3.2. According to McKenzie *et al.* (1994), the sp^3 content in amorphous carbon films depends on the energy per incident C ions. They observed that the maximum sp^3 content for ion beam deposited films occurs at an energy per C atom/ion of 100 eV, and for higher energies, the sp^3 content is less, the sp^2 content is larger and the films are more graphitic. The same trend was found in this investigation.

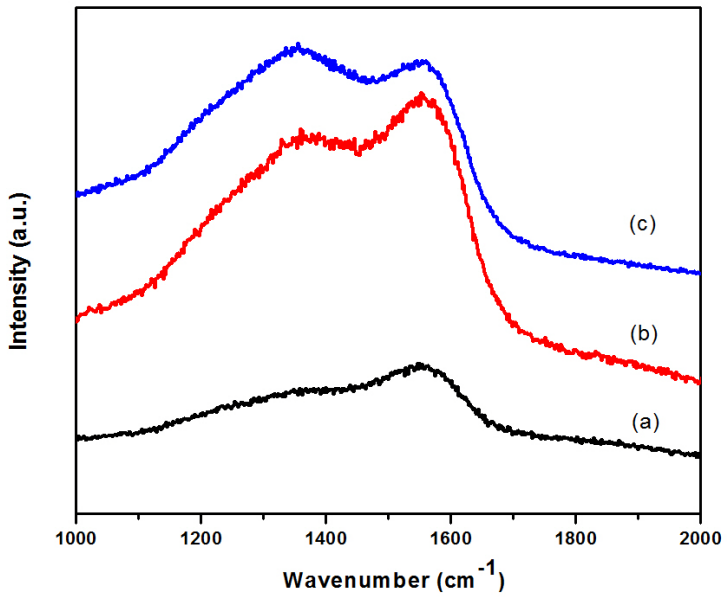

Figure 5.3. Raman spectra of carbon films deposited at different ion energies of (a) 300 eV, (b) 600 eV, (c) 700 eV.

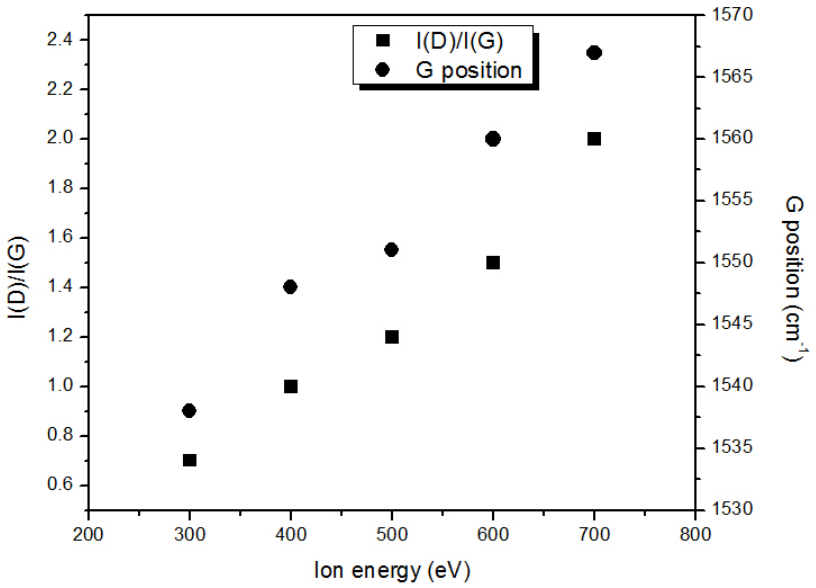

Figure 5.4. Raman G peak position and I(D)/I(G) of the films versus ion energy.

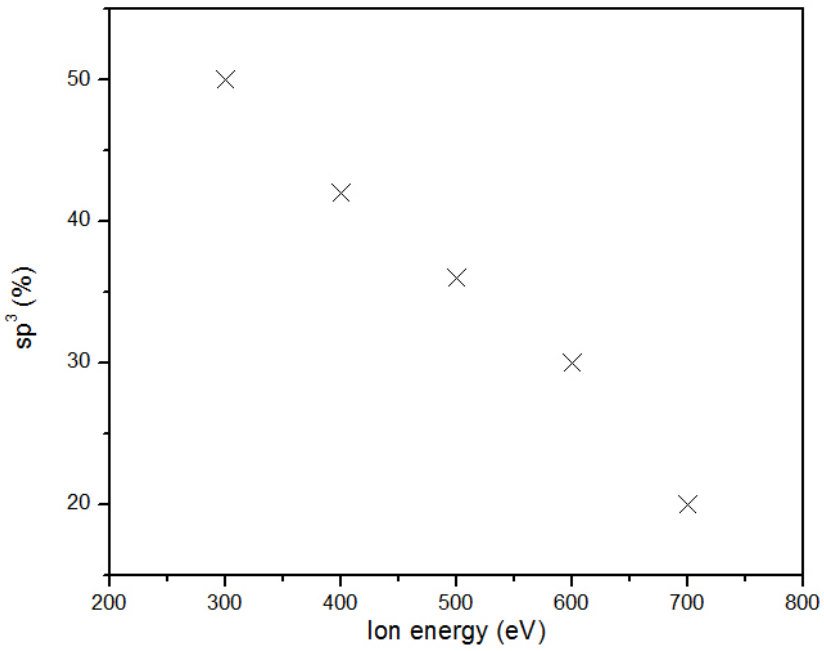

Figure 5.5. sp^3 percentage for as-deposited carbon films versus ion energy.

5.3.3 Mechanical Properties

The variation of hardness and Young's modulus of the DLC films with ion energy are illustrated in Figure 5.6. It can be seen that the hardness reduced from 11.5 GPa to 5 GPa, and the Young's modulus decreased from 125 GPa to 61 GPa with raising ion energy (from 300 eV to 700 eV). The trends of variation of hardness and Young's modulus with the ion energy are consistent with those of Raman spectra, more specifically, sp^3 content of the films. Since the high hardness and Young's modulus values obtained for DLC films are due to the sp^3 tetrahedral carbon, as sp^3 content reduced, the hardness and Young's modulus of the film decreased (exact mechanism explained in section 4.3.3). Therefore, the trends of variation of the hardness and Young's modulus of the hydrogenated DLC films can be ascribed to the variation trend of the sp^3

content of the films due to the ion energy changes, and the hardness and Young's modulus values show almost same agreement with the Raman spectroscopy results.

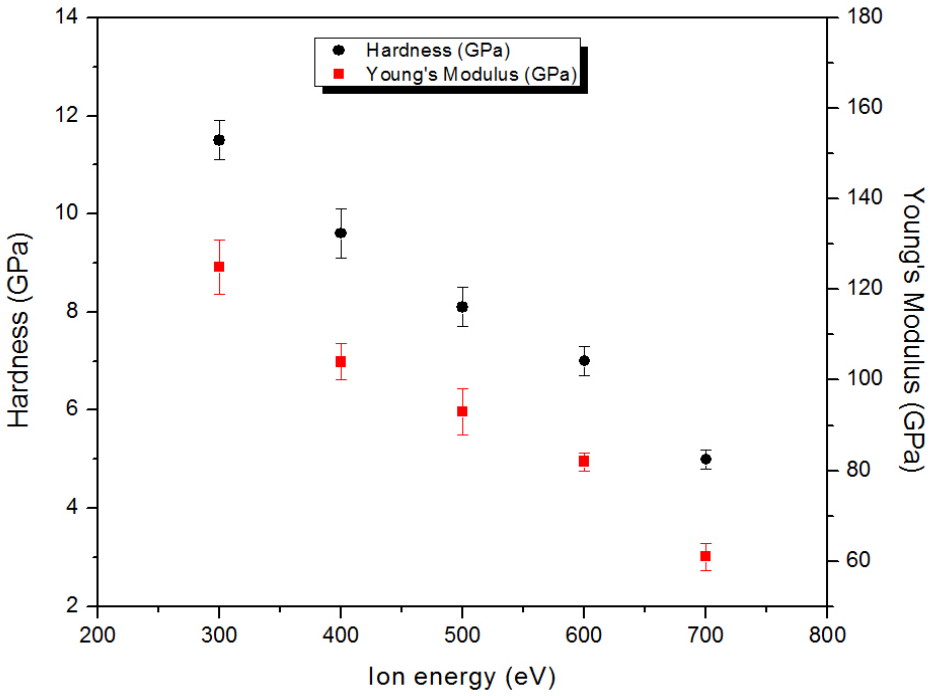

Figure 5.6. Hardness and Young's modulus of DLC films deposited at different ion energy values.

5.3.4 Tribological Properties

Figure 5.7 shows the coefficient of friction (COF) and wear coefficient, k, of the hydrogenated DLC films after 1000 cycle of sliding versus the ion energy which they deposited. It can be observed that by rising the ion energy from 300 eV to 700 eV, COF and k increase monotonously (COF from 0.08 to 0.3 and k from 2.5×10^{-6} to 15.3×10^{-6} $mm^3N^{-1}m^{-1}$). The raise of friction coefficient (COF) with the increase of deposition ion energy must be induced by the decreased film hardness, Young's modulus and sp^3 content, an increase in graphitization and the

raised surface roughness of the films, as described in section 4.3.4.The increase of the wear coefficient of the hydrogenated DLC films with the raise of ion energy is also related to the decreased film hardness with the raise of ion energy.

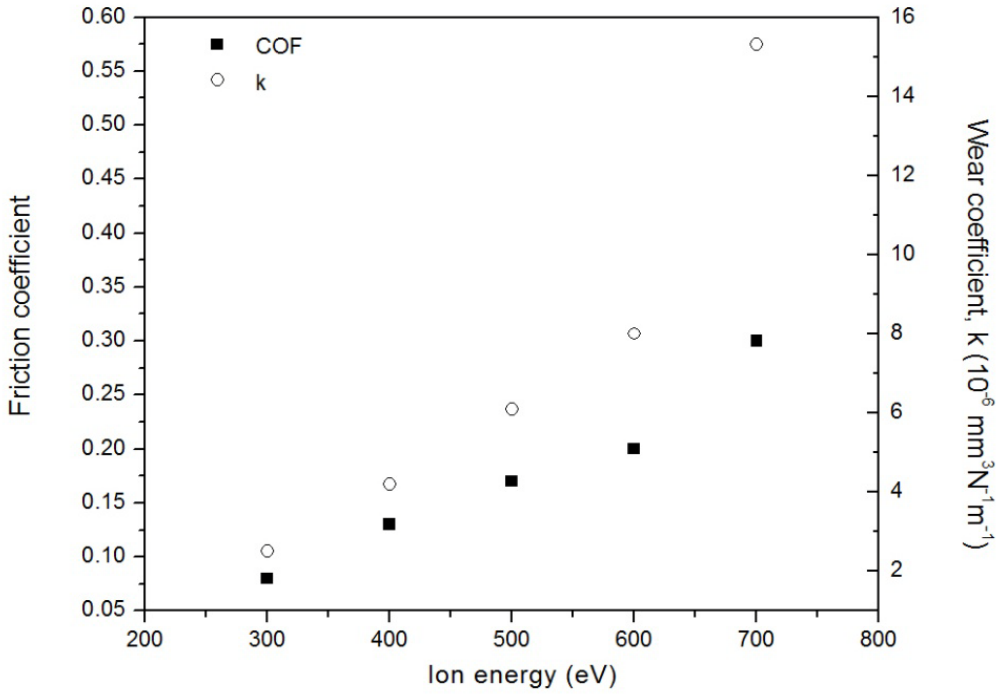

Figure 5.7. Coefficient of friction (COF) and wear coefficient (k) of hydrogenated DLC films versus ion energy of deposition.

5.3.5 Corrosion Resistance

Potentiodynamic polarization tests were conducted in 3.5% NaCl solution at room temperature. The corrosion potential and corrosion current were achieved from the Tafel analysis. Table 5.2 demonstrates the corrosion potential and corrosion current of the hydrogenated DLC films deposited with different ion energies. By rising the ion energy from 300 to 700 eV, corrosion potential decreases. It implies that the anti-corrosion behavior (nobility)

of the carbon films reduces with ion energy rising from 300 to 700 eV. As presented in Table 5.2, when the ion energy increases, the corrosion current raises accordingly, i.e. higher corrosion rate. The decreased corrosion resistance for films with the increased ion energy from 300 to 700 eV can be attributed to the increased electrical conductivity, decreased electrical resistivity and reduced films density due to the decreased sp^3 content of the DLC films, as discussed in section 4.3.5.

Table 5.2. Corrosion potential and corrosion current of the hydrogenated DLC thin films.

Ion energy (eV)	Corrosion potential, E_{corr}, (mV)	Corrosion current, I_{corr}, (nA)
300	195	2.01
400	162	4.4
500	145	5.6
600	83	19
700	22	57

5.4 Conclusions

The hydrogenated DLC thin films prepared by ion beam deposition method using a Kaufman-type gridded ion source at an average ion energy of 300 eV show the lowest roughness, COF and wear coefficient and the highest sp^3 content, hardness, Young's modulus and corrosion resistance. For higher ion energies, the sp^3 fraction content, corrosion resistance, mechanical properties and tribological properties begin to decrease and the surface roughness increases.

CHAPTER 6 STRUCTURAL CHARACTERIZATION AND PROPERTIES OF HYDROGENATED DLC THIN FILMS SYNTHESIZED BY ION BEAM DEPOSITION USING END-HALL ION SOURCE

Transition

Synthesis of hydrogenated DLC thin films by a Kaufman-type gridded ion source was reported in chapter 5. The ion energy which was accessible by the Kaufman source was over 300 eV. In this chapter, deposition of hydrogenated DLC thin films by ion beam deposition method using a gridless end-Hall ion source is investigated. The energy range provided by this end-Hall ion source is from 50 to 110 eV. The influence of ion energy, as a processing parameter, on the structure and properties of the films will also be studied to optimize the processing parameters of hydrogenated DLC thin films synthesized by end-Hall ion source for desired mechanical, tribological and corrosion properties. This chapter has not yet been submitted as a journal paper.The PhD candidate designed and conducted the experiments, analyzed the results of the experiments and prepared the paper under the supervision of Profs. Qiaoqin Yang and Jerzy Szpunar.

6.1 Introduction

The main limitations of gridded ion sources are that the beam current is low, less than 500 mA, and the ion energy is high, usually more than 300 eV. To address these limitations, gridless end-Hall (EH) ion sources were designed to supply low energy ion beams (with mean ion energy ranging from 30 to 120 eV) with high beam current (Kaufman *et al.*, 1987). End-Hall ion sources have the benefit of less complex installation, operation and maintenance in comparison with the gridded ion sources such as Kaufman ion source. Some investigations have been done to synthesize DLC thin films by end-Hall ion sources (Tang *et al.*, 2011b). However,

there are few studies on the bonding structure, tribomechanical and corrosion resistance properties of the synthesized DLC thin films, especially in the ion energy range used for this investigation. In the present study, deposition of hydrogenated DLC thin films using a gridless end-Hall ion source is reported. The effect of ion energy ranging from 50 to 110 eV, on the structure and properties of the synthesized films were further investigated to determine the processing-structure-property relationships of the hydrogenated DLC thin films.

6.2 Experimental

6.2.1 Synthesis of Hydrogenated DLC Thin Films Using End-Hall Ion Source

Mirror polished p-type Si (100) wafers were used as substrate for growth of the DLC thin films. The substrates were cleaned before being put into the vacuum deposition chamber as described in section 4.2.1. The deposition experiments were carried out using the deposition system explained in section 3.1.1. A gridless end-Hall ion source (KRI EH-1000, manufactured by Kaufman & Robinson, Inc. USA) was used to synthesize hydrogenated DLC thin films. Prior to the deposition, the surface of substrates was cleaned and etched by introducing Ar gas at a flow rate of 5 sccm into the ion source with an average ion energy of 50 eV for 10 min. Methane (CH_4) gas was introduced into the ion source to produce hydrocarbon ions using the parameters listed in Table 6.1. The ion energy was varied to determine the influences of processing conditions on the structure and properties of the produced films.

Table 6.1. Deposition conditions for hydrogenated DLC thin films.

Mean ion energy (eV)	50-110
CH_4 flow rate (sccm)	5
Ion current (A)	2
Time (hr)	6
Substrate temperature (°C)	<50
Working pressure (Torr)	1×10^{-4}

6.2.2 Characterization of Hydrogenated DLC Thin Films

After the film deposition, the specimens were analyzed using atomic force microscopy (AFM) and Raman spectroscopy. The surface roughness was determined by AFM as described in section 3.2.1. Raman spectra were obtained using a micro-Raman system which explained in section 3.2.2. Mechanical properties (hardness and Young's modulus) of the films were measured by nanoindentation technique which described in section 3.2.7. The tribological characteristics of the films were obtained using a ball-on-disc tribometer as discussed in section 3.2.8. Potentiodynamic polarization measurements were conducted to evaluate the corrosion resistance of the films as explained in section 3.2.9.

6.3 Results and Discussion

6.3.1 Surface Morphology and Roughness

All the deposited films were continuous and uniform with a thickness of approximately 600 nm as measured by profilometry. The variation of measured root-mean squared (RMS) roughness of the specimens with ion energy is shown in Figure 6.1. The RMS roughness

decreased gradually with raising ion energy up to 100 eV, and then increased with further increase in ion energy. The results can be explained by the mechanism of continuous film formation as discussed in section 5.3.1.

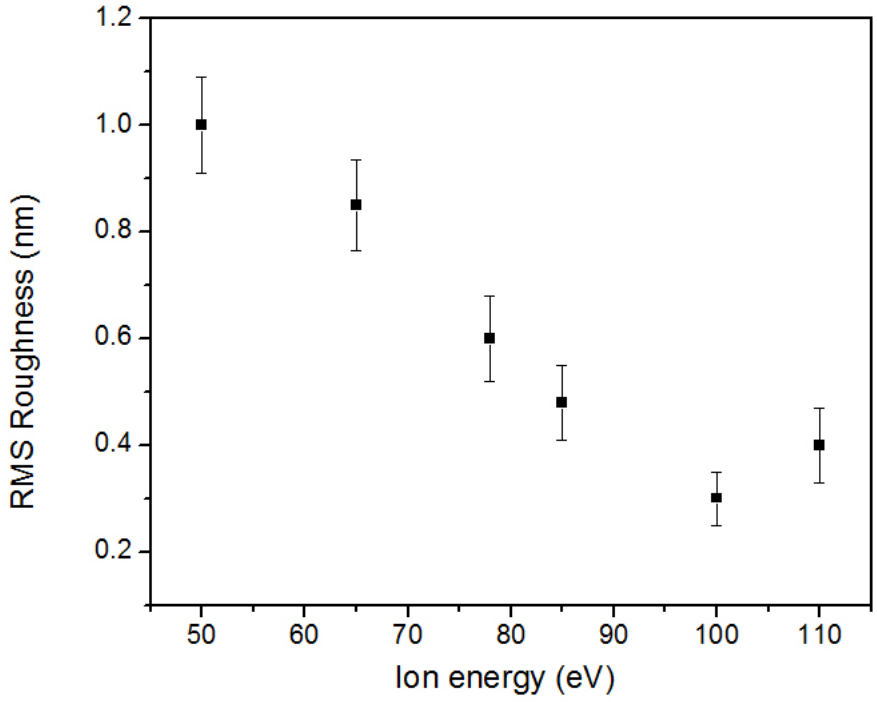

Figure 6.1. RMS roughness values of hydrogenated DLC films synthesized by end-Hall ion source at various ion energies.

6.3.2 Bonding Structure

Figure 6.2 illustrates the Raman spectrum obtained for DLC thin film synthesized by the IBD technique using an end-Hall ion source with ion energy of 78 eV (before and after deconvolution). For ion energies in the range of 50-110 eV, similar spectra were obtained and the signature of a typical DLC film was observed in the spectra (D and G peaks). After deconvolution and fitting of the Raman spectra (mixed Gaussian/Lorentzian) into the D and G peaks, the G peak position and the intensity ratio of the G and D peaks (I(D)/I(G)) were derived,

as plotted in Figure 6.3. It can be seen that G peak position and I(D)/I(G) peak intensity ratio reduced as the ion energy increased from 50 eV to 100 eV. However, with a further increase in the ion energy (from 100 to 110 eV), both G peak position and I(D)/I(G) ratio started to increase. The reduction in I(D)/I(G) ratio and the downward shift of G peak position imply an increase in the sp^3 content of DLC films (see section 4.3.2 for exact mechanism). Based on the correlation between sp^3 content of the DLC thin films and I(D)/I(G) ratio, which discussed in section 4.3.2, the sp^3 content of the DLC films was estimated and the results are shown in Figure 6.4. These results demonstrate that the sp^3 bonding content in the hydrogenated DLC films increases when the ion energy increases from 50 to 100 eV and decreases when the ion energy is higher than 100 eV. Such trend can be attributed to the deposition mechanism of DLC films (subplantation model) which was explained in sections 4.3.2 and 5.3.2.

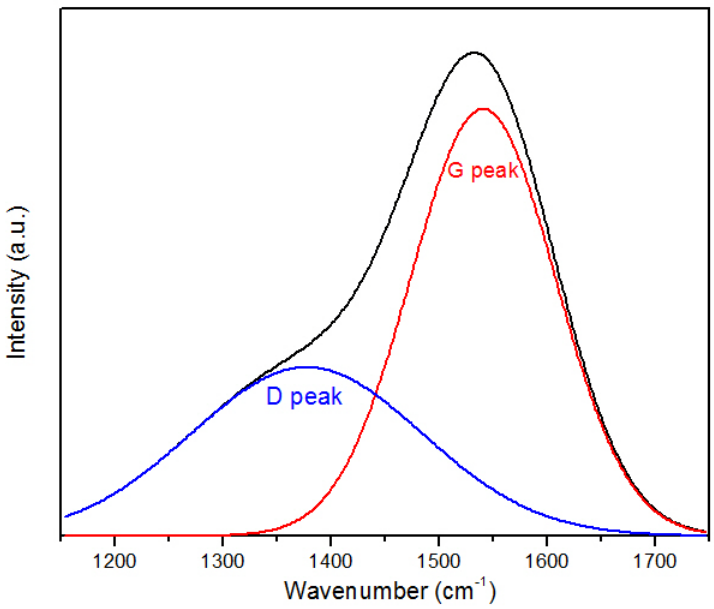

Figure 6.2. Raman spectrum of hydrogenated DLC thin film synthesized at deposition ion energy of 78 eV.

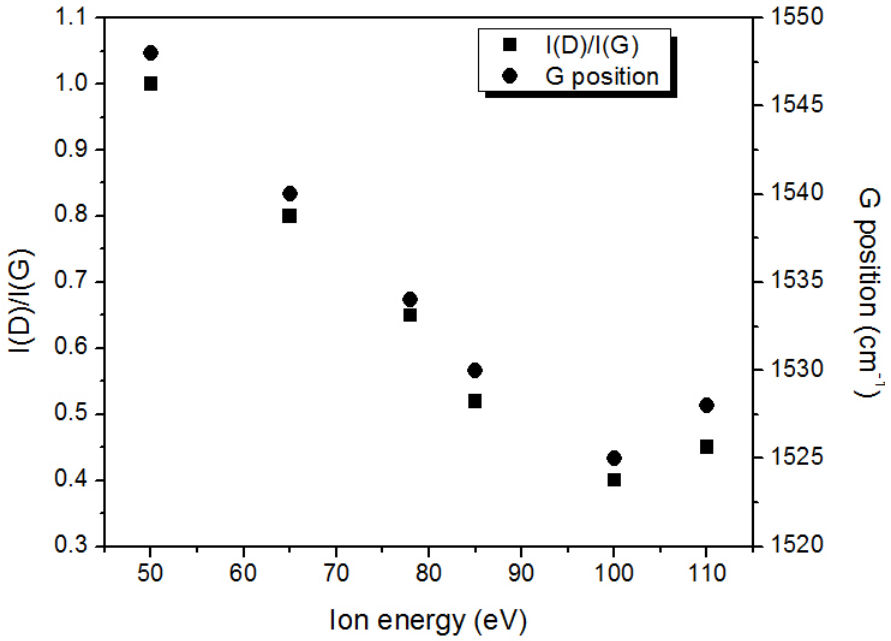

Figure 6.3. Raman G peak position and I(D)/I(G) of the DLC films versus ion energy.

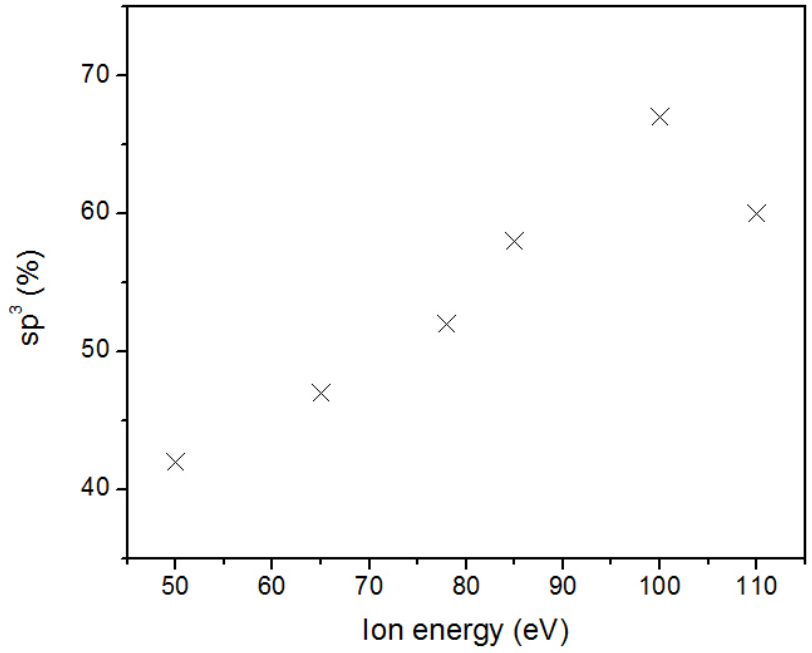

Figure 6.4. sp^3 percentage for as-deposited DLC films versus ion energy.

6.3.3 Mechanical Properties

Hardness and Young's modulus values of the deposited DLC films as a function of ion energy are presented in Figure 6.5. It can be observed that the hardness increases from 9.5 GPa to 17.5 GPa, and the Young's modulus raises from 104 GPa to 182 GPa with increasing ion energy from 50 eV to 100 eV, while the hardness decreases to 15 GPa and the Young's modulus reduces to 167 GPa for ion energy of 110 eV which correlate with the sp^3 content of the DLC films. The hardness values are reasonable for hydrogenated DLC films. According to Robertson (2002), for hydrogenated DLC films, hardness values going beyond 20 GPa would be an excessively high estimate except when there is a special cause to explain it. Since the great mechanical properties of DLC films are due to the sp^3 tetrahedral carbon, as sp^3 content rises, the hardness and Young's modulus increase (mechanism discussed in section 4.3.3). So the variation trend of the hardness and the Young's modulus of the hydrogenated DLC films can be attributed to the variation trend of the sp^3 content of the films caused by the ion energy changes, and the hardness and the Young's modulus values reveal almost same agreement with the Raman spectroscopy analysis.

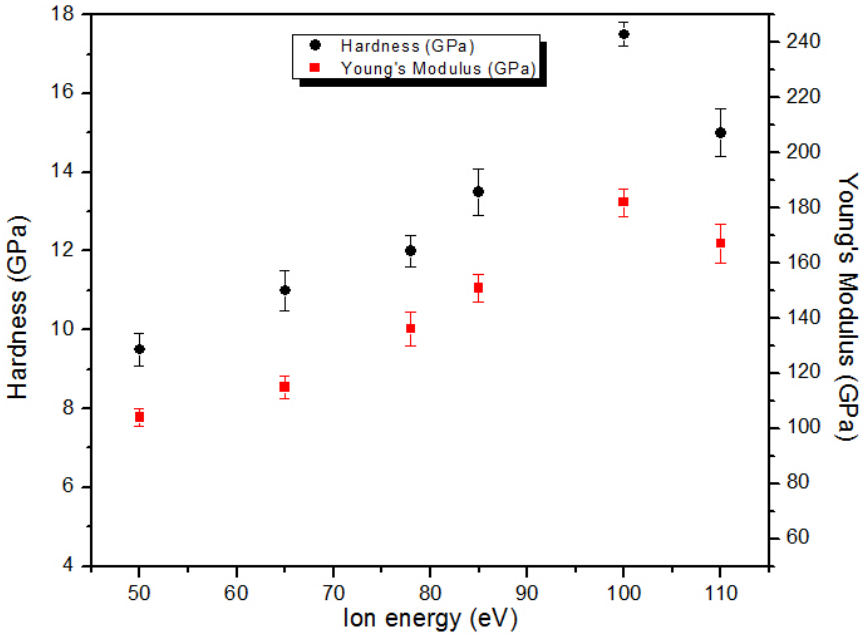

Figure 6.5. Hardness and Young's modulus of hydrogenated DLC thin films synthesized at different ion energy values.

6.3.4 Tribological Properties

Figure 6.6 illustrates the coefficient of friction (COF) and wear coefficient, k, of the hydrogenated DLC films after 1000 cycle of sliding versus the ion energy which they synthesized. It can be seen that by increasing the ion energy from 50 to 100 eV, COF and k decrease monotonously (COF from 0.13 to 0.04 and k from 4.2×10^{-6} to 1.2×10^{-6} $mm^3N^{-1}m^{-1}$). But at 110 eV, COF again increases to 0.05 and k raises to 1.5×10^{-6} $mm^3N^{-1}m^{-1}$. The variation trend of friction coefficient (COF) with deposition ion energy must be resulted from the variation trend of film hardness and Young's modulus, sp^3 content and surface roughness of the films, as explained in section 4.3.4.The variation trend of wear coefficient of the hydrogenated DLC films with ion energy is also originated from the variation trend of the film hardness with the raise of ion energy.

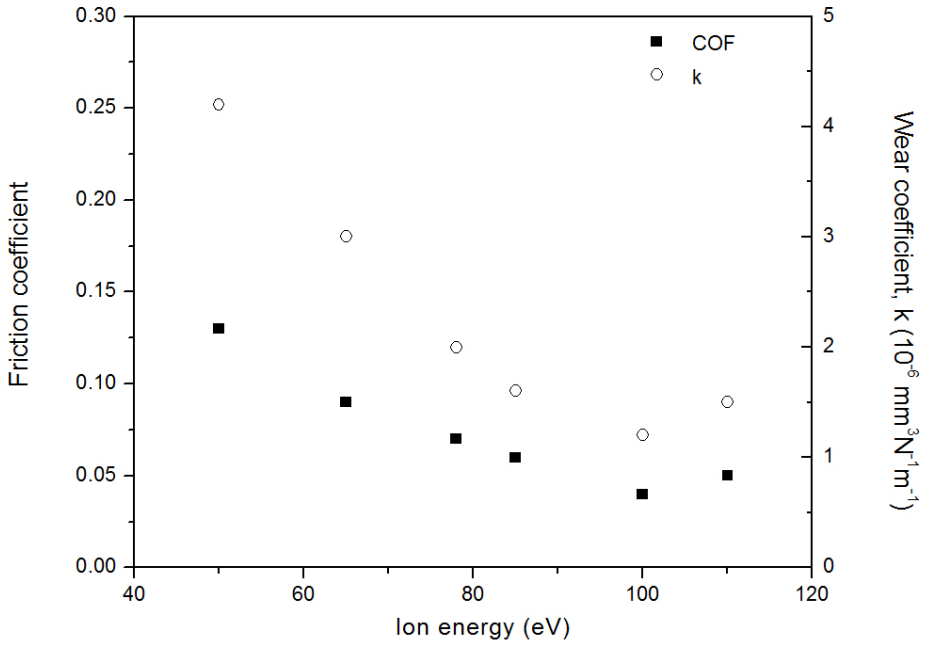

Figure 6.6. Coefficient of friction (COF) and wear coefficient (k) of hydrogenated DLC films versus deposition ion energy.

6.3.5 Corrosion Resistance

Potentiodynamic polarization tests were done in 3.5% NaCl solution at room temperature. The corrosion potential and corrosion current were obtained from the Tafel analysis. Table 6.2 presents the corrosion potential and corrosion current of the hydrogenated DLC films synthesized with various ion energies. By increasing the ion energy from 50 to 100 eV, corrosion potential increases. It shows that the anti-corrosion behavior (nobility) of the DLC films increases with ion energy increasing from 50 to 100 eV. However, with a further increase in the ion energy (from 100 to 110 eV), corrosion potential reduces indicating a decrease in the anti-corrosion behavior (nobility) of the hydrogenated DLC film. As shown in Table 6.2, when the ion energy rises from 50 to 100 eV, the corrosion current reduces correspondingly. However, with a further increase in the ion energy (from 100 to 110 eV), the corrosion current increases

accordingly. The increased corrosion resistance for films with the increased ion energy from 50 to 100 eV can be ascribed to the reduced electrical conductivity, increased electrical resistivity and raised films density caused by the increased sp^3 content of the DLC films which discussed in section 4.3.5. With increasing the ion energy from 100 eV to 110 eV, a reverse mechanism happens leading to a decrease in sp^3 content and consequently corrosion resistance of the hydrogenated DLC film.

Table 6.2. Corrosion potential and corrosion current of the hydrogenated DLC thin films.

Ion energy (eV)	Corrosion potential, E_{corr}, (mV)	Corrosion current, I_{corr}, (nA)
50	160	5.33
65	190	2.34
78	228	1.40
85	261	1.2
100	295	0.98
110	268	1.06

6.4 Conclusions

The hydrogenated DLC thin films synthesized by ion beam deposition technique using a gridless end-Hall ion source at an average ion energy of 100 eV show the lowest roughness, friction coefficient and wear coefficient and the highest sp^3 content, hardness, Young's modulus and corrosion resistance. For higher or lower ion energies, the sp^3 fraction content, corrosion resistance, mechanical properties and tribological properties begin to reduce and the surface roughness rises.

CHAPTER 7 SYNTHESIS AND CHARACTERIZATION OF DLC-MOS_2 THIN FILMS

Transition

In this chapter, synthesis and characterization of DLC-MoS_2 composite thin films, which are employed to improve the tribological properties of pure DLC films in ambient air environment, is investigated. The influence of MoS_2 target bias voltage, as a processing parameter, on the structure and properties of the DLC-MoS_2 films will also be studied in comparison with a pure DLC film. This chapter has been published in "*Journal of Physics and Chemistry of Solids*" as follows: "Niakan H., C. Zhang, L. Yang, Q. Yang, J.A. Szpunar. 2014. Structure and properties of DLC-MoS_2 thin films synthesized by BTIBD method. Journal of Physics and Chemistry of Solids 75: 1289-1294".The PhD candidate designed and conducted the experiments, analyzed the results of the experiments and prepared the manuscript for publication under the supervision of Profs. Qiaoqin Yang and Jerzy Szpunar. C. Zhang helped regarding the preparation of the specimens for DLC-MoS_2 thin film deposition, while L. Yang assisted in conducting XRD characterization. This manuscript has not been included in other theses. It has been reformatted from the original version for inclusion in this thesis and the text has been slightly modified to ensure clarity and avoid repetition.

7.1 Introduction

As mentioned before, DLC films do not have a sufficiently low coefficient of friction and endurance on some working environments. Therefore, investigations on expanding the application environment and improving the performance of the film by means of the addition of metal or non-metal elements have been extensively conducted since Dimigen *et al.* (1987) reported on the synthesis of metal-containing amorphous hydrogenated carbon films (a-C:H) in the early 80s. The use of transition metal dichalcogenides for solid lubricant coatings (sulfides,

selenides or tellurides of molybdenum, tungsten, and niobium) is usually limited to vacuum or dry air environments, where they demonstrate exceptional self-lubricating behaviors (Prasad *et al.*, 2000; Jamison *et al.*, 1971). Due to their low hardness values and triboreaction of these coatings with the ambient air environment, they cannot be used for the ambient air applications (Teer, 2001). Among these transition metal dichalcogenides, sputter deposited molybdenum disulfide (MoS_2) coating with a hexagonal structure is widely used in aerospace industry as solid lubricant due to its ultra low friction coefficient in a high vacuum environment (Donnet *et al.*, 1996). Although MoS_2 films have been employed in high vacuum aerospace environments, the attempts to apply such films in ambient air have been unsuccessful because of the high sensitivity of MoS_2 to humid air environment (Zhang *et al.*, 2001). Fabricating a composite coating containing MoS_2 can be one of the methods not only to hinder the oxidation of MoS_2 during its exposure to humid air environment, but also to improve the tribological performance of the coating under ambient air conditions or elevated temperatures. The first investigation to modify MoS_2 films was done by doping metals into the structure to decrease the porosity and increase the hardness. From the commercial point of view, titanium doped MoS_2 coating (known as MOST) was the most successful one. Nevertheless, Ti addition could not result in low friction in ambient air environment (Teer *et al.*, 1997). As stated earlier in the previous chapters, hydrogenated DLC coatings exhibit low friction coefficient in some environments and low permeability of oxygen (Vasquez-Borucki *et al.*, 2000). A composite coating including both hydrogenated DLC and MoS_2 might exhibit desirable tribomechanical properties at various environments. Also, the effect of MoS_2 content on the structure (e.g. sp^3 content of DLC), mechanical properties (hardness and Young's modulus), tribological properties (coefficient of

friction and wear resistance), and corrosion resistance of the composite films is important for their applications.

In the present chapter, the synthesis of DLC-MoS_2 composite thin films using biased target ion beam deposition (BTIBD) is reported, in which MoS_2 was produced by sputtering a biased MoS_2 target by Ar ion beam under various target bias voltages while DLC was deposited by an end-Hall ion source with CH_4 gas as carbon source simultaneously. DLC film without MoS_2, and pure MoS_2 film were also deposited for comparison. The structure, the mechanical and tribological properties, and the corrosion resistance of the films were studied and the effect of MoS_2 target bias voltage as a key processing parameter on the structure and properties of the composite films was also evaluated.

7.2 Experimental

7.2.1 Synthesis of DLC-MoS_2 Thin Films Using BTIBD Technique

Mirror polished p-type Si (100) wafers were employed as substrate for deposition of DLC-MoS_2 thin films. The substrates were cleaned before being inserted into the vacuum chamber for the film deposition as explained in section 4.2.1. The deposition experiments were conducted using the deposition system described in section 3.1.1, which is equipped with two end-hall ion sources: ion source I was used for substrate precleaning and depositing DLC, and ion source II was used for simultaneous sputtering of MoS_2. Before the deposition, the surface of substrates was cleaned and etched by introducing Ar gas at a flow rate of 5 sccm into the ion source I with the average ion energy of 50 eV for 10 min. Hydrogenated DLC thin film synthesis was performed by introducing Methane (CH_4) gas into the deposition ion source I to produce hydrocarbon radicals and ions. For synthesis of DLC-MoS_2 composite thin films, a MoS_2 target of 99.99% purity, sputtered by Ar ion beam from ion source II, was employed to produce MoS_2

simultaneously with the deposition of DLC by ion source I. The target biasing voltage was varied from -200 V to -800 V to incorporate different amount of MoS_2 into the DLC. The deposition parameters are listed in Table 7.1.

Table 7.1. Deposition conditions for DLC-MoS_2 thin films.

Mean ion energy (eV) (for DLC)	85
Discharge current (A) (for DLC)	2
CH_4 flow rate (sccm) (for DLC)	5
Target bias voltage (-V) (for MoS_2)	200-800
Discharge current (A) (for MoS_2)	4
Time (hr)	6
Substrate temperature (°C)	<50
Working pressure (Torr)	1×10^{-4}

7.2.2 Characterization of DLC-MoS_2 Thin Films

After the film deposition, the samples were analyzed using electron probe microanalysis (EPMA), X-ray Diffraction (XRD), X-ray absorption near edge structure (XANES) and Raman spectroscopy. Electron probe microanalysis (EPMA) was used to evaluate the chemical composition of the films. X-ray diffraction (XRD) patterns were recorded with the Bruker diffractometer which explained in section 3.2.5. Synchrotron-based XANES spectra of the samples were achieved using the Soft X-ray Microanalysis Beamline of the Canadian Light Source as described in section 3.2.4. The WINXAS software was employed to normalize raw data and subtract background. Raman spectra were obtained using a micro-Raman system which mentioned in section 3.2.2. Mechanical properties (hardness and Young's modulus) of the films

were evaluated by nanoindentation method as explained in section 3.2.7. The tribological properties of the films were measured using a ball-on-disc tribometer as described in section 3.2.8. Potentiodynamic polarization measurements were carried out to evaluate the corrosion resistance of the films as discussed in section 3.2.9.

7.3 Results and Discussion

7.3.1 Surface Morphology and Chemical Composition

All the synthesized films were continuous and uniform with a thickness of approximately 600 nm as measured by profilometry. Table 7.2 presents the chemical composition of the DLC-MoS_2 thin films measured by EPMA. The relative atomic percentage of Mo, S and O components increase with the raise of MoS_2 target bias voltage from -200 V to -800 V. A raise in MoS_2 concentration results in a reduction of carbon content, and this could be related to the reduction of CH_n radicals in the plasma, induced by the excess of energetic MoS_2 radicals (Bharathy *et al.*, 2010b). More importantly, an increased sputtering rate of MoS_2 at higher bias voltages occurs. The S/Mo ratio decreases from 1.80 to 1.65 and the O/Mo ratio increases from 0.20 to 0.44 when the target bias voltage increases from -200 V to -800 V. Sub-stoichiometry of molybdenum disulfide, represented by MoS_{2-x}, in the synthesized thin films is probably related to the reaction with residual oxygen in the deposition chamber (Lévy *et al.*, 1994). However, the S/Mo ratio in the synthesized thin films is higher than the amount which molybdenum disulfide still exhibits self-lubricating behaviors (Lansdown, 1999). The increase of oxygen in the synthesized films with the increase of Mo and S content (by increasing the target bias voltage from -200 V to -800 V) can be attributed to the incident of chemical reactions in the deposition chamber during the synthesis. The existence of active carbon species in the chamber induces the reaction with oxygen atoms and formation of CO_2 or CO molecules. The reactions which can happen between

oxygen and hydrogen atoms also lead to a lower inclusion of oxygen in the synthesized films with more carbon content. The atomic percentage of Mo, S and O in table 7.2 indicates the formation of $MoS_{2-x}O_x$ in the films. According to Fleischauer *et al.* (1999), the formation of a solid solution of $MoS_{2-x}O_x$ in the structure has positive effects on the performance of the films ($MoS_{2-x}O_x$ is a solid solution of oxygen in the MoS_2 phase which MoS_2 is the solvent and oxygen atoms substitute for sulfur atoms in the MoS_2 lattice). So, the DLC-MoS_2 composite thin films are consisted of MoS_2 / $MoS_{2-x}O_x$ embedded into an amorphous carbon (DLC) matrix and the content of DLC matrix in the composite films decreases with the rise of negative bias voltage on the target.

Table 7.2. Chemical composition of DLC-MoS_2 thin films.

Target bias voltage of MoS_2 (-V)	Chemical composition (at.%)						
	C	Mo	S	O	MoS_2	S/Mo	O/Mo
200	82.00	6.00	10.8	1.2	16.8	1.80	0.20
300	77.50	7.50	13.50	1.50	21	1.80	0.20
400	74.50	8.50	14.50	2.50	23	1.71	0.29
500	67.00	11.00	18.75	3.25	29.75	1.70	0.30
600	63.90	12.00	20.00	4.10	32	1.67	0.34
700	57.00	14.10	23.50	5.40	37.60	1.67	0.38
800	53.00	15.20	25.10	6.70	40.3	1.65	0.44

7.3.2 Crystalline Structure

The crystalline structure of pure MoS_2 film (as a reference) and the DLC-MoS_2 composite films was characterized using XRD and the results are presented in Figure 7.1. It can be seen that pure MoS_2 film shows MoS_2 peaks of (100) at $2\theta \approx 33°$ and (110) at $2\theta \approx 59°$ in its pattern. When comparing to the pure MoS_2 XRD pattern, peak position of DLC-MoS_2 films shifted to higher diffraction angles (from 33 to $\approx 35°$ for (100) and from 59 to $\approx 61°$ for (110)) indicating a lower lattice constant. According to Fleischauer *et al.* (1999), this shift is due to the formation of a solid solution of $MoS_{2-x}O_x$ in the structure. This is because the atomic radius of O is smaller than that of S, so the replacement of S with O decreases the lattice parameters. Actually, peak shifting to higher angular positions is due to the uniform compressive stress (strain) in the lattice structure, i.e. lattice contraction (uniform macrostrain). Also, some peak broadening and some peak asymmetry in the XRD patterns are observed which might be due to non-uniform microstrain as a consequence of interstitials or vacancies. In addition, it can be seen that with the raise of carbon content (by decreasing target bias voltage from 800 to 200 V), the peaks become broadened and the peak intensity reduces correspondingly, indicating a gradual decrease in crystallinity and a raise in amorphization. According to Evaristo *et al.* (2008), DLC-WS_2 films show the same trend of gradual decrease in crystallinity with the raise of carbon content in the films.

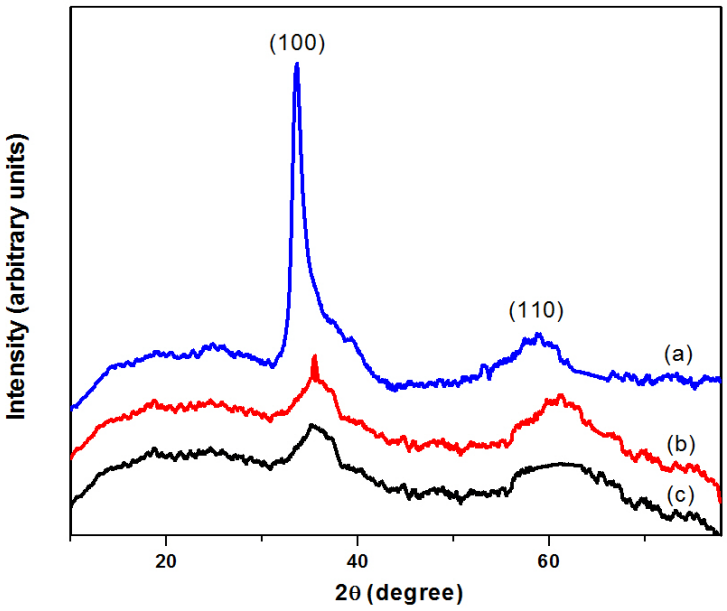

Figure 7.1. XRD pattern of (a) pure MoS_2 film, (b) DLC-MoS_2 film deposited at target bias voltage of -800 V, (c) DLC-MoS_2 film deposited at target bias voltage of -200 V.

7.3.3 Electronic and Bonding Structure

Figure 7.2 shows S K and Mo L_{III} edge XANES spectra of the DLC-MoS_2 thin films deposited under different target bias voltages, recorded in the total electron yield (TEY), a surface sensitive mode. The results demonstrate that for all DLC-MoS_2 films, the main peaks are Mo^{4+} and S^{2-}, indicating the formation of MoS_2 and $MoS_{2-x}O_x$ structures, which is in agreement with the XRD and chemical composition results (Zubavichus *et al.*, 1997). With increasing the absolute value of sputtering target bias voltage from 200 V to 800 V, the Mo^{4+} and S^{2-} peak signals have been intensified revealing an increase in MoS_2 and $MoS_{2-x}O_x$ components, in consistent with the chemical composition results. At the same time, by increasing the voltage from 200 V to 800 V, Mo^{6+} and S^{6+} signals have been intensified a bit, revealing the formation of structures such as $Mo(SO_4)_3$ in a small amount (a little more oxidation at the surface).

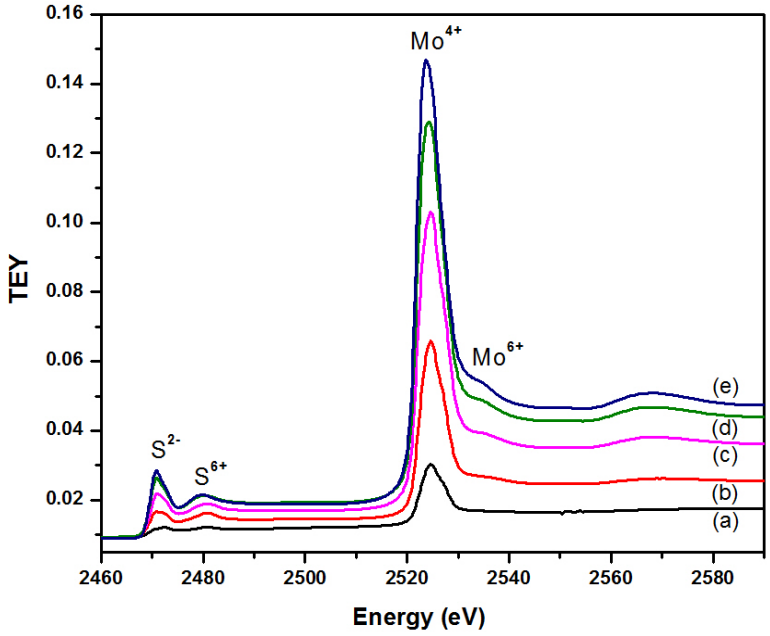

Figure 7.2. S K and Mo L_{III} edge XANES spectra of DLC-MoS_2 thin films deposited at different target bias voltage of (a) -200 V, (b) -300 V, (c) -400 V, (d) -600 V, (e) -800 V.

Figure 7.3 shows typical Raman spectra of DLC-MoS_2 films with different MoS_2 content synthesized under different target bias voltages. For DLC-MoS_2 films, not only the typical D and G peaks of DLC, but also two peaks approximately at 383 and 408 cm^{-1} corresponding to MoS_2 (Frey *et al.*, 1999), were observed. Moreover, by increasing the target bias voltage value from 200 to 800 V, the relative intensity of MoS_2 peaks raised which correlate well with the chemical composition and XANES results and demonstrate the increase of MoS_2 component in the composite film. After deconvolution and fitting of the Raman spectra (mixed Gaussian/Lorentzian) into the D and G peaks, the intensity ratio of the G and D peaks (I(D)/I(G)) and the G peak position were extracted. Figure 7.4 presents the results of I(D)/I(G) and G peak position calculated from the spectra of the pure DLC sample (MoS_2 target bias voltage= 0) and DLC-MoS_2 samples deposited at different target bias voltage. It can be observed that G peak

position shifts up and the I(D)/I(G) increases with increasing the absolute value of MoS_2 target bias voltage from 0 to 800 V. The increase in I(D)/I(G) ratio and the G-band upward shift position are accompanied by raised graphitic content in the film (see section 4.3.2 for detailed mechanism). Also based on the correlation between sp^3 content of the DLC thin films and I(D)/I(G) ratio, which explained in section 4.3.2, it can be understood that the sp^3 content of the DLC films decreases by increasing the I(D)/I(G) or G position. So, it can be deduced that sp^3 bonding content in the DLC-MoS_2 films decreases when the absolute value of target bias voltage increases from 200 to 800 V which directly implies an increase in sp^2 content. This increase in sp^2 content with increase of MoS_2 concentration indicates that the addition of MoS_2 induces and promotes the formation and clustering of graphitic (sp^2) bonds in DLC matrix by modifying the DLC network (the presence and inclusion of MoS_2 domains in DLC matrix increases the C-sp^2 sites by degrading the stress-induced C-sp^3 bonds, so the content of sp^2-C is increased and the sp^3-C content is decreased with increasing MoS_2 content in the composite thin films). According to Bharathy *et al.* (2010b), Ti causes the same effect in Ti-DLC composite coatings.

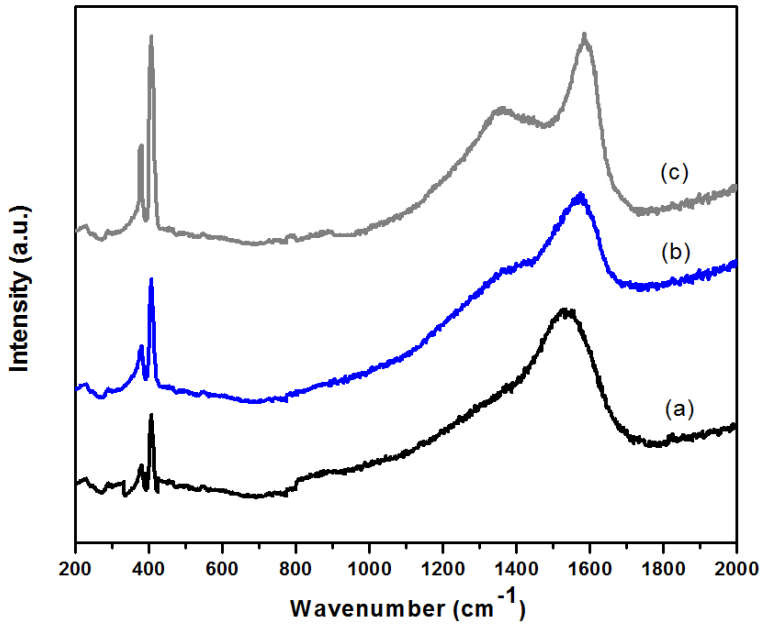

Figure 7.3. Raman spectra of DLC-MoS_2 films deposited at different target bias voltage of (a) -200 V, (b) -500 V, (c) -800 V.

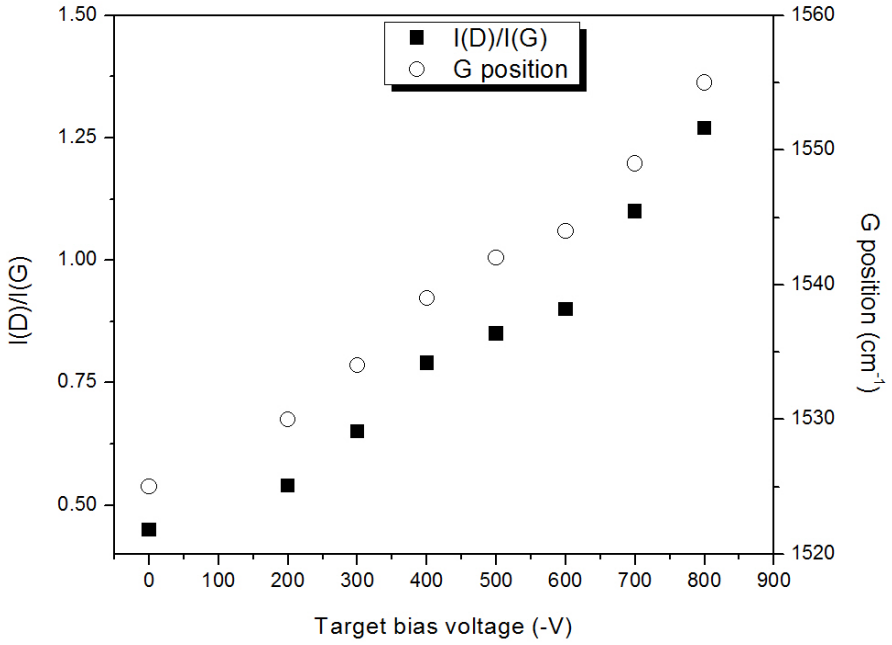

Figure 7.4. Raman G peak position and I(D)/I(G) of pure DLC and DLC-MoS_2 films versus target bias voltage.

7.3.4 Mechanical Properties

Hardness and Young's modulus values of the pure DLC film (MoS_2 content= 0) and DLC-MoS_2 films as a function of the MoS_2 content are displayed in Figure 7.5. It can be seen that for the DLC-MoS_2 films the hardness decreases from 9.1 GPa to 7 GPa, and the Young's modulus decreases from 100 GPa to 78 GPa with increasing the MoS_2 content from 16.8 to 40.3 at.% (for the films synthesized with the target bias voltage from -200 V to -800 V respectively). Considering the pure DLC film, which was prepared for comparison with MoS_2 content= 0, the hardness and Young's modulus values were 12 GPa and 136 GPa respectively. The variation trends of the hardness and Young's modulus with the MoS_2 content are consistent with those of the Raman spectra, more specifically, sp^3 content of the films. Since the high hardness and Young's modulus values of DLC films are due to the sp^3 tetrahedral carbon, as sp^3 content reduces, the hardness and Young's modulus decrease (exact mechanism explained in section 4.3.3). By increasing the MoS_2 content, an increase in the sp^2 content (graphitization) of the DLC-MoS_2 films happens, which results in softening of the composite films. Previously, the same trend of softening induced by graphitization has been observed in the Ti-doped DLC thin films (Bharathy *et al.*, 2010b). Furthermore, MoS_2 is much softer than DLC and in the DLC-MoS_2 composite films, with increasing the absolute value of MoS_2 target bias voltage, the MoS_2 content increases while carbon (DLC) content decreases. So, by raise of the MoS_2 content, the percentage of harder component (DLC) would be reduced and the percentage of softer component (MoS_2) would be increased in the composite thin films. Consequently, by raise of the MoS_2 content, gradually the hardness of the DLC-MoS_2 composite thin films decreases.

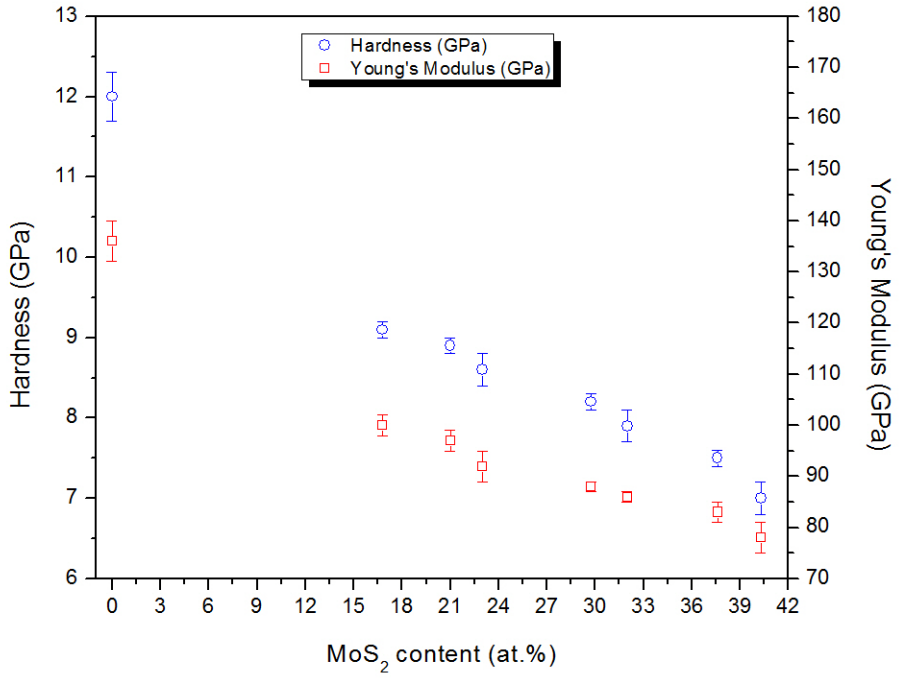

Figure 7.5. Hardness and Young's modulus of pure DLC and DLC-MoS_2 films versus MoS_2 content.

7.3.5 Tribological Properties

Figure 7.6 presents the typical graph of DLC-MoS_2 friction coefficient as a function of the number of sliding cycles for the films with various MoS_2 contents, synthesized at different target bias voltages. All curves measured for the pure MoS_2, pure DLC and DLC-MoS_2 films with different MoS_2 content were similar to these typical graphs, in which the short running-in period was described by higher friction, and then reduced down to a smaller value (the steady state level) after a few cycles. Figure 7.7 shows the coefficient of friction (COF) and wear coefficient, k, of the pure DLC film (MoS_2 content= 0) and DLC-MoS_2 films after 1000 cycle of sliding versus the MoS_2 content of the films. It can be observed that for the DLC-MoS_2 films by increasing the MoS_2 content from 16.8 to 40.3 at.%, COF and k raise (COF from 0.02 to 0.17

and k from 5×10^{-7} to 5×10^{-6} $mm^3N^{-1}m^{-1}$). Considering the pure DLC and pure MoS_2 films which were prepared for comparison of tribological properties; for pure DLC film, COF and k values were 0.05 and 1.5×10^{-6} $mm^3N^{-1}m^{-1}$ respectively, and in the case of pure MoS_2 film, COF and k values were 0.14 and 4×10^{-5} $mm^3N^{-1}m^{-1}$ respectively. So, it can be understood that for DLC-MoS_2 films with lower MoS_2 content e.g. 16.8 at.%, this composite coating demonstrates better tribological performances than pure DLC and pure MoS_2 films in ambient air environment. The variation trend of friction coefficient (COF) for the DLC-MoS_2 films with the increase of MoS_2 content could be related to the variation trend of film hardness and Young's modulus, and sp^3 content of the films, as discussed in section 4.3.4.The variation trend of wear coefficient of the DLC-MoS_2 films with MoS_2 content is also resulted from the variation trend of the film hardness with the raise of MoS_2 content. Also in accordance with Fleischauer *et al.* (1999), $MoS_{2-x}O_x$ has a positive effect on lubricant performance of MoS_2 films while more oxidation and formation of oxides such as $Mo(SO_4)_3$ has a negative influence on that leading to very low value of COF and k for DLC-MoS_2 films synthesized with low MoS_2 contents e.g. 16.8 at.% and gradually raise of those with higher MoS_2 contents e.g. 40.3 at.%.

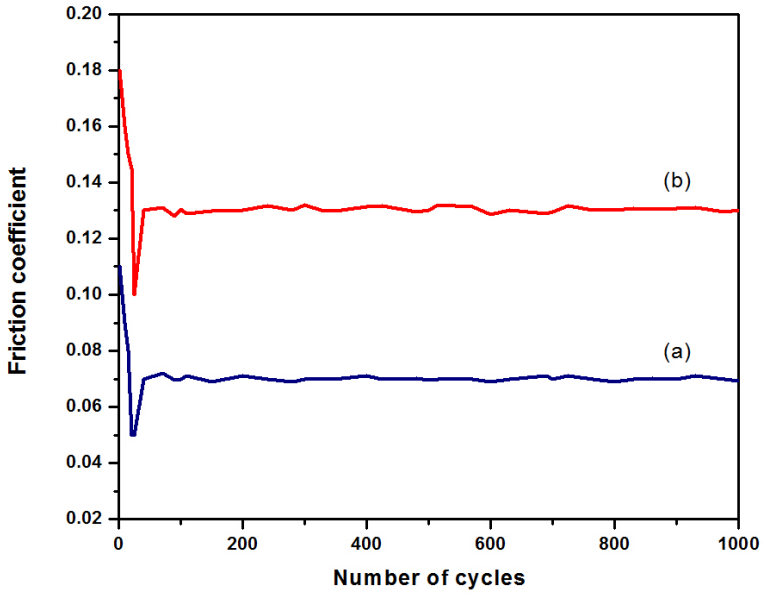

Figure 7.6. Typical graph of friction coefficient versus number of sliding cycles for DLC-MoS_2 films synthesized at different target bias voltage of (a) -400 V, (b) -700 V.

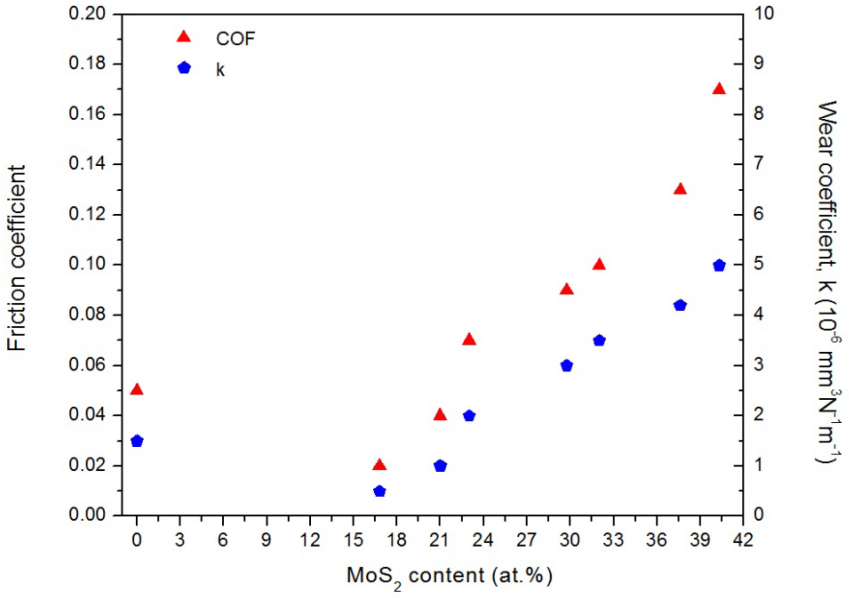

Figure 7.7. Coefficient of friction (COF) and wear coefficient (k) of pure DLC and DLC-MoS_2 films versus MoS_2 content.

7.3.6 Corrosion Resistance

Potentiodynamic polarization tests were carried out in 3.5% NaCl solution at room temperature. The corrosion potential and corrosion current were achieved from the Tafel analysis. Table 7.3 shows the corrosion potential and corrosion current of the pure DLC film (MoS_2 content= 0) and DLC-MoS_2 films with different MoS_2 content. By increasing the MoS_2 content from 0 to 40.3 at.%, corrosion potential decreases. It shows that the anti-corrosion behavior (nobility) of the DLC-MoS_2 films decreases with MoS_2 content increasing from 0 to 40.3 at.%. As presented in Table 7.3, when the MoS_2 content increases, the corrosion current raises slightly. But, one can say that for the whole range of MoS_2 content, the synthesized DLC and DLC-MoS_2 films showed promising corrosion resistance, i.e. very low corrosion rate. The decreased corrosion resistance for films with the increased MoS_2 content from 0 to 40.3 at.% (for the films synthesized with the target bias voltage from 0 to 800 V respectively) can be attributed to the raised electrical conductivity, reduced electrical resistivity and decreased films density induced by the reduced sp^3 content of the DLC-MoS_2 films which explained in section 4.3.5. According to the previous chapter results, pure DLC films show the same trend of decreasing the corrosion resistance with the drop of sp^3 content in the film.

Table 7.3. Corrosion potential and corrosion current of the pure DLC and DLC-MoS_2 thin films.

MoS_2 content (at.%)	Corrosion potential, E_{corr}, (mV)	Corrosion current, I_{corr}, (nA)
0 (pure DLC)	268	1.09
16.8	260	1.21
21	233	1.42
23	192	2.3
29.75	181	3.2
32	174	4.1
37.6	165	5.2
40.3	160	5.6

7.4 Conclusions

The DLC-MoS_2 composite thin films with low content of MoS_2 show better tribological properties, i.e. lower friction coefficient and lower wear coefficient, than either MoS_2 or DLC films, demonstrating great potential to be used as a protective coating for industrial applications in which the film is exposed to ambient air environment. The hardness, Young's modulus, and corrosion resistance of the composite films drop and the coefficient of friction and the wear coefficient increase with the increase of incorporation of MoS_2 into the film. The composite films are composed of DLC, MoS_2 and $MoS_{2-x}O_x$ and the content of Mo, S, and O in the form of MoS_2 and $MoS_{2-x}O_x$ in the films increase with the rise of negative bias voltage on the target. The incorporation of MoS_2 enhances the formation of graphitic (sp^2) bonds and decreases the sp^3 content in DLC.

CHAPTER 8 THERMAL STABILITY OF DLC-MOS_2 THIN FILMS IN DIFFERENT ENVIRONMENTS

Transition

In this chapter, improving the thermal stability of pure DLC thin film by making a composite coating including MoS_2 and hydrogenated DLC (DLC-MoS_2 composite thin film) is investigated. The effect of thermal annealing on the structure, mechanical and tribological properties of the pure DLC and DLC-MoS_2 thin films in ambient air and low pressure environments will be discussed. This chapter has been published in "*Thin Solid Films*" as follows: "Niakan H., C. Zhang, Y. Hu, J.A. Szpunar, Q. Yang. 2014. Thermal stability of diamond-like carbon-MoS_2 thin films in different environments. Thin Solid Films 562: 244-249".The PhD candidate designed and conducted the experiments, analyzed the results of the experiments and prepared the manuscript for publication under the supervision of Profs. Qiaoqin Yang and Jerzy Szpunar. C. Zhang assisted regarding the preparation of the specimens for DLC-MoS_2 thin film deposition, while Y. Hu helped in conducting XANES characterization and interpretation of XANES results. This manuscript has not been included in other theses. It has been reformatted from the original version for inclusion in this thesis and the text has been slightly modified to ensure clarity and avoid repetition.

8.1 Introduction

For most of industrial applications, the coatings may be exposed to elevated temperatures or localized heating induced by friction. Therefore, the thermal stability of DLC films not only determines the temperature range in which the DLC films can be used but also is very important for their long-term performance. As stated in previous chapters, DLC films consist of high fraction of sp^3-bonded carbon, a metastable structure, which has a natural tendency to turn to

stable graphitic structure, sp^2-bonded carbon. Previous investigations have already revealed that DLC films are unable to keep their superior properties at higher working temperatures because of this irreversible conversion in their structure, which restricts the application of these films (Zhang *et al.*, 2006; Peng *et al.*, 1998). This instability, so-called graphitization process, is highly noticeable in one of the major DLC categories, the hydrogenated DLC thin films (Louro *et al.*, 2011). According to Wang *et al.* (1996), annealing of the hydrogenated DLC films at elevated temperatures causes hydrogen evolution, the conversion of sp^3-bonded carbon to sp^2-bonded carbon, and thus deteriorating their diamond-like characteristics. Recently, doping metal or non-metal elements such as Ti, W, and Si to DLC coating to form nanocomposite coatings has been shown to be effective in improving thermal stability and other properties (Choi *et al.*, 2007b). However, most of these studies have been conducted to investigate the thermal stability of the DLC films in a vacuum environment rather than in ambient air or low pressure environments.

As studied in chapter 7, tribological properties of DLC films doped with MoS_2 are improved as comparing with pure MoS_2 or pure DLC films under ambient air environment which it might be favorable in some industrial applications. As stated earlier in this chapter, most of these industrial applications may expose the coatings to elevated temperatures or localized elevated temperatures induced by friction. Thus the thermal stability of the DLC-MoS_2 composite coatings is crucial for their application and it has not been investigated previously. In this study, the synthesis of DLC-MoS_2 composite thin films using biased target ion beam deposition (BTIBD) was carried out, in which MoS_2 was produced by sputtering a biased MoS_2 target by Ar ion beam while DLC was deposited by an end-Hall ion source with CH_4 gas as carbon source simultaneously. DLC films without MoS_2 were also deposited for comparison. The thermal stability (both the structure and properties) of the DLC based composite and DLC

films were studied by annealing the films in ambient air and low pressure atmospheres (to investigate the effect of changing the annealing atmosphere) at different temperatures.

8.2 Experimental

8.2.1 Synthesis of DLC and DLC-MoS_2 Thin Films

Mirror polished p-type Si (100) wafers were used as substrate for this investigation. Firstly, the substrates were cleaned as explained in section 4.2.1. The deposition experiments were carried out using the deposition system mentioned in section 3.1.1. Hydrogenated DLC thin film deposition was carried out by introducing Methane (CH_4) gas into the deposition ion source to produce hydrocarbon radicals and ions. For deposition of DLC-MoS_2 composite thin films, a MoS_2 target of 99.99% purity, sputtered by Ar ion beam, was used to produce MoS_2 simultaneously with the deposition of DLC. The synthesis parameters are shown in Table 8.1.

Table 8.1. Deposition conditions for DLC and DLC-MoS_2 thin films.

Mean ion energy (eV) (for DLC)	85
Target bias voltage (-V) (for MoS_2)	400
Discharge current (A) (for MoS_2)	4
Time (hr)	6
Substrate temperature (°C)	<50
Working pressure (Torr)	1×10^{-4}

8.2.2 Thermal Annealing and Microstructural Characterization

In order to investigate the thermal stability of the deposited films, thermal annealing was performed in ambient air and low pressure environments as explained in section 3.1.2. The

annealing temperatures ranged from 100 to 600 ºC at an interval of 100 ºC. After annealing, the samples were analyzed using Raman spectroscopy, synchrotron-based X-ray absorption near edge structure (XANES), and scanning electron microscope (SEM). Raman spectra were obtained using a micro-Raman system which described in section 3.2.2. Synchrotron-based XANES spectra of the samples were obtained using the Soft X-ray Microanalysis Beamline of the Canadian Light Source as explained in section 3.2.4. The WINXAS software was used to normalize raw data and subtract background. Sample surfaces were analyzed using a Hitachi SU-6600 field emission SEM with an Oxford Instrument energy dispersive X-ray spectroscopy (EDS) attachment as discussed in section 3.2.6. EDS was mainly used to obtain the elemental mapping of the samples, and the chemical composition of the films was evaluated by electron probe microanalysis (EPMA). Mechanical properties (hardness and Young's modulus) of the films were measured by nanoindentation technique as described in section 3.2.7. The tribological characteristics of the films were obtained using a ball-on-disc tribometer which explained in section 3.2.8.

8.3 Results and Discussion

8.3.1 Chemical Composition of DLC-MoS_2 Thin Films

Table 8.2 shows the chemical composition of the DLC-MoS_2 thin film before and after thermal annealing in ambient air and low pressure atmospheres. For as-deposited DLC-MoS_2 film, the S/Mo and O/Mo ratio are approximately 1.7 and 0.3, respectively. The atomic percentage of Mo, S and O indicates the formation of $MoS_{2-x}O_x$ in the film. According to Fleischauer *et al.* (1999), the formation of a solid solution of $MoS_{2-x}O_x$ in the structure has positive influences on the performance of the film. Also, Sub-stoichiometry of molybdenum disulfide, represented by MoS_{2-x}, in the deposited thin film is probably originated from the

reaction with residual oxygen in the deposition chamber (Lévy *et al.*, 1994). However, the S/Mo ratio in the deposited thin film is higher than the amount which molybdenum disulfide still exhibits self-lubricating behaviors (Lansdown, 1999). The chemical composition of the DLC-MoS_2 films after annealing scarcely changes up to 400 °C in air and 500 °C in low pressure atmosphere. Afterwards, the C and S content, and S/Mo ratio decrease and the O content increases significantly with increasing the annealing temperature up to 600 °C indicating further oxidation at the surface and formation of structures such as MoO_2, MoO_3 and $Mo(SO_4)_3$ at this situation.

Table 8.2. Chemical composition of DLC-MoS_2 thin film before and after thermal annealing.

Samples	Chemical composition (at.%)				
	C	Mo	S	O	S/Mo
As-deposited DLC-MoS_2	74.50	8.50	14.50	2.50	1.70
DLC-MoS_2-Air-400 °C	72.50	8.50	14.00	5.00	1.65
DLC-MoS_2-Air-500 °C	65.00	8.50	2.50	24.00	0.30
DLC-MoS_2-Air-600 °C	62.00	8.50	2.00	27.50	0.24
DLC-MoS_2-Low P-400 °C	74.00	8.50	14.00	3.50	1.65
DLC-MoS_2-Low P-500 °C	73.00	8.50	14.00	4.50	1.65
DLC-MoS_2-Low P-600 °C	66.00	8.50	3.00	22.50	0.35

8.3.2 Electronic and Bonding Structure of DLC and DLC-MoS_2 Thin Films

Figure 8.1 illustrates typical Raman spectra of as-deposited DLC film, as-deposited DLC-MoS_2 film, and DLC-MoS_2 film annealed in low pressure environment at 600 ºC. For DLC thin

film (before and after thermal annealing), the signature of a typical DLC film was observed in the spectra (D and G peaks). For DLC-MoS_2 films (before and after thermal annealing), not only the typical D and G peaks of DLC, but also two peaks corresponding to MoS_2 (approximately at 383 and 408 cm^{-1}) were observed. In the case of DLC-MoS_2 film annealed in low pressure at 600 ºC (or in air at 500 and 600 ºC), the relative intensity of MoS_2 peaks decreased and a new peak corresponding to MoO_3 (approximately at 820 cm^{-1}) was identified, which correlate well with the chemical composition results and demonstrate the increase of oxidation in the film. After deconvolution and fitting of the Raman spectra (mixed Gaussian/Lorentzian) into the D and G peaks, the intensity ratio of the G and D peaks (I(D)/I(G)) and the G peak position were derived. Figure 8.2 describes the results of I(D)/I(G) and G peak position calculated from the spectra of the pure DLC and DLC-MoS_2 samples annealed at various temperatures in air and low pressure environments. For pure DLC in air and low pressure environments, it can be seen that I(D)/I(G) and G peak position scarcely change as the temperature increases up to 200 and 300 °C, respectively. Afterwards, the G peak position shifts up and the I(D)/I(G) raises with increasing the annealing temperature, and the pure DLC film does not show carbon peaks in the Raman spectrum after annealing at over 400 °C in air and over 500 °C in low pressure. But for DLC-MoS_2 samples in air and low pressure environments, the I(D)/I(G) and G peak position scarcely change as the temperature increases up to 400 and 500 °C, respectively. Afterwards, the G peak position shifts up and the I(D)/I(G) raises with increasing the annealing temperature, and the DLC-MoS_2 films still show carbon peaks after annealing at 600 °C. Based on the theoretical analysis of Raman spectra from amorphous carbon (Zou *et al.*, 2009), the G-band upward shift implies that some bond-angle disorders have been annealed out and the tetrahedral bonds (sp^3-bonded carbon) have been broken and converted to trigonal bonds (sp^2-bonded carbon),

accompanied by raised graphitic content in the film. Also the rise in I(D)/I(G) indicates a rise in the graphitic content of the films and a reduction in the sp^3 content of the DLC films (Zhang *et al.*, 2000). Additionally based on the correlation between sp^3 content of the DLC thin films and the I(D)/I(G) ratio, which discussed in section 4.3.2, it can be understood that the sp^3 content of the DLC films reduces by increasing the I(D)/I(G) or G position. So, it can be concluded that the DLC thin films were gradually graphitized and oxidized at elevated temperatures, and the number or size of graphitic sp^2 domains raised (Fu *et al.*, 2005). Tallant *et al.* (1995) have found that in pure DLC films, sp^3 began to transform to sp^2 at around 200–300 ºC and completely transformed at around 450 ºC, which is in consistent with the results of this investigation. A relative constant ratio of I(D)/I(G) and G-peak position for DLC-MoS_2 films throughout a wider range of annealing temperatures indicates a slower rate of graphitization and higher thermal stability compared to the DLC films.

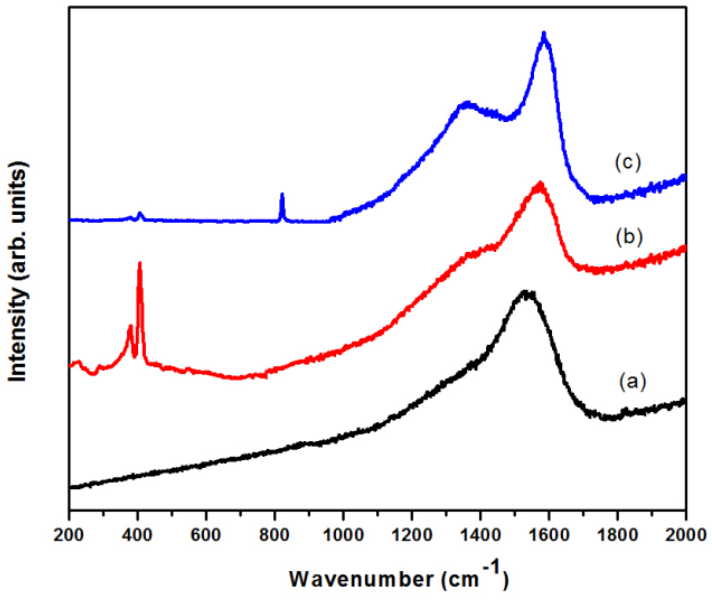

Figure 8.1. Raman spectra of (a) as-deposited DLC film, (b) as-deposited DLC-MoS_2 film, (c) DLC-MoS_2 film annealed in low pressure at 600 ºC.

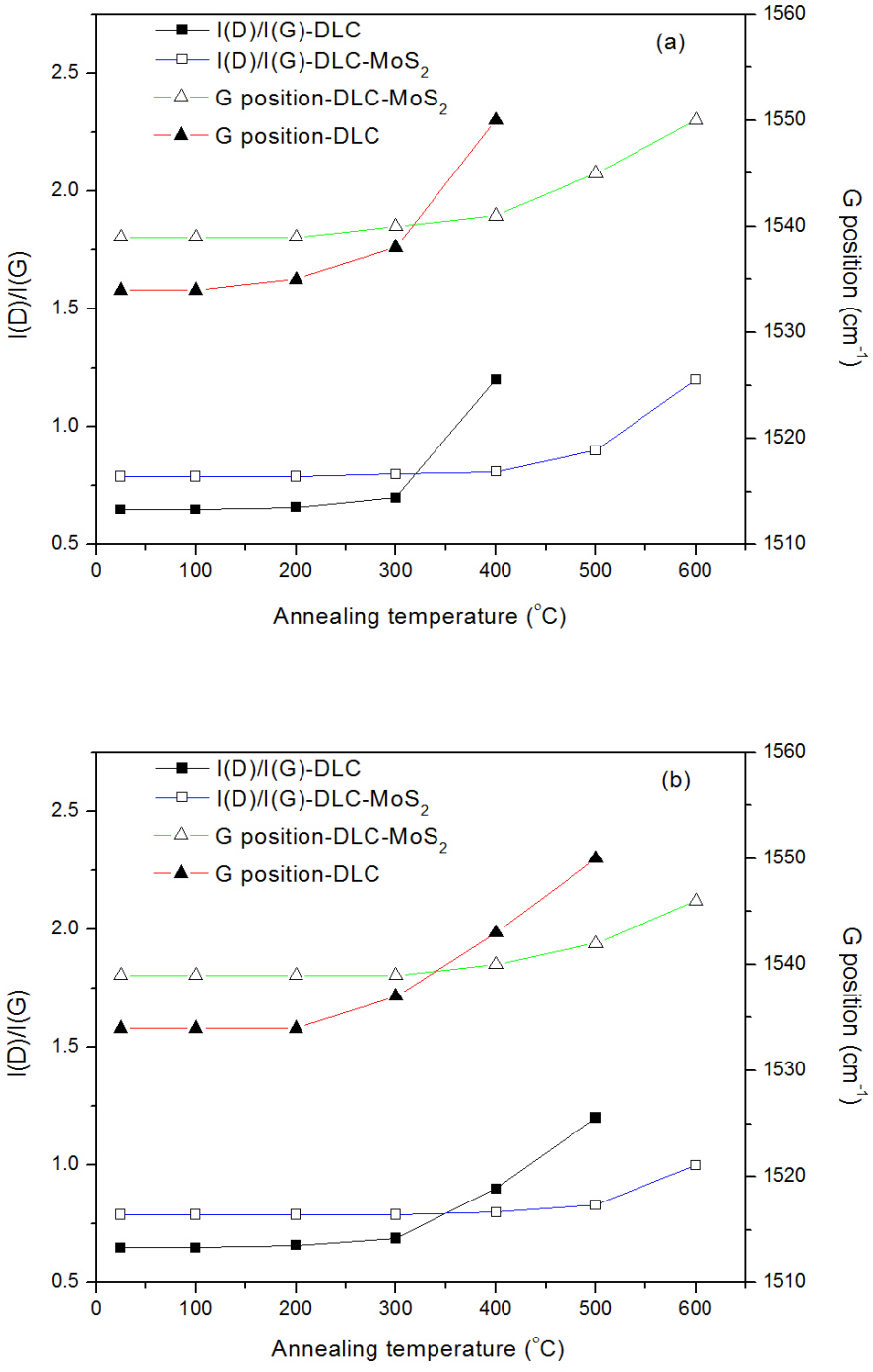

Figure 8.2. Raman G peak position and I(D)/I(G) of DLC and DLC-MoS_2 films before and after annealing at various temperatures in (a) air, (b) low pressure.

Figure 8.3 presents S K and Mo L_{III} edge XANES spectra of as-deposited and annealed DLC-MoS_2 thin films recorded in the total electron yield (TEY), a surface sensitive mode. The results show that for as-deposited DLC-MoS_2 film, the main peaks are Mo^{4+} and S^{2-}, revealing the formation of MoS_2 and $MoS_{2-x}O_x$ structures, which is in agreement with the chemical composition analysis (Zubavichus *et al.*, 1997). For the film annealed in low pressure at 500 ºC, similar pattern is observed but with increased oxidation. For the films annealed in low pressure at 600 ºC or in air at 500 ºC, S^{2-} signal is very weak while Mo^{4+}, Mo^{6+} and S^{6+} signals are much stronger, indicating the formation of oxides such as MoO_2, $Mo(SO_4)_3$, or MoO_3 and consequently deterioration of the film performance, which is in agreement with the chemical composition and Raman spectroscopy results.

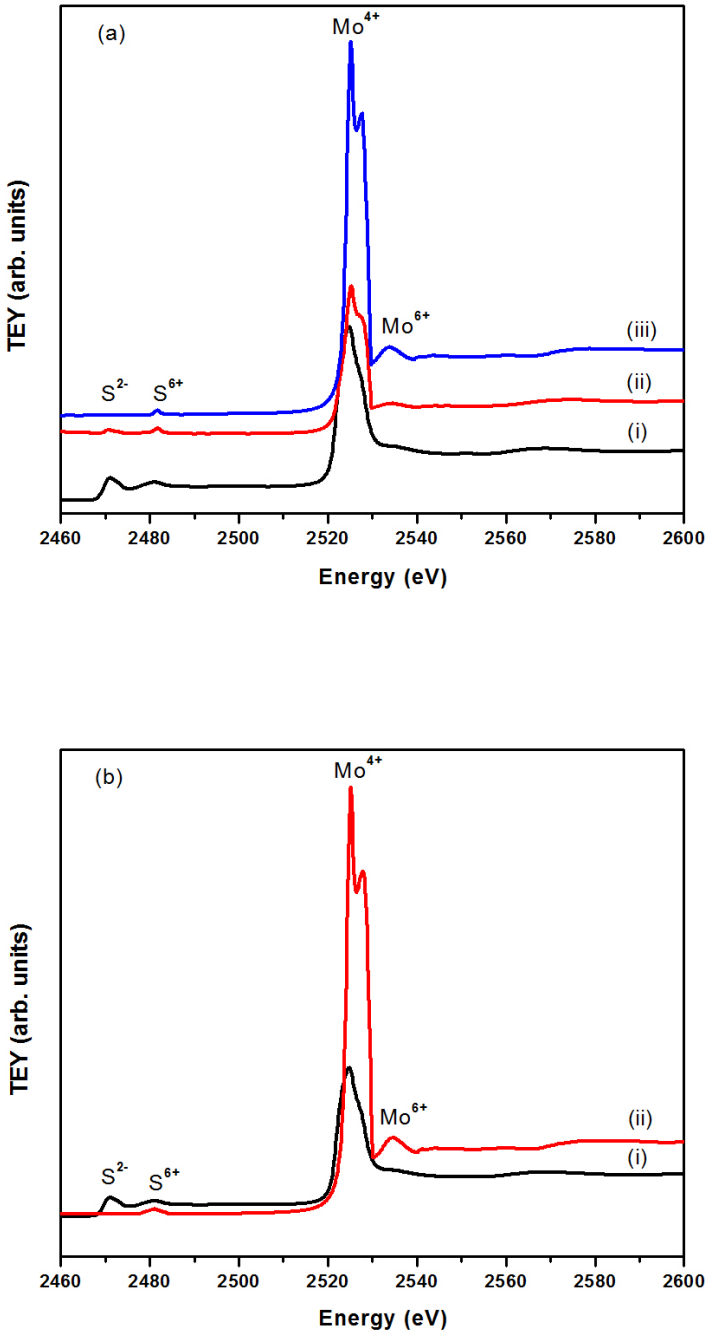

Figure 8.3. S K and Mo L_{III} edge XANES spectra of as-deposited and annealed DLC-MoS_2 thin films in (a) low pressure atmosphere: (i) as-deposited DLC-MoS_2 film, (ii) DLC-MoS_2 film annealed at 500 ºC, (iii) DLC-MoS_2 film annealed at 600 ºC; and (b) air atmosphere: (i) as-deposited DLC-MoS_2 film, (ii) DLC-MoS_2 film annealed at 500 ºC.

8.3.3 Surface Morphology and Elemental Mapping

Figure 8.4 presents morphology and elemental mapping of as-deposited DLC-MoS_2 film samples and DLC-MoS_2 samples after thermal annealing in low pressure atmosphere at 500 ºC. SEM micrographs show that the as-deposited DLC and DLC-MoS_2 films were very compact and homogeneous with featureless morphologies (an amorphous-like morphology). It can be seen that for as-deposited DLC-MoS_2 film (Figure 8.4 (a)), a homogeneous structure with uniformly distributed Mo, S, O, (MoS_2/$MoS_{2-x}O_x$) and C (DLC) has formed, in consistent with the chemical composition and XANES results. But, after annealing at high temperature (e.g. 500 ºC) the carbon matrix becomes heterogeneous with many voids (cavities), and regions containing Mo, S, and O (probably $MoS_{2-x}O_x$) are topographically lying on top of the matrix after thermal annealing at 500 ºC (Figure 8.4 (b)).

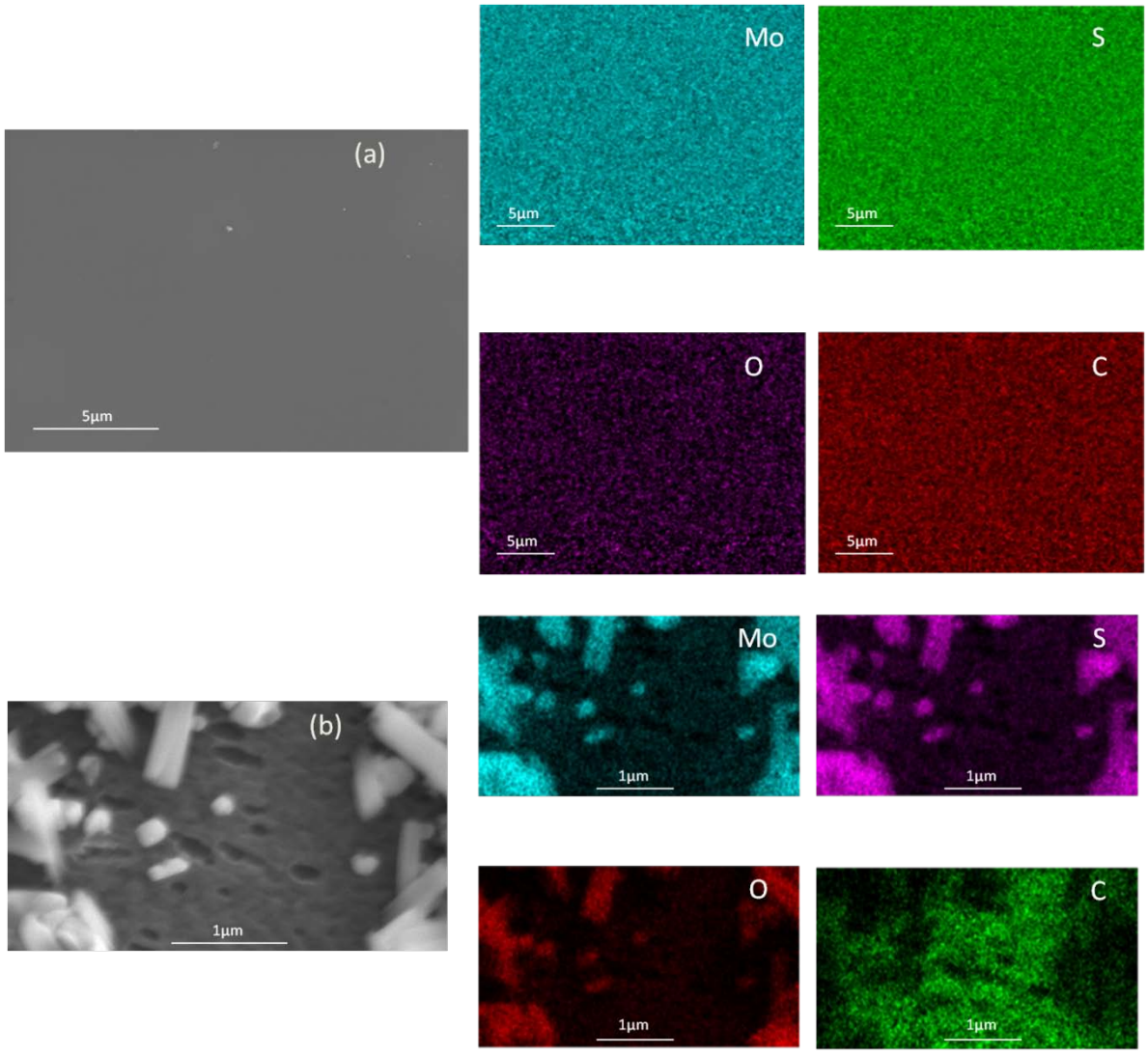

Figure 8.4. Surface morphology and elemental mapping of (a) as-deposited DLC-MoS_2 film samples, (b) DLC-MoS_2 film samples after thermal annealing in low pressure at 500 ºC.

8.3.4 Mechanical Properties of DLC and DLC-MoS_2 Thin Films

Hardness and Young's modulus values of the DLC and DLC-MoS_2 films as a function of the annealing temperature in air and low pressure are presented in Figure 8.5. For pure DLC heat treated in air, a slight decrease of the hardness and Young's modulus values in films was observed at the annealing temperature less than 200 °C, and then reduced significantly when the annealing temperature increases to 400 °C. In terms of DLC-MoS_2 films heat treated in air, the

hardness and Young's modulus values scarcely change but remain as high as the original values up to 400 °C. Afterwards, they start to drop a little (up to 600 °C). Regarding the pure DLC heat treated in low pressure, a slight decrease of the hardness and Young's modulus values in films was observed at the annealing temperature less than 300 °C, and then reduced significantly when the annealing temperature increases to 500 °C. In terms of DLC-MoS_2 films heat treated in low pressure, the hardness and Young's modulus values scarcely change but remain as high as the original values up to 500 °C. Afterwards, they start to drop a little (up to 600 °C). The variation trends of the hardness and Young's modulus with annealing temperature are consistent with those of the Raman spectra, more specifically, sp^3 content of the films. Since the great mechanical properties of DLC films are resulted from the sp^3 tetrahedral carbon, as sp^3 content decreases, the hardness and Young's modulus reduce (detailed mechanism explained in section 4.3.3). During the annealing of DLC films at elevated temperatures, the conversion of sp^3-bonded carbon to sp^2-bonded carbon or the growth of sp^2-bonded clusters occurs, which results in softening of the annealed films. Therefore, for pure DLC hardness and Young's modulus dramatically decrease when annealing temperature increases to 400 °C in air and 500 °C in low pressure as sp^3 content of the films severely drops at these temperatures. But in terms of DLC-MoS_2 film, hardness and Young's modulus gradually and slowly decrease when annealing temperature increases up to 600 °C in air and low pressure atmospheres because of the mild and slow drop of the sp^3 content.

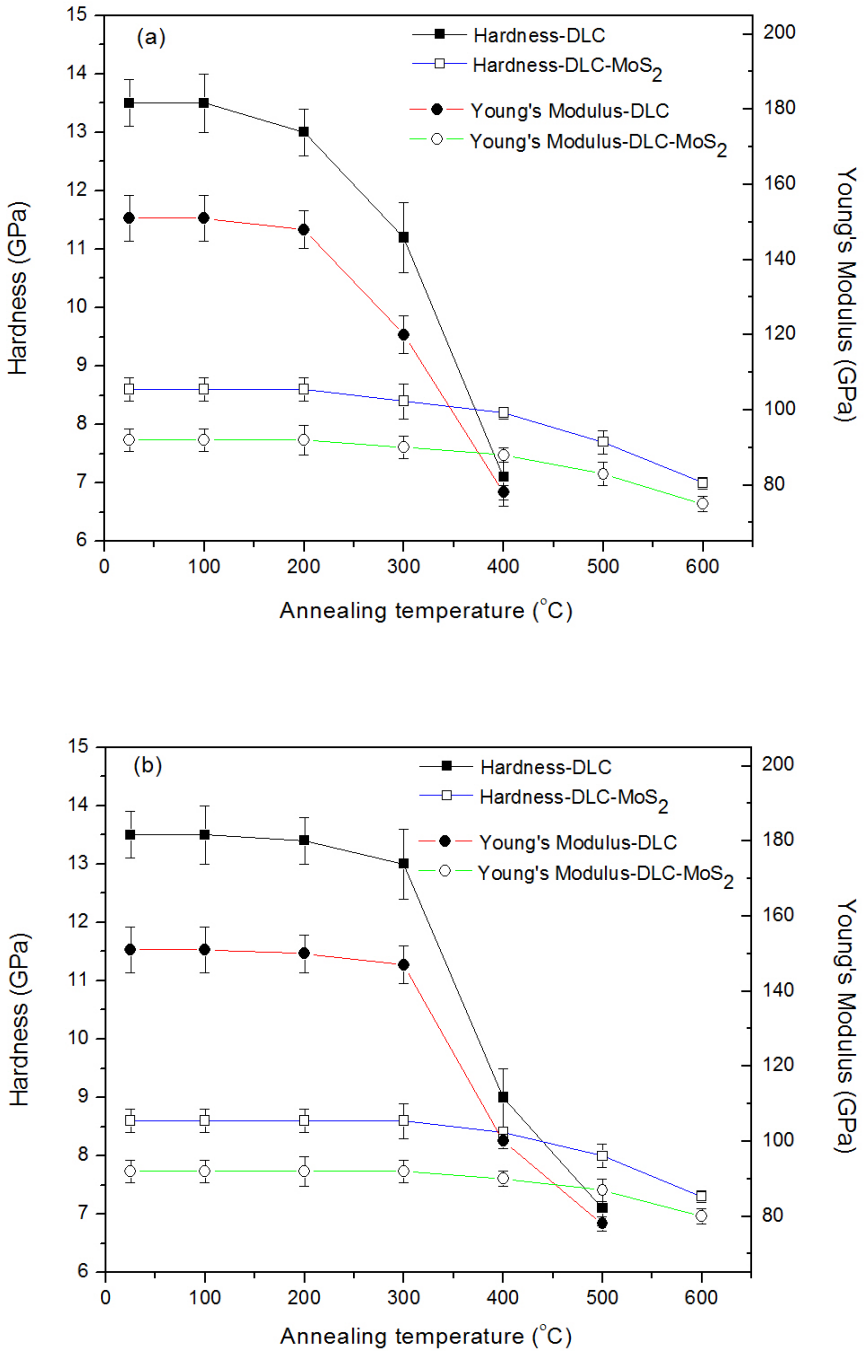

Figure 8.5. Hardness and Young's modulus of DLC and DLC-MoS_2 films annealed at different temperatures in (a) air, (b) low pressure.

8.3.5 Tribological Properties of DLC and DLC-MoS_2 Thin Films

Figure 8.6 illustrates the typical graph of DLC-MoS_2 friction coefficient as a function of the number of sliding cycles for the as-deposited film and the film annealed in low pressure at 600 °C. All curves measured for DLC and DLC-MoS_2 films before and after annealing in air and low pressure at different temperatures were similar to this typical graph, in which the short running-in period was described by higher friction, and then reduced down to a smaller value (the steady state level) after a few cycles. Figure 8.7 presents the coefficient of friction (COF) and wear coefficient, k, of the DLC and DLC-MoS_2 films after 1000 cycle of sliding versus the temperature at which they annealed in air and low pressure atmospheres. For pure DLC heat treated in air, COF and k remain relatively constant until 200 °C, and then rise significantly when the annealing temperature increases to 400 °C (COF from 0.04 to 0.4 and k from 1.5×10^{-6} to 19.5×10^{-6} $mm^3N^{-1}m^{-1}$). Considering the DLC-MoS_2 film heat treated in air, COF and k remain relatively constant until 400 °C. Afterwards, they start to increase moderately (comparing to pure DLC) up to 600 °C (COF from 0.07 to 0.18, and k from 2×10^{-6} to 6×10^{-6} $mm^3N^{-1}m^{-1}$). Regarding the pure DLC heat treated in low pressure atmosphere, COF and k remain relatively constant until 300 °C, and then raise significantly when the annealing temperature increases to 500 °C (COF from 0.04 to 0.3 and k from 1.5×10^{-6} to 15×10^{-6} $mm^3N^{-1}m^{-1}$). In terms of the DLC-MoS_2 film heat treated in low pressure environment, COF and k remain relatively constant until 500 °C. Afterwards, they start to increase moderately (comparing to pure DLC) up to 600 °C (COF from 0.07 to 0.14 and k from 2×10^{-6} to 5×10^{-6} $mm^3N^{-1}m^{-1}$). The variation trend of friction coefficient (COF) for the DLC and DLC-MoS_2 films with annealing temperature could be ascribed to the variation trend of film hardness and Young's modulus with annealing, and sp^3 content of the films, as explained in section 4.3.4. On the other hand, based on Li *et al.* (2006),

the friction mainly results from the chemical interactions induced by the strong dangling σ-bonds at the sliding interfaces, and the weak π–π interactions of sp^2 bonds will also cause an extra friction force. By annealing the film at elevated temperatures, large amount of hydrogen effusion from the film happens, and the dangling σ-bonds and π–π interactions will appear on the sliding surface. Therefore, the COF of the annealed DLC films rises with the raised temperature. The variation trend of wear coefficient of the DLC and DLC-MoS_2 films with annealing temperature is also related to the variation trend of the film hardness with the raise of annealing temperature. Since harder surfaces wear less, the decreased film hardness with annealing leads to the rise of wear coefficient of the annealed DLC films with the increase of temperature. Also in accordance with Fleischauer *et al.* (1999), $MoS_{2-x}O_x$ has a positive influence on lubricant performance of MoS_2 films while more oxidation and formation of oxides such as MoO_2, $Mo(SO_4)_3$, or MoO_3 has a negative effect on that leading to relatively stable value of COF and k up to high temperatures for DLC-MoS_2 film and gradually degrading of those at higher temperatures. Actually, MoS_2 has a higher thermal stability than the DLC (the thermal stability of MoS_2 in non-oxidizing atmospheres is nearly up to 1100 °C, while in ambient air atmosphere, substantial oxidation occurs at around 400 °C) (Booser, 1989). Even though MoS_2 has a higher thermal stability than the DLC, if there is no synergistic effect from combining both, the thermal stability of the composite coating would not be that much higher than the DLC because DLC is the matrix. The synergistic effect is probably from the uniformly distributed MoS_2 molecules which increase the energy barrier to transform metastable sp^3 to sp^2 carbon due to the thermal treatment.

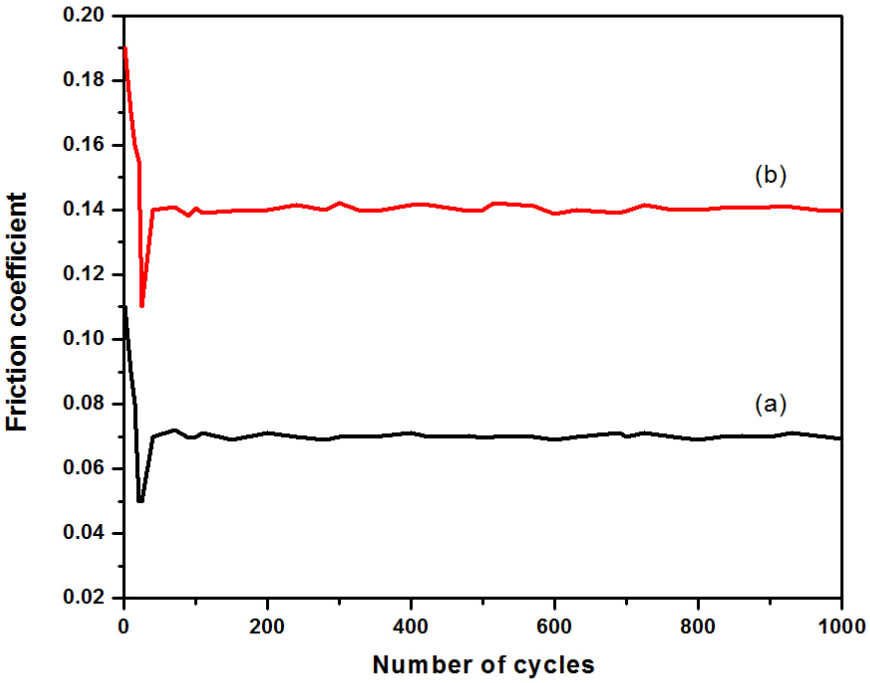

Figure 8.6. Typical graph of friction coefficient versus number of sliding cycles for (a) as-deposited DLC-MoS_2 film, (b) DLC-MoS_2 film annealed in low pressure at 600 ºC.

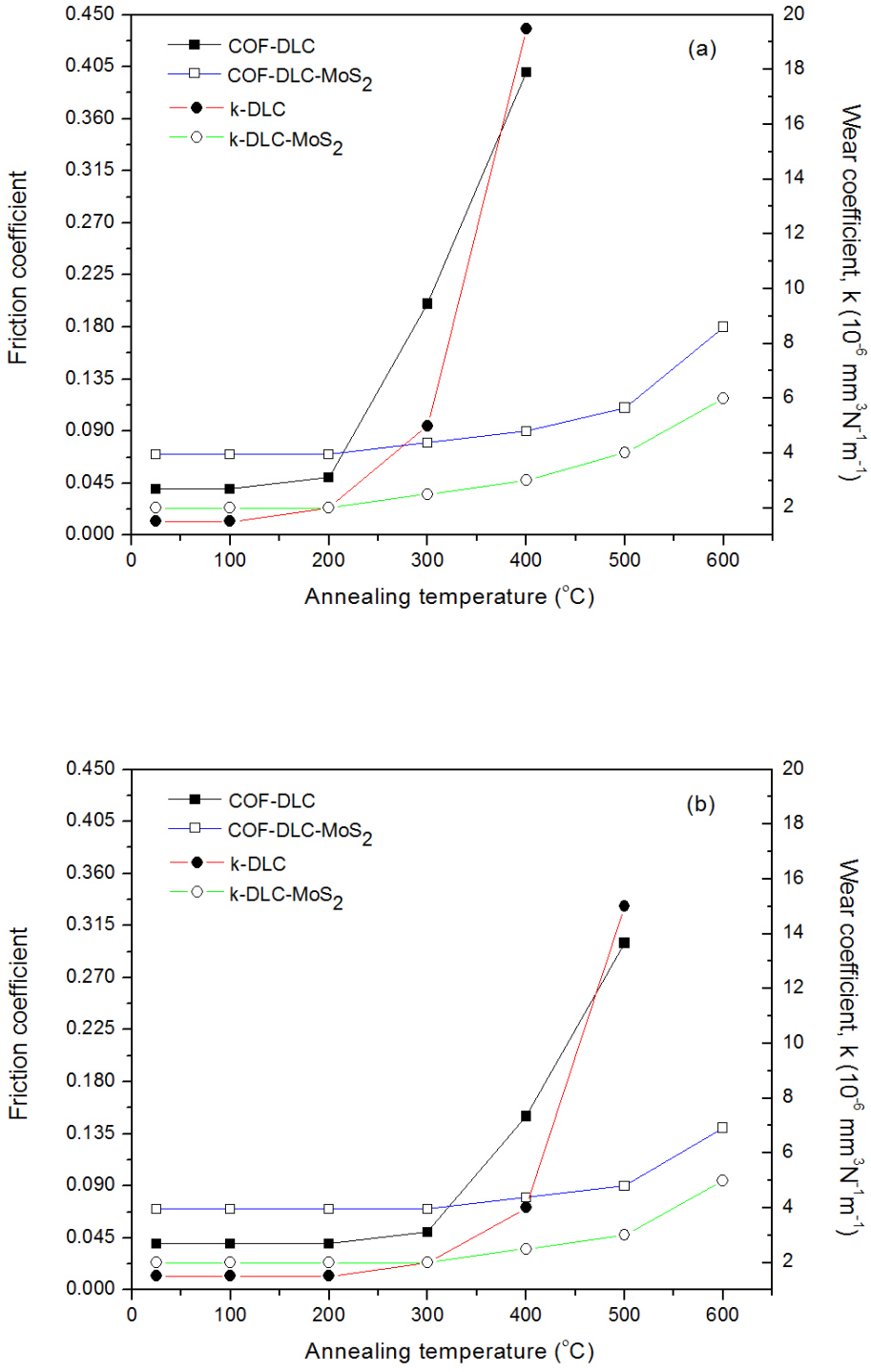

Figure 8.7. Coefficient of friction (COF) and wear coefficient (k) of DLC and DLC-MoS_2 films versus annealing temperature in (a) air, (b) low pressure.

8.4 Conclusions

The thermal stability of DLC films can be improved by fabricating a composite film including DLC and MoS_2, and the DLC-MoS_2 coating is promising to be employed as a protective coating for industrial applications in which the coating may be exposed to elevated temperatures. Pure DLC is thermally stable up to 200 °C in air and 300 °C in low pressure, after which, film mechanical and tribological performances drastically drop with the increase of treating temperature because of graphitization, which leads to an increase in sp^2 and decrease in sp^3 bonding structure. DLC-MoS_2 film is thermally stable up to 400 °C in air and 500 °C in low pressure. Afterwards, the mechanical and tribological performances of the film drop moderately up to 600 °C. Annealing in low pressure atmosphere slows down the oxidation and degradation of DLC and DLC-MoS_2 films at elevated temperatures. Structural characterization shows that formation of $MoS_{2-x}O_x$ structure is responsible for higher thermal stability of DLC-MoS_2 film, while more oxidation and formation of oxides such as MoO_2, $Mo(SO_4)_3$, or MoO_3 at higher temperatures causes the gradual degradation of the film.

CHAPTER 9 CONCLUSIONS AND FUTURE WORK

9.1 Conclusions

The major findings of this thesis work are summarized as follows:

(1) Hydrogen-free DLC thin films have been successfully synthesized by biased target sputtering of graphite target without additional ion bombardment either by negative bias of substrate or assisting ion source, while additional ion bombardment is essential to obtain DLC by other sputtering techniques. The films obtained by this method are continuous and uniform with different structure and properties depending on the target bias voltage. The films prepared at target bias voltage of -800 V show the lowest roughness, friction coefficient (COF) and wear coefficient (k) and the highest sp^3 content, hardness, Young's modulus and corrosion resistance. For higher or lower biasing voltages, the sp^3 fraction content, corrosion resistance, mechanical properties and tribological properties begin to reduce and the surface roughness rises.

(2) The hydrogenated DLC thin films prepared by ion beam deposition method using a Kaufman-type gridded ion source at an average ion energy of 300 eV show the lowest roughness, COF and wear coefficient and the highest sp^3 content, hardness, Young's modulus and corrosion resistance. For higher ion energies, the sp^3 fraction content, corrosion resistance, mechanical properties and tribological properties begin to decrease and the surface roughness increases.

(3) The hydrogenated DLC thin films synthesized by ion beam deposition technique using a gridless end-Hall ion source at an average ion energy of 100 eV show the lowest roughness, friction coefficient and wear coefficient and the highest sp^3 content, hardness, Young's modulus and corrosion resistance. For higher or lower ion energies, the sp^3 fraction content, corrosion

resistance, mechanical properties and tribological properties begin to reduce and the surface roughness rises.

(4) The DLC-MoS_2 composite thin films with low content of MoS_2 show better tribological properties, i.e. lower friction coefficient and lower wear coefficient, than either MoS_2 or DLC films, demonstrating great potential to be used as a protective coating for industrial applications in which the film is exposed to ambient air environment. The hardness, Young's modulus, and corrosion resistance of the composite films drop and the coefficient of friction and the wear coefficient increase with the increase of incorporation of MoS_2 into the film. The composite films are composed of DLC, MoS_2 and $MoS_{2-x}O_x$ and the content of Mo, S, and O in the form of MoS_2 and $MoS_{2-x}O_x$ in the films increase with the rise of negative bias voltage on the target. The incorporation of MoS_2 enhances the formation of graphitic (sp^2) bonds and decreases the sp^3 content in DLC.

(5) The thermal stability of DLC films can be improved by fabricating a composite film including DLC and MoS_2, and the DLC-MoS_2 coating is promising to be employed as a protective coating for industrial applications in which the coating may be exposed to elevated temperatures. Pure DLC is thermally stable up to 200 °C in air and 300 °C in low pressure, after which, film mechanical and tribological performances drastically drop with the increase of treating temperature because of graphitization, which leads to an increase in sp^2 and decrease in sp^3 bonding structure. DLC-MoS_2 film is thermally stable up to 400 °C in air and 500 °C in low pressure. Afterwards, the mechanical and tribological performances of the film drop moderately up to 600 °C. Annealing in low pressure atmosphere slows down the oxidation and degradation of DLC and DLC-MoS_2 films at elevated temperatures. Structural characterization shows that formation of $MoS_{2-x}O_x$ structure is responsible for higher thermal stability of DLC-MoS_2 film,

while more oxidation and formation of oxides such as MoO_2, $Mo(SO_4)_3$, or MoO_3 at higher temperatures causes the gradual degradation of the film.

9.2 Recommendations for Future Work

DLC-MoS_2 composite thin films with low content of MoS_2 have shown interesting properties such as lower friction coefficient, lower wear coefficient, and higher thermal stability than pure DLC films in ambient air environment. In order to make these films useful for practical applications, further investigations are recommended as follows:

(1) In the present thesis, hydrogenated amorphous carbon (a-C:H) was synthesized and used as DLC component in the composite film. It would be interesting if tetrahedral amorphous carbon (ta-C) or hydrogenated tetrahedral amorphous carbon (ta-C:H) with a high percentage of sp^3 bonding could be employed as DLC component for the composite thin films. Because of the high content of sp^3 bonding in ta-C and ta-C:H, the mechanical properties and other properties (e.g. thermal stability) of the composite films might be improved.

(2) In the present study, tribological properties (friction and wear) of pure DLC and DLC-MoS_2 composite thin films in ambient air environment were investigated. For some industrial applications, the coatings may be exposed to vacuum or N_2 atmospheres. Thus it would be interesting and useful to evaluate the tribological behaviors of these films in the other environments such as vacuum and N_2.

(3) Erosion-corrosion is able to deteriorate materials or thin films at elevated rates than anticipated, due to a synergistic influence between corrosion and wear, and it can occur in some industrial applications. Therefore, the study of tribocorrosion behavior of DLC-MoS_2 composite thin films in comparison with pure DLC films is another area for further investigations.

LIST OF REFERENCES

Abrasonis G., R. Gayo, M. Vinnichenko, U. Kreissig, A. Kolitsch, W. Moller. 2006. Sixfold ring clustering in sp^2-dominated carbon and carbon nitride thin films: A Raman spectroscopy study. Physical Review B 73 (12): 125427-125440

Aisenberg S., R. Chabot. 1971. Ion-beam deposition of thin films of diamond-like carbon. Journal of Applied Physics 42 (7): 2953-2958

Aisenberg S., F.M. Kimock. 1991. Properties and characterization of amorphous carbon films. Materials Science Forum 52-53: 1-40

Bai L., G. Zhang, Z. Wu, J. Wang, P. Yan. 2011. Effect of different ion beam energy on properties of amorphous carbon film fabricated by ion beam sputtering deposition (IBSD). Nuclear Instruments and Methods in Physics Research B 269: 1871-1877

Bhandari H., S.A. Kumar, S.K. Dhawan. 2012. Conducting polymer nanocomposites for anticorrosive and antistatic applications. InTech Open Science p. 332

Bharathy P.V., Y. Chang, D. Nataraj, Q. Yang, S.M.Yang, D. Mangalaraj, L.Yang, T.J. Webster. 2010a. Effect of nickel incorporation on structural, nanomechanical and biocompatible properties of amorphous hydrogenated carbon thin films prepared by low energy biased target ion beam deposition. Thin Solid Films 519: 1623-1628

Bharathy P.V., D. Nataraj, P.K. Chu, H. Wang, Q. Yang, M. Kiran, J. Silvestre-Albero, D. Mangalaraj. 2010b. Effect of titanium incorporation on the structural, mechanical and biocompatible properties of DLC thin films prepared by reactive-biased target ion beam deposition method. Applied Surface Science 257: 143-150

Booser E.R. 1989. Handbook of lubrication: theory and practice of tribology, volume II. CRC-Press, Boca Raton

Casiraghi C., J. Robertson, A.C. Ferrari. 2007. Diamond-like carbon for data and beer storage. Materials Today 10: 44-53

Chan W.C., B. Zhou, Y.W. Chung, C.S. Lee, S.T. Lee. 1998. Synthesis, composition, surface roughness and mechanical properties of thin nitrogenated carbon films. Journal of Vacuum Science and Technology A 16: 1907-1911

Chen W., D.N.H. Nam, J. Lu, K.G. West, S.A. Wolf. 2009. Effects of target bias voltage in magnetic tunnel junctions grown by ion beam deposition. Journal of Applied Physics 106: 13905-13909

Chen X., Z. Peng, X. Yu, Z. Fu, W. Yue, C. Wang. 2011. Microstructure and tribological performance of self-lubricating diamond/tetrahedral amorphous carbon composite film. Applied Surface Science 257: 3180-3186

Choi J., S. Nakao, J. Kim, M. Ikeyama, T. Kato. 2007a. Corrosion protection of DLC coatings on magnesium alloy. Diamond and Related Materials 16: 1361-1364

Choi J., S. Nakao, S. Miyagawa, M. Ikeyama, Y. Miyagawa. 2007b. The effects of Si incorporation on the thermal and tribological properties of DLC films deposited by PBII&D with bipolar pulses. Surface and Coatings Technology 201: 8357-8361

Chowdhury S., M.T. Laugier, I.Z. Rahman. 2004. Characterization of DLC coatings deposited by rf magnetron sputtering. Journal of Materials Processing Technology 153-154: 804-810

Cuomo J.J., J.P. Doyle, J. Bruley, J.C. Liu. 1991. Sputter deposition of dense diamond-like carbon films at low temperature. Applied Physics Letters 58: 466-468

Cutiongco E.C., D. Li, Y.W. Chung, C.S. Bhatia. 1996. Tribological behavior of amorphous carbon nitride overcoats for magnetic thin film rigid disks. Journal of Tribology 118: 543-548

Dahan I., U. Admon, N. Frage, J. Sariel, M.P. Dariel. 2001. The development of a functionally graded TiC-Ti multilayer hard coating. Surface and Coatings Technology 137: 111-115

Dimigen H., H. Hubsch, R. Memming. 1987. Tribological and electrical properties of metal-containing hydrogenated carbon films. Applied Physics Letters 50: 1056-1058

Dimigen H., C.P. Klages. 1991. Microstructure and wear behavior of metal-containing diamond-like coatings. Surface and Coatings Technology 49: 543-547

Donnet C., J.M. Martin, T.L. Mogne, M. Belin. 1996. Super-low friction of MoS_2 coatings in various environments. Tribology International 29: 123-128

Donnet C., A. Grill. 1997a. Friction control of diamond-like carbon coatings. Surface and Coatings Technology 94-95: 456-462

Donnet C., J. Fontaine, A. Grill, V. Patel, C. Patel, M. Belin. 1997b. Wear-resistant fluorinated diamond like carbon films. Surface and Coatings Technology 94-95: 531-536

Donnet C., A. Erdemir. 2008. Tribology of diamond-like carbon films. Springer, NewYork

Erdemir A., G.R. Fenske. 1996. Tribological performance of diamond and diamond-like carbon films at elevated temperatures. Tribology Transactions 39 (4): 787-794

Erdemir A., O.L. Eryilmaz, G. Fenske. 2000. Synthesis of diamond like carbon films with super low friction and wear properties. Journal of Vacuum Science and Technology A 18 (4): 1987-1992

Erdemir A., C. Donnet. 2006. Tribology of diamond-like carbon films: recent progress and future prospects. Journal of Physics D: Applied Physics 39: R311-R327

Evaristo M., T. Polcar, A. Cavaleiro. 2008. Tribological behaviour of C-alloyed transition metal dichalcogenides (TMD) coatings in different environments. International Journal of Mechanics and Materials in Design 4: 137-143

Ferrari A.C., J. Robertson. 2004. Raman spectroscopy of amorphous, nanostructured, diamond-like carbon, and nanodiamond. Philosophical Transactions of the Royal Society A 362: 2477-2512

Fleischauer P.D., J.R. Lince. 1999. A comparison of oxidation and oxygen substitution in MoS_2 solid film lubricants. Tribology International 32: 627-636

Franceschini D.F., C.A. Achete, F.L. Freire. 1992. Internal stress reduction by nitrogen incorporation in hard amorphous carbon thin films. Applied Physics Letters 60: 3229-3231

Frey G.L., R. Tenne, M.J. Matthews, M.S. Dresselhaus, G. Dresselhaus. 1999. Raman and resonance Raman investigation of MoS_2 nanoparticles. Physical Review B 60 (4) 2883-2892

Fu R.K.Y., Y.F. Mei, M.Y. Fu, X.Y. Liu, P.K. Chu. 2005. Thermal stability of metal-doped diamond-like carbon fabricated by dual plasma deposition. Diamond and Related Materials 14:1489-1493

Gangopadhyay A.K., P.A. Willermet, M.A. Tamor, W.C. Vassell. 1997. Amorphous hydrogenated carbon films for tribological applications I. Development of moisture insensitive films having reduced compressive stress. Tribology International 30: 9-18

Gangopadhyay A. 1998. Mechanical and tribological properties of amorphous carbon films. Tribology Letters 5: 25-39

Gao F., A. Erdemir, W.T. Tysoe. 2005. The tribological properties of low-friction hydrogenated diamond-like carbon measured in ultrahigh vacuum. Tribology Letters 20 (3-4): 221-227

Ge S., S. Wang, N. Gitis, M. Vinogradov, J. Xiao. 2008. Wear behavior and wear debris distribution of UHMWPE against Si_3N_4 ball in bi-directional sliding. Wear 264: 571-578

Gilmer G.H., H. Huang, C. Roland. 1998. Thin film deposition: fundamentals and modeling. Computational Materials Science 12: 354-380

Gitis N., I. Hermann, S. Kuiry. 2008. Nano and micro indentation and scratch tests of mechanical properties of thin films. Proceedings of the 7th International Conference "The Coatings in Manufacturing Engineering": 371-378

Grill A., V. Patel, B.S. Meyerson. 1991. Temperature and bias effects on the physical and tribological properties of diamond-like carbon. Journal of the Electrochemical Society 138 (8): 2362-2367

Grill A. 1993. Review of the tribology of diamond-like carbon. Wear 168: 143-153

Grill A., Patel V. 1996. Wear resistant fluorinated diamond like carbon films. New Diamond and Frontier Carbon Technology 6: 13-21

Grill A. 1997. Tribology of diamond like carbon and related materials: an updated review. Surface and Coatings Technology 94-95: 507-513

Hauert R., A. Glisenti, S. Metin, J. Goitia, J.H. Kaufman, P.H.M. van Loosdrecht. 1995. Influence of nitrogen doping on different properties of a-C:H. Thin Solid Films 268: 22-29

Hauert R., U. Muller, G. Francz, F. Birchler, A. Schroeder, J. Mayer. 1997. Surface analysis and bioreactions of F and Si containing a-C:H. Thin Solid Films 308-309: 191-194

He B.B. 2009. Two-dimensional X-ray diffraction. Wiley, Hoboken

He X.M., M. Hakovirta, M. Nastasi. 2005. Hardness, hydrophobic and optical properties of fluorine and boron co-alloyed diamond-like carbon films. Materials Letters 59: 1417-1421

Holmberg K., H. Ronkainen, A. Laukkanen, K. Wallin, S. Hogmark, S. Jacobson. 2009. Residual stresses in TiN, DLC and MoS_2 coated surfaces with regard to their tribological fracture behavior. Wear 267: 2142-2156

Hylton T.L., B. Ciorneiu, D.A. Baldwin, O. Escorcia, J. Son, M.T. McClure, G. Waters. 2000. Thin film processing by biased target ion beam deposition. IEEE Transactions on Magnetics 36: 2966-2971

Jamison W.E., S.L. Cosgrove. 1971. Friction characteristics of transition-metal disulphides and diselenides. ASLE Transactions 14: 62 -72

Jellesen M.S., T.L. Christiansen, L.R. Hilbert, P. Moller. 2009. Erosion-corrosion and corrosion properties of DLC coated low temperature gas-nitrided austenitic stainless steel. Wear 267: 1709-1714

Jeong S.M., W.H. Koo, S.H. Choi, H.K. Baik. 2005. Enhanced passivation characteristics in OLEDs by modification of aluminum cathodes using Ar^+ ion beam. Solid-State Electronics 49: 838-846

Jung H.S., H.H. Park, S.S. Pang, S.Y. Lee. 1999. The structural and electron field emission characteristics of pulsed laser deposited diamond-like carbon films with thermal treatment. Thin Solid Films 355-356: 151-156

Kaufmann H.R. 1978. Technology of ion beam sources used in sputtering. Journal of Vacuum Science and Technology 15 (2): 272-276

Kaufman H.R., R.S. Robinson, R.I. Seddon. 1987. End-Hall ion source. Journal of Vacuum Science and Technology A 5: 2081-2084

Khun N.W., E. Liu, X.T. Zeng. 2009. Corrosion behavior of nitrogen doped diamond-like carbon thin films in NaCl solutions. Corrosion Science 51: 2158-2164

Khun N.W., E. Liu, G.C. Yang. 2010. Structure, scratch resistance and corrosion performance of nickel doped diamond-like carbon thin films. Surface and Coatings Technology 204: 3125-3130

Khurshudov A., K. Kato, S. Daisube. 1996. Comparison of tribological properties of carbon and carbon nitride protective coatings over magnetic media. Journal of Vacuum Science and Technology A 14: 2935-2939

Kim H.G., S.H. Ahn, J.G. Kim, S.J. Park, K.R. Lee. 2005. Corrosion performance of diamond-like carbon (DLC)-coated Ti alloy in the simulated body fluid environment. Diamond and Related Materials 14: 35-41

Konca E., Y.T. Cheng, A.M. Weiner, J.M. Dasch, A.T. Alpas. 2006. Elevated temperature tribological behavior of non-hydrogenated diamond-like carbon coatings against 319 aluminum alloy. Surface and Coatings Technology 200: 3996-4005

Lansdown A.R. 1999. Molybdenum disulphide lubrication. Elsevier, Amsterdam

Leng Y.X., J.Y. Chen, P. Yang, H. Sun, G.J. Wan, N. Huang. 2003. Mechanical properties and thermomechanical stability of diamond-like carbon films synthesized by pulsed vacuum arc plasma deposition. Surface and Coatings Technology 173: 67-73

Lévy F., J. Moser. 1994. High-resolution cross-sectional studies and properties of molybdenite coatings. Surface and Coatings Technology 68-69: 433-438

Li H., T. Xu, C. Wang, J. Chen, H. Zhou, H. Liu. 2006. Annealing effect on the structure, mechanical and tribological properties of hydrogenated diamond-like carbon films. Thin Solid Films 515: 2153-2160

Lieberman M.A., A.J. Lichtenberg. 1994. Principles of plasma discharges and materials processing. Wiley, NewYork

Lifshitz Y. 1996. Hydrogen-free amorphous carbon films: correlation between growth conditions and properties. Diamond and Related Materials 5: 388-400

Lifshitz Y. 1999. Diamond-like carbon - present status. Diamond and Related Materials 8: 1659-1676

Lifshitz Y. 2003. Pitfalls in amorphous carbon studies. Diamond and Related Materials 12: 130-140

Lince J.R., M.R. Hilton, A.S. Bommannavar. 1990. Oxygen substitution in sputter-deposited MoS_2 films studied by extended X-ray absorption fine structure, X-ray photoelectron spectroscopy and X-ray diffraction. Surface and Coatings Technology 43-44: 640-651

Liu C., D. Hu, J. Xu, D. Yang, M. Qi. 2006. In vitro electrochemical corrosion behavior of functionally graded diamond-like carbon coatings on biomedical Nitinol alloy. Thin Solid Films 496: 457-462

Liu H., A. Tanaka, K. Umeda. 1999. The tribological characteristics of diamond-like carbon films at elevated temperatures. Thin Solid Films 346: 162-168

Liu Y., E.I. Meletis. 1997. Evidence of graphitization of diamond-like carbon films during sliding wear. Journal of Materials Science 32: 3491-3495

Liu Z.T., N.K. Xu, D.S. Geng, X.L. Zheng.1993. Thermostability of diamond-like carbon films. Surface Engineering 9 (2): 148-150

Louro C., C.W. Moura, N. Carvalho, M. Stueber, A. Cavaleiro. 2011. Thermal stability in oxidative and protective environments of a-C:H cap layer on a functional gradient coating. Diamond and Related Materials 20: 57-63

Martin J.M., C. Donnet, T. Lemogne, T. Epicier. 1993. Superlubricity of molybdenum disulphide. Physical Review B 48 (14): 10583-10586

Martinez E., J.L. Andujar, M.C. Polo, J. Esteve, J. Robertson, W.I. Milne. 2001. Study of the mechanical properties of tetrahedral amorphous carbon films by nanoindentation and nanowear measurements. Diamond and Related Materials 10: 145-152

Masami I., N. Setsuo, S. Tsutomu, C. Junho. 2009. Improvement of corrosion protection property of Mg-alloy by DLC and Si–DLC coatings with PBII technique and multi-target DC-RF magnetron sputtering. Nuclear Instruments and Methods in Physics Research B 267: 1675-1679

McKenzie D.R., D. Muller, B.A. Pailthorpe. 1991. Compressive-stress-induced formation of thin-film tetrahedral amorphous carbon. Physical Review Letters 67 (6): 773-776

McKenzie D.R., Y. Yin, N.A. Yin, C.A. Davis, B.A. Pailthorpe, G.A.J. Amaratunga, V.S. Veerasamy. 1994. Hydrogen-free amorphous carbon preparation and properties. Diamond and Related Materials 3: 353-360

Memming R., H.J. Tolle, P.E. Wierenga. 1986. Properties of polymeric layers of hydrogenated amorphous carbon produced by a plasma-activated chemical vapour deposition process II: tribological and mechanical properties. Thin Solid Films 143: 31-41

Meneve J., R. Jacobs, L. Eersels, J. Smeets, E. Dekempeneer. 1993. Friction and wear behavior of amorphous hydrogenated Si_{1-x} C_x films. Surface and Coatings Technology 62: 577-582

Merel P., M. Tabbal, M. Chaker, S. Moisa, J. Margot. 1998. Direct evaluation of the sp^3 content in diamond-like-carbon films by XPS. Applied Surface Science 136: 105-110

Michler T., M. Grischke, K. Bewilogna, A. Hieke. 1999. Continuously deposited duplex coatings consisting of plasma nitriding and a-C:H:Si deposition. Surface and Coatings Technology 111: 41-45

Miyake S., R. Kaneko, Y. Kikuya, I. Sugimoto. 1991. Micro-tribological studies on fluorinated carbon films. Journal of Tribology 113: 384-389

Miyoshi K., J.J. Pouch, A. Alterovitz. 1989. Plasma-deposited amorphous hydrogenated carbon films and their tribological properties. NASA TM-102379. Cleveland, Ohio

Monteiro O.R. 2001. Synthesis, properties and applications of pure and covalently doped DLC films prepared by energetic condensation. Lawrence Berkeley National Laboratory

Müller U., R. Hauert, B. Oral, M. Tobler. 1995. Temperature stability of fluorinated amorphous hydrogenated carbon films. Surface and Coatings Technology 76-77: 367-371

Nakazawa H., A. Sudoh, M. Suemitsu, K. Yasui, T. Itoh, T. Endoh, Y. Narita, M. Mashita. 2010. Mechanical and tribological properties of boron, nitrogen- coincorporated diamond-like carbon films prepared by reactive radio-frequency magnetron sputtering. Diamond & Related Materials 19: 503-506

Oguri K., T. Arai. 1990. Low friction coatings of diamond-like carbon with silicon prepared by plasma-assisted chemical vapor deposition. Journal of Materials Research 5: 2567-2571

Oliver W.C., G.M. Phar. 2004. Measurement of hardness and elastic modulus by instrumented indentation: Advances in understanding and refinements to methodology. Journal of Materials Research 19: 3-20

Ostrovskaya Y.L., V.E. Strel'nitskij, V.I. Kuleba, G.D. Gamulya. 2001. Friction and wear behaviour of hard and superhard coatings at cryogenic temperatures. Tribology International 34: 255-263

Pandey M., D. Bhatacharyya, D.S. Patil, K. Ramachandran, N. Venkatramani. 2004. Diamond-like carbon coatings: AFM and ellipsometric studies. Surface and Coatings Technology 182: 24-34

Patterson A.L. 1939. The Scherrer formula for X-ray particle size determination. Physical Review 56: 978-982

Pauleau Y., P.B. Barna. 1997. Protective coatings and thin films: synthesis, characterization and applications. Kluwer Academic Publishers, Amsterdam

Peng X.L., T.W. Clyne. 1998. Mechanical stability of DLC films on metallic substrates Part II-Interfacial toughness, debonding and blistering. Thin Solid Films 312: 219 -227

Peng X.L., Z.H. Barber, T.W. Clyne. 2001. Surface roughness of diamond-like carbon films prepared using various techniques. Surface and Coatings Technology 138: 23-32

Prasad S.V., N.T. McDevitt, J.S. Zabinski. 2000. Tribology of tungsten disulfide-nanocrystalline zinc oxide adaptive lubricant films from ambient to 500 °C. Wear 237: 186-196

Quan J.J., S.A. Wolf, H.N.G. Wadley. 2007. Low energy ion beam assisted deposition of a spin valve. Journal of Applied Physics 101: 74302-74305

Rey S., F. Antoni, B. Prevot, E. Fogarassy, J.C. Arnault, J. Hommet, F. LeNormand, P. Bohe. 2000. Thermal stability of amorphous carbon films deposited by pulsed laser ablation. Applied physics A 71: 433-439

Robertson J. 1986. Amorphous carbon. Advances in Physics 35: 317-374

Robertson J. 1994. The deposition mechanism of diamond-like a-C and a-C:H. Diamond and Related Materials 3: 361-368

Robertson J. 1995. Structural models of a-C and a-C:H. Diamond and Related Materials 4: 297-301

Robertson J. 2002. Diamond-like amorphous carbon. Materials Science and Engineering R 37: 129-281

Robertson J. 2003. Requirements of ultrathin carbon coatings for magnetic storage technology. Tribology International 36: 405-415

Schwan J., S. Ulrich, H. Roth, H. Ehrhardt, S.R.P. Silva, J. Robertson, R. Samlenski. 1996. Tetrahedral amorphous carbon films prepared by magnetron sputtering and dc ion plating. Journal of Applied Physics 79 (3): 1416-1422

Shaha K.P., Y.T. Pei, D. Martinez, J.Th.M. De Hosson. 2011. Influence of surface roughness on the transfer film formation and frictional behavior of TiC/a-C nanocomposite coatings. Tribology Letters 41: 97-101

Sharma R., P.K. Barhai, N. Kumari. 2008. Corrosion resistant behavior of DLC films. Thin Solid Films 516: 5397-5403

Silva S.R. 2003. Properties of amorphous carbon. INSPEC, London

Singh K., O. Anil, S.K. Dhawan. 2012. Polymer-graphene nanocomposites: preparation, characterization, properties, and applications. In F. Ebrahimi (Ed.), Nanocomposites-New Trends and Developments (pp. 37-72). InTech, Hampshire

Sundaram V.S. 2006. Diamond like carbon film as a protective coating for high strength steel and titanium alloy. Surface and Coatings Technology 201 (6): 2707-2711

Tallant D.R., J.E. Parmeter, M.P. Diegal, R.L. Simpson. 1995. The thermal stability of diamond-like carbon. Diamond and Related Materials 4: 191-199

Tang Y. 2010. Plasma and ion beam enhanced chemical vapour deposition of diamond and diamond-like carbon. Ph.D. Thesis, University of Saskatchewan

Tang Y., Y.S. Li, C.Z. Zhang, J. Wang, Q. Yang, A. Hirose. 2011a. Synthesis of cobalt/diamond-like carbon thin films by biased target ion beam deposition. Diamond and Related Materials 20: 538-541

Tang Y., Y.S. Li, Q. Yang, A. Hirose. 2011b. Characterization of hydrogenated amorphous carbon thin films by end-Hall ion beam deposition. Applied Surface Science 257: 4699-4705

Teer D.G., J. Hampshire, V. Fox, V. Bellido-Gonzalez. 1997. The tribological properties of MoS_2/metal composite coatings deposited by closed field magnetron sputtering. Surface and Coatings Technology 94: 572-577

Teer D.G. 2001. New solid lubricant coatings. Wear 251: 1068-1074

Trojan K., M. Grischke, H. Dimigen. 1994. Network modification of DLC coatings to adjust a defined surface energy. Physica Status Solidi A 145: 575-585

Vanhulsel A., F. Velasco, R. Jacobs, L. Eersels, D. Havermans, E.W. Roberts, I. Sherrington, M.J. Anderson, L. Gaillard. 2007. DLC solid lubricant coatings on ball bearings for space applications. Tribology International 40 (7): 1186-1194

Vasquez-Borucki S., W. Jacob, C.A. Achete. 2000. Amorphous hydrogenated carbon films as barrier for gas permeation through polymer films. Diamond and Related Materials 9: 1971-1978

Venkatraman C., C. Brodbeck, R. Lei. 1999. Tribological properties of diamond-like nanocomposite coatings at high temperatures. Surface and Coatings Technology 115: 215-221

Voevodin A.A., C. Rebholz, J.M. Schneider, P. Stevenson, A. Matthews. 1995. Wear resistant composite coatings deposited by electron enhanced closed field unbalanced magnetron sputtering. Surface and Coatings Technology 73: 185-197

Voevodin A.A., M.S. Donley. 1996a. Preparation of amorphous diamond-like carbon by pulsed laser deposition: a critical review. Surface and Coatings Technology 82 (3): 199-213

Voevodin A.A., A.W. Phelps, J.S. Zabinski, M.S. Donley. 1996b. Friction induced phase transformation of pulsed laser deposited diamond-like carbon. Diamond and Related Materials 5: 1264-1269

Wang P., X. Wang, T. Xu, W. Liu, J. Zhang. 2007. Comparing internal stress in diamond-like carbon films with different structure. Thin Solid Films 515: 6899-6903

Wang W.J., T.M. Wang, B.L. Chen. 1996. Hydrogen release from diamondlike carbon films due to thermal annealing in vacuum. Nuclear Instruments and Methods in Physics Research B 117: 140-144

Wei Q., R.J. Narayan, J. Narayan, J. Sankar, A.K. Sharma. 1998. Improvement of wear resistance of pulsed laser deposited diamond-like carbon films through incorporation of metals. Materials Science and Engineering B 53: 262-266

Weise G., N. Mattern, H. Hermann, A. Teresiak, I. Bacher, W. Bruckner, H.D. Bauer, H. Vinzelberg, G. Reiss, U. Kreissig, M. Mader, P. Markschlager. 1997. Preparation, structure and properties of MoS_x films. Thin Solid Films 298 (1-2): 98-106

Wild C., P. Koidl. 1987. Thermal gas effusion from hydrogenated amorphous carbon films. Applied Physics Letters 51 (19): 1506-1508

Wolf B. 1995. Handbook of ion sources. CRC Press p. 222

Wu W.J., M.H. Hon. 1999. Thermal stability of diamond-like carbon films with added silicon. Surface and Coatings Technology 111: 134-140

Yang W.J., Y.H. Choa, T. Sekino, K.B. Shim, K. Niihara, K.H. Auh. 2003. Thermal stability evaluation of diamond-like nanocomposite coatings. Thin Solid Films 434: 49-54

Zhang L. 2012. Synthesis and characterization of boron incorporated diamond-like carbon thin films. M.Sc.Thesis, University of Saskatchewan

Zhang S., X.T. Zeng, H. Xie, P. Hing. 2000. A phenomenological approach for the I_d/I_g ratio and sp^3 fraction of magnetron sputtered a-C films. Surface and Coatings Technology 123: 256-260

Zhang S., X.L. Bui, X. Li. 2006. Thermal stability and oxidation properties of magnetron sputtered diamond-like carbon and its nanocomposite coatings. Diamond and Related Materials 15: 972-976

Zhang X., R.G. Vitchev, W. Lauwerens, L. Stals, J. He, J.P. Celis. 2001. Effect of crystallographic orientation on fretting wear behavior of MoS_x coatings in dry and humid air. Thin Solid Films 396: 69-77

Zhurin V.V., H.R. Kaufman, J.R. Kahn, T.L. Hylton. 2000. Biased target deposition. Journal of Vacuum Science and Technology A 18: 37-41

Zou Y.S., Y.F. Wu, R.F. Huang, C. Sun, L.S. Wen. 2009. Mechanical properties and thermal stability of nitrogen incorporated diamond-like carbon films. Vacuum 83: 1406-1410

Zubavichus Y.V., A.S. Golub, Y.N. Novikov, Y.L. Slovokhotov, A.N. Nesmeyanov, P.J. Schilling, R.C. Tittsworth. 1997. XAFS study of MoS_2 intercalation compounds. Journal de Physique IV 7: 1057-1059

APPENDIX: COPYRIGHT INFORMATION

The chapters 4, 7 and 8 have been published in the three Elsevier journals. For manuscripts published by Elsevier, the authors retain the right to include their article in a thesis or dissertation without the need to obtain a written permission:

"As an author, you retain rights for a large number of author uses, including use by your employing institute or company. These rights are retained and permitted without the need to obtain specific permission from Elsevier. These include: the right to include the article in full or in part in a thesis or dissertation (provided that this is not to be published commercially)" (http://support.elsevier.com/app/answers/detail/a_id/565/session/L3RpbWUv).

Copyright Permissions for Figures

Figures 2.1, 2.5, 2.9 and 3.5:

ELSEVIER LICENSE

TERMS AND CONDITIONS

Dec 15, 2014

This is a License Agreement between Hamid Niakan ("You") and Elsevier ("Elsevier") provided by Copyright Clearance Center ("CCC").

Supplier Elsevier Limited

The Boulevard,Langford Lane

Kidlington, Oxford, OX5 1GB, UK

Registered Company Number 1982084

Customer name Hamid Niakan

License number 3530431251119

License date Dec 15, 2014

Licensed content publisher Elsevier

Licensed content publication Materials Science and Engineering: R: Reports

Licensed content title Diamond-like amorphous carbon

Licensed content author J. Robertson

Licensed content date 24 May 2002

Licensed content volume number 37

Licensed content issue number 4-6

Number of pages 153

Start Page 129

End Page 281

Type of Use reuse in a thesis/dissertation

Intended publisher of new work other

Portion figures/tables/illustrations

Number of figures/tables/illustrations 4

Format both print and electronic

Are you the author of this Elsevier article? No

Will you be translating? No

Title of your thesis/dissertation Synthesis and Characterization of Diamond-Like Carbon and DLC-MoS_2 Composite Thin Films

Expected completion date Dec 2014

Estimated size (number of pages) 168

Elsevier VAT number GB 494 6272 12

Permissions price 0.00 USD

VAT/Local Sales Tax 0.00 USD / 0.00 GBP

Total 0.00 USD

Figure 2.2:

The source of this figure is InTech Open Access Platform. According to their Copyright Policy, "Creative Commons Attribution 3.0 Unported License", "The CC BY 3.0 license permits Works to be freely shared in any medium or format, as well as reuse and adaptation of the original contents of Works (e.g. figures and tables created by the authors), as long as the source Work is cited" (http://www.intechopen.com/copyright-policy.html).

Figure 2.3:

ELSEVIER LICENSE

TERMS AND CONDITIONS

Dec 15, 2014

This is a License Agreement between Hamid Niakan ("You") and Elsevier ("Elsevier") provided by Copyright Clearance Center ("CCC").

Supplier Elsevier Limited

The Boulevard,Langford Lane

Kidlington, Oxford, OX5 1GB, UK

Registered Company Number 1982084

Customer name Hamid Niakan

License number 3530430719853

License date Dec 15, 2014

Licensed content publisher Elsevier

Licensed content publication Materials Today

Licensed content title Diamond-like carbon for data and beer storage

Licensed content author Cinzia Casiraghi,John Robertson,Andrea C. Ferrari

Licensed content date January–February 2007

Licensed content volume number 10

Licensed content issue number 1-2

Number of pages 10

Start Page 44

End Page 53

Type of Use reuse in a thesis/dissertation

Intended publisher of new work other

Portion figures/tables/illustrations

Number of figures/tables/illustrations 1

Format both print and electronic

Are you the author of this Elsevier article? No

Will you be translating? No

Title of your thesis/dissertation Synthesis and Characterization of Diamond-Like Carbon and DLC-MoS_2 Composite Thin Films

Expected completion date Dec 2014

Estimated size (number of pages) 168

Elsevier VAT number GB 494 6272 12

Permissions price 0.00 USD

VAT/Local Sales Tax 0.00 USD / 0.00 GBP

Total 0.00 USD

Figure 2.4:

ELSEVIER LICENSE

TERMS AND CONDITIONS

Dec 15, 2014

This is a License Agreement between Hamid Niakan ("You") and Elsevier ("Elsevier") provided by Copyright Clearance Center ("CCC").

Supplier Elsevier Limited

The Boulevard,Langford Lane

Kidlington, Oxford, OX5 1GB, UK

Registered Company Number 1982084

Customer name Hamid Niakan

License number 3530430317285

License date Dec 15, 2014

Licensed content publisher Elsevier

Licensed content publication Diamond and Related Materials

Licensed content title Structural models of a-C and a-C:H

Licensed content author J. Robertson

Licensed content date 15 April 1995

Licensed content volume number 4

Licensed content issue number 4

Number of pages 5

Start Page 297

End Page 301

Type of Use reuse in a thesis/dissertation

Intended publisher of new work other

Portion figures/tables/illustrations

Number of figures/tables/illustrations 1

Format both print and electronic

Are you the author of this Elsevier article? No

Will you be translating? No

Title of your thesis/dissertation Synthesis and Characterization of Diamond-Like Carbon and DLC-MoS_2 Composite Thin Films

Expected completion date Dec 2014

Estimated size (number of pages) 168

Elsevier VAT number GB 494 6272 12

Permissions price 0.00 USD

VAT/Local Sales Tax 0.00 USD / 0.00 GBP

Total 0.00 USD

Figure 2.6:

ELSEVIER LICENSE

TERMS AND CONDITIONS

Dec 15, 2014

This is a License Agreement between Hamid Niakan ("You") and Elsevier ("Elsevier") provided by Copyright Clearance Center ("CCC").

Supplier Elsevier Limited

The Boulevard,Langford Lane

Kidlington, Oxford, OX5 1GB, UK

Registered Company Number 1982084

Customer name Hamid Niakan

License number 3530391391216

License date Dec 15, 2014

Licensed content publisher Elsevier

Licensed content publication Solid-State Electronics

Licensed content title Enhanced passivation characteristics in OLEDs by modification of aluminum cathodes using Ar^+ ion beam

Licensed content author Soon Moon Jeong,Won Hoe Koo,Sang Hun Choi,Hong Koo Baik

Licensed content date May 2005

Licensed content volume number 49

Licensed content issue number 5

Number of pages 9

Start Page 838

End Page 846

Type of Use reuse in a thesis/dissertation

Intended publisher of new work other

Portion figures/tables/illustrations

Number of figures/tables/illustrations 1

Format both print and electronic

Are you the author of this Elsevier article? No

Will you be translating? No

Title of your thesis/dissertation Synthesis and Characterization of Diamond-Like Carbon and DLC-MoS_2 Composite Thin Films

Expected completion date Dec 2014

Estimated size (number of pages) 168

Elsevier VAT number GB 494 6272 12

Permissions price 0.00 USD

VAT/Local Sales Tax 0.00 USD / 0.00 GBP

Total 0.00 USD

Figure 2.7:

AMERICAN PHSICAL SOCIETY LICENSE

TERMS AND CONDITIONS

This is a License Agreement between Hamid Niakan ("You") and American Physical Society provided by Copyright Clearance Center ("CCC").

License Number 3530370237639

License date Dec 15, 2014

Licensed content publisher American Physical Society

Licensed content publication Physical Review Letters

Licensed content title Compressive-stress-induced formation of thin-film tetrahedral amorphous carbon

Licensed copyright line © 1991 The American Physical Society

Licensed content author D. R. McKenzie, D. Muller, and B. A. Pailthorpe

Licensed content date Aug 5, 1991

Volume number 67

Type of use Thesis/Dissertation

Requestor type Student

Format both print and electronic

Portion image/photo

Number of images/photos requested 1

Rights for Main product

Duration of use Life o f current edition

For distribution to World

In the following language(s) Original language o f publication

The requesting person/organization Hamid Niakan

Order reference number None

Title of your thesis /dissertation Synthesis and Characterization of Diamond-Like Carbon and DLC-MoS_2 Composite Thin Films

Expected completion date Dec 2014

Expected size (number of pages) 168

Total 0.00 CAD

Figures 2.8 and 2.10:

SPRINGER LICENSE

TERMS AND CONDITIONS

This is a License Agreement between Hamid Niakan ("You") and Springer ("Springer") provided by Copyright Clearance Center ("CCC").

License Number 3530381293071

License date Dec 15, 2014

Licensed content publisher Springer

Licensed content publication Springer eBook

Licensed content title Classification of Diamond-like Carbons

Licensed content author J. Robertson

Licensed content date Jan 1, 2008

Type of Use Thesis/Dissertation

Portion Figures

Number of images/photos requested 2

Format both print and electronic

Author of this Springer article No

Title of your thesis /dissertation Synthesis and Characterization of Diamond-Like Carbon and DLC-MoS_2 Composite Thin Films

Expected completion date Dec 2014

Estimated size (pages) 168

Total 0.00 USD

Figure 2.11:

SPRINGER LICENSE

TERMS AND CONDITIONS

This is a License Agreement between Hamid Niakan ("You") and Springer ("Springer") provided by Copyright Clearance Center ("CCC").

License Number 3530380594331

License date Dec 15, 2014

Licensed content publisher Springer

Licensed content publication Springer eBook

Licensed content title Doping and Alloying Effects on DLC Coatings

Licensed content author J. C. Sánchez -López

Licensed content date Jan 1, 2008

Type of Use Thesis/Dissertation

Portion Figures

Number of images/photos requested 1

Format both print and electronic

Author of this Springer article No

Title of your thesis /dissertation Synthesis and Characterization of Diamond-Like Carbon and DLC-MoS_2 Composite Thin Films

Expected completion date Dec 2014

Estimated size (pages) 168

Total 0.00 USD

Figure 3.10:

CAMBRIDGE UNIVERSITY PRESS LICENSE

TERMS AND CONDITIONS

This is a License Agreement between Hamid Niakan ("You") and Cambridge University Press ("Cambridge University Press") provided by Copyright Clearance Center ("CCC").

License Number 3530390822388

License date Dec 15, 2014

Licensed content publisher Cambridge University Press

Licensed content publication Journal of Materials Research

Licensed content title Measurement of hardness and elastic modulus by instrumented indentation: Advances in understanding and refinements to methodology

Licensed content author W.C. Oliver and G.M. Pharr

Licensed content date Mar 3, 2011

Volume number 19

Issue number 01

Start page 3

End page 20

Type of Use Dissertation/Thesis

Requestor type Not-for-profit

Portion image/photo

Number of images/photos requested 1

Format both print and electronic

Order reference number None

Territory for reuse World

Title of your thesis /dissertation Synthesis and Characterization of Diamond-Like Carbon and DLC-MoS_2 Composite Thin Films

Expected completion date Dec 2014

Estimated size (pages) 168

Billing Type Invoice

TAX (0.00%) 0.00 USD

Total 0.00 USD

Figure 3.11:

ELSEVIER LICENSE

TERMS AND CONDITIONS

Dec 15, 2014

This is a License Agreement between Hamid Niakan ("You") and Elsevier ("Elsevier") provided by Copyright Clearance Center ("CCC").

Supplier Elsevier Limited

The Boulevard,Langford Lane

Kidlington, Oxford, OX5 1GB, UK

Registered Company Number 1982084

Customer name Hamid Niakan

License number 3530440771568

License date Dec 15, 2014

Licensed content publisher Elsevier

Licensed content publication Wear

Licensed content title Wear behavior and wear debris distribution of UHMWPE against Si_3N_4 ball in bi-directional sliding

Licensed content author Shirong Ge,Shibo Wang,Norm Gitis,Michael Vinogradov,Jun Xiao

Licensed content date 15 March 2008

Licensed content volume number 264

Licensed content issue number 7-8

Number of pages 8

Start Page 571

End Page 578

Type of Use reuse in a thesis/dissertation

Intended publisher of new work other

Portion figures/tables/illustrations

Number of figures/tables/illustrations 1

Format both print and electronic

Are you the author of this Elsevier article? No

Will you be translating? No

Title of your thesis/dissertation Synthesis and Characterization of Diamond-Like Carbon and DLC-MoS_2 Composite Thin Films

Expected completion date Dec 2014

Estimated size (number of pages) 168

Elsevier VAT number GB 494 6272 12

Permissions price 0.00 USD

VAT/Local Sales Tax 0.00 USD / 0.00 GBP

Total 0.00 USD